University of Kentucky

UKnowledge

2022

PARAMETRIC AVERAGE-VALUE MODELING, SIMULATION, AND CHARACTERIZATION OF MACHINE-RECTIFIER SYSTEMS

Isuje Ojo
University of Kentucky, Ojoisuje@gmail.com
Digital Object Identifier: https://doi.org/10.13023/etd.2022.354

Right click to open a feedback form in a new tab to let us know how this document benefits you.

STUDENT AGREEMENT:

I represent that my thesis or dissertation and abstract are my original work. Proper attribution has been given to all outside sources. I understand that I am solely responsible for obtaining any needed copyright permissions. I have obtained needed written permission statement(s) from the owner(s) of each third-party copyrighted matter to be included in my work, allowing electronic distribution (if such use is not permitted by the fair use doctrine) which will be submitted to UKnowledge as Additional File.

I hereby grant to The University of Kentucky and its agents the irrevocable, non-exclusive, and royalty-free license to archive and make accessible my work in whole or in part in all forms of media, now or hereafter known. I agree that the document mentioned above may be made available immediately for worldwide access unless an embargo applies.

I retain all other ownership rights to the copyright of my work. I also retain the right to use in future works (such as articles or books) all or part of my work. I understand that I am free to register the copyright to my work.

REVIEW, APPROVAL AND ACCEPTANCE

The document mentioned above has been reviewed and accepted by the student's advisor, on behalf of the advisory committee, and by the Director of Graduate Studies (DGS), on behalf of the program; we verify that this is the final, approved version of the student's thesis including all changes required by the advisory committee. The undersigned agree to abide by the statements above.

<div align="right">

Isuje Ojo, Student

Dr. Aaron Cramer, Major Professor

Dr. Daniel Lau, Director of Graduate Studies

</div>

PARAMETRIC AVERAGE-VALUE MODELING, SIMULATION, AND

CHARACTERIZATION OF MACHINE-RECTIFIER SYSTEMS

DISSERTATION

A dissertation submitted in partial

fulfillment of the requirements for

the degree of Doctor of Philosophy

in the College of Engineering at the

University of Kentucky

By

Isuje T. Ojo

Lexington, Kentucky

Director: Dr. Aaron M. Cramer, Professor of Electrical and Computer Engineering

Lexington, Kentucky

2022

ABSTRACT OF DISSERTATION

PARAMETRIC AVERAGE-VALUE MODELING, SIMULATION, AND

CHARACTERIZATION OF MACHINE-RECTIFIER SYSTEMS

There are many techniques for modeling and simulation of synchronous machine-rectifier systems. The more common approaches are the detailed and average-value modeling techniques. The detailed simulation technique takes into account the details of the diode switching and is both very accurate and very expensive in terms of computational resources. To alleviate this disadvantage, the average-value modeling technique is often utilized. In this approach, the details of diode switching are neglected or averaged. In that light, the work presented herein proposes a unique saliency-sensitive parametric average-value model (SSPAVM) of the synchronous machine-rectifier system. This model extends existing parametric average-value models to account for machine saliency by includng the angle of the machine's ac current as an input to the parameterized rectifier relationships. The performance of the proposed SSPAVM is compared with both detailed simulation and prior AVM in steady and transient state scenarios. The proposed SSPAVM more accurately predicts the detailed model waveforms in comparison to the existing AVM, while retaining the extensive computational cost savings associated with average-value models.

In addition, parametric average-value models (PAVMs) of synchronous machine-rectifier systems have proven to be very useful in studying the behavior of these systems. PAVMS are able to represent the system's dynamic characteristics in a computationally efficient manner. They require characterization using the detailed model simulation. Hence, to develop a PAVM of the synchronous machine-rectifier system, the essential parametric functions are extracted once from the detailed model of the system. Herein, it is shown that the rectifier parametric functions can be represented as functions of both the dynamic loading condition of the rectifier and the current angle of the synchronous machine's ac currents, and a method of extracting these two-dimensional relationships is proposed. It is also shown that previous PAVMs are unable to represent the rectifier parametric functions during transient events, particularly for more salient synchronous machines.

Furthermore, the characterization method is extended to a fast procedure, wherein instead of multiple steady state simulations with a single value of the load resistance

and machine's ac current angle at each simulation loop, the method adopted in this study involves a single transient exponential load increase for each current angle at each simulation loop. This multidimensional fast procedure greatly improves simulation times; and computational overhead associated with the multidimensional steady state approach.

Finally, an exact detailed model of the rectifier, in which all modes of operation/switching are accounted for is developed using stateflow-simulink hybrid state variable simulation environments. To achieve this, the exact differential equations with their appropriate state variable governing each state is utilized.

KEYWORDS: Average-value model, machines, rectifiers, salient, characterization,

    simulation

<div align="right">

_____
Isuje T. Ojo

_____
August 25, 2022

</div>

PARAMETRIC AVERAGE-VALUE MODELING, SIMULATION, AND CHARACTERIZATION OF MACHINE-RECTIFIER SYSTEMS

By

Isuje T. Ojo

Aaron M. Cramer

Director of Dissertation

Daniel Lau

Director of Graduate Studies

August 25, 2022

Date

I dedicate this work to Almighty God and my lovely family.

ACKNOWLEDGMENTS

Very important to the success of my research and dissertation is the very adept, intelligent, and timely contributions of my advisor, Dr. Aaron Cramer. Your technical expertise and scholarly depth have made my entire Ph.D. pursuit worthwhile. Thank you for your patience, calm demeanor and everything. My other Ph.D. dissertation committee members; Dr. Yuan Liao, Dr. Jiangbiao He, Dr. Joseph Sottile, and my outside examiner, Dr. Donald Colliver. Thank you all for agreeing to serve in your various capacities.

To my family; Dad & Mum; Mr & Mrs E.O. Ojo, My siblings; Isoiza K. Ojo, Oremeyi Ojo (of blessed memory), Alaba U. Ojo and Omeiza P. Ojo. Thanks for your support and prayers. My cousin; Victoria O. Oyannah, thanks for your support. My lovely and beautiful wife Ngozi J. Isuje-Ojo; your love, prayers and understanding are well appreciated. To my Uncles; Asishana B. Okauru and Nelson K. Adeloye; thank you for believing in me and committing your finances to my academic pursuit. My lab mates; Allen W. Flath III, you are the first lab mate I met and you helped with the initial MATLAB help I needed. Musharrat Sabah, and other members of the Power & Energy lab, thank you for being good colleagues.

To all my friends, thank you for being there for me throughout this journey.

TABLE OF CONTENTS

LIST OF TABLES

Chapter 1 Introduction

An important component of the electrical power system is the synchronous machine [2]. The power system may be described as a network of electrical components interconnected for the generation, transmission, and distribution of electrical energy to the consumer. In many electricity networks, the synchronous machine serves as a generator [3, 4]. The utilization of synchronous machines is paramount to the production of electricity and has accounted for almost all the electric power production world wide [1]. In addition, the synchronous generator can be driven by hydro, wind and steam turbines.

Modeling of the synchronous machine has been the subject of research and interest to many researchers (e.g. [5–18]). It is useful for understanding the power system, as many behaviors of the system may be predicated upon the behavior of the electromechanical devices connected to it. Furthermore, synchronous machine modeling and simulation is important for power system analysis, and it affords the engineer an insight into the complex workings of the system, as experiments may not be feasible on the real power network itself. In [5], a unified formulation approach wherein the synchronous machine model's magnetizing path saturation and rotor circuit are represented using linear networks is presented. The work in [6] proposes a model of the synchronous machine using a modified multiple reference frame theory. Various synchronous machine models and how they are implemented using EMT-type solvers is the major focus of [7]. The research works in [8–11] focuses on different aspects of the phase-domain approach of modeling the synchronous machine. The authors in [12] extends the voltage-behind reactance model of the synchronous machine by including magnetic saturation using the saliency-factor to the main-flux saturation. The voltage-behind reactance model was simulated on FPGA in [13] with an increased

speed compared to MATLAB simulations. Stability of the synchronous machine is the main idea in [14–16], and finally, the authors of [17] hints on the merits of the model of the synchronous machine in the direct time-phase domain over the model in the traditional $q - d$ axis domain.

According to [18], depending on the required fidelity and objective, the modeling approach for synchronous machines may be generally divided into three categories, namely finite element method [19], equivalent magnetic circuit approach [20, 21], and coupled electric circuit approach. The finite element analysis (FEA) model (e.g. [22–27]) is generally considered to be the most accurate model in comparison to its equivalent magnetic (for instance [28, 29]) and coupled electric circuits counterparts, but its simulation is time-consuming. Also, the FEA requires relatively large amount of machine parameters that make it impracticable for system analysts to do system-level studies. The equivalent magnetic circuit approach, even though it has faster simulation time and relatively fewer parameters than the FEA, yet contains more details than are required for studies like power system transients. Thus, the FEA and equivalent magnetic circuits approach are better suited for studying internal machine details early in the design stage. Therefore, in this work, the equivalent electric circuit approach, that is well suited for the simulation studies considered herein is utilized. The equivalent electric circuit approach comes originally in the phase-domain (PD) form, but it could also be in the quadrature and direct axes (qd) and voltage-behind-reactance (VBR) forms. The machine equations can be transformed from the PD form to the qd form using the Park's transformation. The advantage of this transformation is that the machine equations become rotor-position independent, hence time invariant, and the state variables become constant in the steady state. The VBR model tends to combine the advantages of both the PD and qd models, in that it is able to provide concurrent solution to the machine and network electrical variables and improves simulation efficiency and numerical accuracy [18].

2

The VBR model of the synchronous machine is also useful for interfacing electrical machine models with power electronics circuits e.g. rectifiers.

A rectifier is an electronic device which converts ac power to dc. This process happens with the aid of diodes in basic rectifiers. Many power electronic devices including the rectifier have become indispensable in systems requiring dc power, e.g. electric vehicles (EVs), battery charging, electric shipboard power systems, etc. Furthermore, synchronous machine-rectifiers are often utilized in the electrical subsystem of aircrafts, ships, electric vehicles (EVs) and in large generators' brushless excitation system. Rectifiers can be used to supply dc power in many applications. Modeling and simulation of synchronous machine-rectifier system can be achieved in various forms, using different techniques. The more common approaches are the detailed and average value modeling techniques. The detailed simulation technique takes into account the details of the diode switching and has proven to be very expensive in terms of computational resources. One of the causes of high computational expense is that accurate modeling of rectifier switching involves zero-crossing detection, and hence requires very small time steps. To alleviate this disadvantage, the average-value modeling (AVM) technique has since been developed. In this approach, the details of diode switching is neglected or averaged. In that light, one of the contributions presented herein is the development of a unique saliency-sensitive parametric average-value model (SSPAVM) of the synchronous machine-rectifier system. The proposed SSPAVM provides an extension to existing PAVMs by introducing the angle of machine's ac current of the synchronous machine to the parametric relationships. By so doing, the machine saliency is accounted for. The proposed SSPAVM's performance is compared with detailed model simulation and previous PAVMs in steady and transient state simulations, and results indicate that the proposed SSPAVM more accurately portrays the detailed model waveforms than the previous AVM, while maintaining comparable computational efficiency of existing average-value models. In

addition, the proposed AVM is valid in all rectifier operating modes, as in previous AVMs; for example [2].

In general, to implement the rectifier AVM, the essential numerical or parametric functions that represent the rectifier averaged behavior are initially extracted from the detailed simulation. Thus, another contribution presented is a method or procedure for systematically extracting the required relationships amongst the rectifier ac and dc variables using the detailed model of the synchronous machine-rectifier system. These essential numerical or parametric functions obtained from these two-dimensional parametric relationships are used in the development of the proposed SSPAVM. It is shown that these functions can be represented as a function of both the dynamic loading condition of the rectifier and the current angle of the machine's ac current. The idea is inspired from the observation that during transient events (with machine of high subtransient saliency), the dynamic impedance alone used in [30] and other works may not be sufficient to represent the system's operating conditions.

In addition, the characterization method is extended to a fast procedure, wherein instead of multiple steady state simulations with a single value of the load resistance and machine's ac current angle at each simulation loop, the method adopted in this study involves a single transient exponential load increase for each current angle at each simulation loop. This multidimensional fast procedure greatly improves simulation times; and computational overhead associated with the multidimensional steady state approach.

Finally, a detailed switched model of the rectifier, where all its modes operation/switching are accounted is developed using stateflow-simulink hybrid state variable simulation environments. To achieve this, the exact differential equations with the appropriate state variables governing each state is utilized.

The organization of the remaining part of this dissertation is as follows. Chap-

ter 2 provides the background to the studies herein, and the relevant literature reviews are presented. The saliency-sensitive parametric average-value model of synchronous machine-rectifier systems is developed and presented in Chapter 3. A discussion of a methodical approach by which the parametric functions required to develop this average-value model are extracted from the detailed model simulations represents the main idea of Chapter 4. A multidimentional fast procedure which can serve as an alternative approach for extracting these parametric functions is discussed exhaustively in Chapter 5. The exact detailed model of a rectifier using stateflow-simulink hybrid simulation environments (with results shown) is the focus of Chapter 6. Finally, this dissertation comes to a conclusion, with future ideas for research suggested in Chapter 7.

Relevant and Notable Nomenclature

q-axis – quadrature magnetic axis

d-axis – direct magnetic axis

r_s – Stator resistance

r'_{kq1} – Resistance of the $kq1$ rotor damper winding of the q-magnetic axis

r'_{kq2} – Resistance of the $kq2$ rotor damper winding of the q-magnetic axis

r'_{kd} – Resistance of the kd rotor damper winding of the d-magnetic axis

r'_{fd} – Resistance of the rotor field winding

v^r_{qs} – q-axis stator voltage in the rotor reference frame

v^r_{ds} – d-axis stator voltage in the rotor reference frame

v'_{qr} – q-axis rotor voltage

v'_{dr} – d-axis rotor voltage

i'_{qr} – q-axis rotor current

i'_{dr} – d-axis rotor current

i^r_{qs} – q-axis stator current in the rotor refrence frame

i^r_{ds} – d-axis stator current in the rotor refrence frame

i'^r_{kq1} – Current of the $kq1$ rotor damper winding of the q-magnetic axis

i'^r_{kq2} – Current of the $kq2$ rotor damper winding of the q-magnetic axis

i'^r_{kq2} – Current of the kd rotor damper winding of the d-magnetic axis

i'^r_{fd} – Current of the rotor field winding

λ^r_{qs} – q-axis stator flux linkage in the rotor reference frame

λ^r_{ds} – d-axis stator flux linkage in the rotor reference frame

λ_{qr} – q-axis rotor flux linkage

λ_{dr} – d-axis rotor flux linkage

λ'^r_{kq1} – Flux linkage of the $kq1$ rotor damper winding of the q-magnetic axis

λ'^r_{kq2} – Flux linkage of the $kq2$ rotor damper winding of the q-magnetic axis

$\lambda_{kd}^{\prime r}$ – Flux linkage of the kd rotor damper winding of the d-magnetic axis

$\lambda_{fd}^{\prime r}$ – Flux linkage of the rotor field winding

L_{mq} – Magnetizing inductance of the q-axis

L_{md} – Magnetizing inductance of the d-axis

L_{ls} – Stator leakage inductance

$L_{lkq1}^{\prime}$ – Leakage inductance of the $kq1$ rotor damper windings of the q-magnetic axis

$L_{lkq2}^{\prime}$ – Leakage inductance of the $kq2$ rotor damper windings of the q-magnetic axis

$L_{lkd}^{\prime}$ – Leakage inductance of the kd rotor damper windings of the d-magnetic axis

$L_{lfd}^{\prime}$ – Field winding leakage inductance

Others may be found in [1].

Chapter 2 Background and Literature Review

2.1 Preamble

Modeling and simulation of synchronous machine-rectifier systems have been studied extensively by researchers. The detailed simulation approach and AVM dominate the techniques used in research endeavors. This chapter provides background information about synchronous machines, rectifiers, and a literature review of past research in AVM of synchronous machine-rectifier systems.

2.2 Synchronous Machine

The synchronous machine is mainly involved with the conversion of mechanical energy to electrical energy. It consists of the rotor and stator, as the two principal construction parts. In the stator lies the three-phase armature windings that are 120 degrees displaced from each other and sinusoidally distributed. The rotor houses the field windings and may also carry one or more shorted damper windings. The rotor requires excitation by an external dc current source for a rotating magnetic field to be established. The rotor may be connected to the external dc source via brushes and slip rings. The magnetic field's strength is dependent on the applied dc current and it aligns with the field winding's axes. Furthermore, the rotor behaves as an electromagnet, and can as well be made from a permanent magnet. Such a synchronous machine is called a permanent magnet synchronous machine (PMSM). The magnetic poles of a synchronous machine can be non-salient or salient(field poles project outward or out of rotor core). Salient pole machines are mostly used for low speed applications, e.g. in machines coupled to hydroelectric turbines, while non-salient constructions are used for high speed applications, such as steam turbine generators. Furthermore,

the salient pole synchronous machine rotors are magnetically unsymmetrical. As a result of these rotor assymmetries, there's no benefit to rotor variable transformation. However, this is not the case with the stator. Hence, it is helpful for the stator variables to be transformed to the rotor reference frame using Park's transformation suitable for computer simulations.

2.3   Synchronous Machine Equations in the Phase Domain

A two-pole, 3-phase, wye connected, salient-pole synchronous machine is shown in Figure 2.1. The electromechanical and electrical behavior of most typical synchronous machines are well represented as being analogous to this arrangement. The windings of the stator are sinusoidally distributed and are displaced 120 degrees from each other. The stator windings' magnetic axes are depicted as as, bs and cs, with N_s equivalent turns and r_s equivalent resistance. The rotor houses a field winding and three damper windings, that are presumed to be sinusoidally distributed. The field windings' equivalent turns and resistance are denoted as N_{fd} and r_{fd} respectively. Specific to Figure 2.1, the magnetic axis of the field windings aligns with the magnetic axis of one of the damper windings, namely the kd damper windings. The kd winding has N_{kd} equivalent turns with r_{kd} resistance. The second $(kq1)$ and third $(kq2)$ damper windings have magnetic axes displaced 90 degrees ahead of the fd and kd windings. The $kq1$ winding has N_{kq1} equivalent turns with r_{kq1} resistance, while the $kq2$ winding has N_{kq2} equivalent turns with r_{kq2} resistance. The quadrature (or q-axis) is the magnetic axis of $kq1$ and $kq2$ windings while the direct axis (d-axis) is the magnetic axis of the fd and kd windings.

By modifying the equations below which describe the performance of the machine shown in Figure 2.1, nearly all synchronous machines' dynamic performance can be described for any number of winding. In addition, positive current into the machine terminals is assumed in the equations.
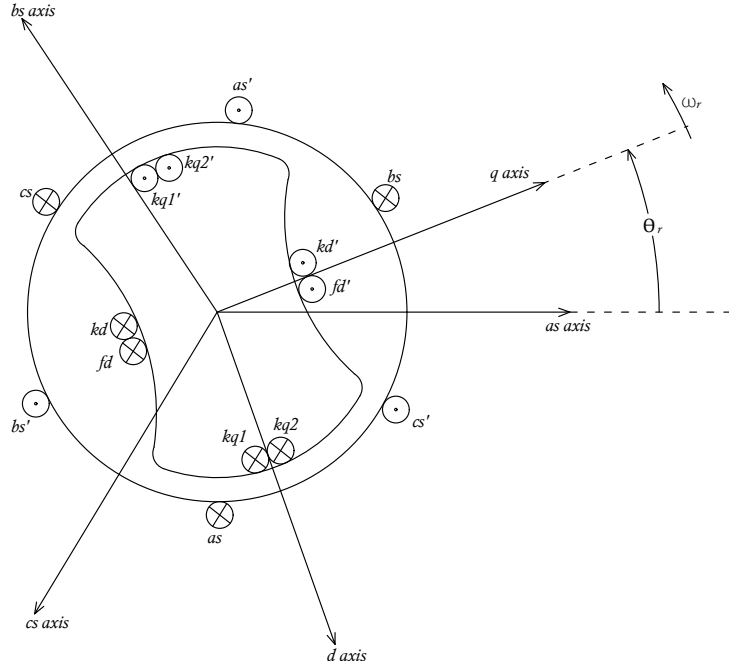
Figure 2.1: Two-pole, 3-phase, wye-connected, salient-pole synchronous machine [1]

The voltage equations in the machine variables may be written in the form of a matrix as

$$\mathbf{v}_{abcs} = \mathbf{r}_s \mathbf{i}_{abcs} + p\lambda_{abcs} \tag{2.1}$$

$$\mathbf{v}_{qdr} = \mathbf{r}_r \mathbf{i}_{qdr} + p\lambda_{qdr} \tag{2.2}$$

where p is a differential operator and

$$\mathbf{f}_{abcs} = \begin{bmatrix} f_{as} & f_{bs} & f_{cs} \end{bmatrix}^{\mathrm{T}} \tag{2.3}$$

$$\mathbf{f}_{qdr} = \begin{bmatrix} f_{kq1} & f_{kq2} & f_{fd} & f_{kd} \end{bmatrix}^{\mathrm{T}} \tag{2.4}$$

10

$$\mathbf{r}_s = \begin{bmatrix} r_s & & \\ & r_s & \\ & & r_s \end{bmatrix} \tag{2.5}$$

and

$$\mathbf{r}_r = \begin{bmatrix} r_{kq1} & & & \\ & r_{kq2} & & \\ & & r_{fd} & \\ & & & r_{kd} \end{bmatrix}. \tag{2.6}$$

The stator and rotor windings' variables are depicted with the subscripts s and r respectively, and $\mathbf{f}$ may be voltage ($\mathbf{v}$), current ($\mathbf{i}$) or flux linkage (λ), $\mathbf{r}_s$ is the resistance matrix of the stator windings, while $\mathbf{r}_r$ is the resistance matrix of the rotor windings. All stator phase windings of a synchronous machine are designed to have the same resistance.

A linear magnetic system's flux linkage can be expressed as:

$$\begin{bmatrix} \lambda_{abcs} \\ \lambda_{qdr} \end{bmatrix} = \begin{bmatrix} \mathbf{L}_s & \mathbf{L}_{sr} \\ \mathbf{L}_{sr}^T & \mathbf{L}_r \end{bmatrix} \begin{bmatrix} \mathbf{i}_{abcs} \\ \mathbf{i}_{qdr} \end{bmatrix} \tag{2.7}$$

where the stator inductance $\mathbf{L}_s$ is

$$\mathbf{L}_s = \begin{bmatrix} L_{ls} + L_A - L_B \cos 2\theta_r & -\frac{1}{2}L_A - L_B \cos 2(\theta_r - \frac{\pi}{3}) & -\frac{1}{2}L_A - L_B \cos 2(\theta_r + \frac{\pi}{3}) \\ -\frac{1}{2}L_A - L_B \cos 2(\theta_r - \frac{\pi}{3}) & L_{ls} + L_A - L_B \cos 2(\theta_r - \frac{2\pi}{3}) & -\frac{1}{2}L_A - L_B \cos 2(\theta_r + \pi) \\ -\frac{1}{2}L_A - L_B \cos 2(\theta_r + \frac{\pi}{3}) & -\frac{1}{2}L_A - L_B \cos 2(\theta_r + \pi) & L_{ls} + L_A - L_B \cos 2(\theta_r + \frac{2\pi}{3}) \end{bmatrix} \tag{2.8}$$

The self ($\mathbf{L}_r$) and mutual inductances ($\mathbf{L}_{sr}$) of the damper windings are expressed

11

as:

$$
\mathbf{L}_{sr} = \begin{bmatrix}
L_{skq1}\cos\theta_r & L_{skq2}\cos\theta_r & L_{sfd}\sin\theta_r & L_{skd}\sin\theta_r \\
L_{skq1}\cos(\theta_r - \frac{2\pi}{3}) & L_{skq2}(\theta_r - \frac{2\pi}{3}) & L_{sfd}\sin(\theta_r - \frac{2\pi}{3}) & L_{skd}\sin(\theta_r - \frac{2\pi}{3}) \\
L_{skq1}\cos(\theta_r + \frac{2\pi}{3}) & L_{skq2}(\theta_r + \frac{2\pi}{3}) & L_{sfd}\sin(\theta_r + \frac{2\pi}{3}) & L_{skd}\sin(\theta_r + \frac{2\pi}{3})
\end{bmatrix}
$$

$$(2.9)$$

and

$$
\mathbf{L}_r = \begin{bmatrix}
L_{lkq1} + L_{mkq1} & L_{kq1kq2} & 0 & 0 \\
L_{kq1kq2} & L_{lkq2} + L_{mkq2} & 0 & 0 \\
0 & 0 & L_{lfd} + L_{mfd} & L_{fdkd} \\
0 & 0 & L_{fdkd} & L_{lkd} + L_{mkd}
\end{bmatrix}
$$

$$(2.10)$$

In the same way that variables can be transformed across a transformer, the rotor variables transformed to the stator windings may be defined as follows:

$$
i'_j = \frac{2}{3}\left(\frac{N_j}{N_s}\right) i_j \tag{2.11}
$$

$$
v'_j = \frac{2}{3}\left(\frac{N_s}{N_j}\right) v_j \tag{2.12}
$$

$$
\lambda'_j = \frac{2}{3}\left(\frac{N_s}{N_j}\right) \lambda_j \tag{2.13}
$$

where j may be $kq1$, $kq2$, fd, or kd.

The flux linkage may now be written as

$$
\begin{bmatrix} \lambda_{abcs} \\ \lambda'_{qdr} \end{bmatrix} = \begin{bmatrix} \mathbf{L}_s & \mathbf{L}'_{sr} \\ \frac{2}{3}(\mathbf{L}'_{sr})^T & \mathbf{L}'_r \end{bmatrix} \begin{bmatrix} \mathbf{i}_{abcs} \\ \mathbf{i}'_{qdr} \end{bmatrix} \tag{2.14}
$$

where

$$\mathbf{L}'_{sr} = \begin{bmatrix} L_{mq}\cos\theta_r & L_{mq}\cos\theta_r & L_{md}\sin\theta_r & L_{md}\sin\theta_r \\ L_{mq}\cos\left(\theta_r - \frac{2\pi}{3}\right) & L_{mq}\cos\left(\theta_r - \frac{2\pi}{3}\right) & L_{md}\sin\left(\theta_r - \frac{2\pi}{3}\right) & L_{md}\sin\left(\theta_r - \frac{2\pi}{3}\right) \\ L_{mq}\cos\left(\theta_r + \frac{2\pi}{3}\right) & L_{mq}\cos\left(\theta_r + \frac{2\pi}{3}\right) & L_{md}\sin\left(\theta_r + \frac{2\pi}{3}\right) & L_{md}\sin\left(\theta_r + \frac{2\pi}{3}\right) \end{bmatrix}$$

$$(2.15)$$

$$\mathbf{L}'_r = \begin{bmatrix} L'_{lkq1} + L_{mq} & L_{mq} & 0 & 0 \\ L_{mq} & L'_{lkq2} + L_{mq} & 0 & 0 \\ 0 & 0 & L'_{lfd} + L_{md} & L_{md} \\ 0 & 0 & L_{md} & L'_{lkd} + L_{md} \end{bmatrix} \qquad (2.16)$$

where

$$L_{mq} = \frac{3}{2}(L_A - L_B) \qquad (2.17)$$

$$L_{md} = \frac{3}{2}(L_A + L_B) \qquad (2.18)$$

2.4   Reference Frame Variables

Some inductances of the machine are rotor position-dependent. This can be observed from the inductance equations expressed in Section 2.3. It therefore means that the differential equations' coefficients that depict the machine's behavior are a function of the rotor position. This causes these set of differential equations to be complex, hence the need for a change or transformation of variables. There exist several change of variables proposed by researchers like R.H. Park [31], H.C. Stanley [32], D.S. Brereton [33], G. Kron [34], etc. at different times. However, it was discovered by P.C Krause and C.H. Thomas [35] that each transformation is nearly a special case of a general variable transformation. With this general transformation, machine

variables are transformed to a reference frame that rotates at an arbitrary electrical angular velocity. Hence, this frame of reference is known as the arbitrary reference frame. Other known transformations can simply be achieved by assigning a rotation speed to the arbitrary reference frame. The commonly used reference frames are the arbitrary reference frame, stationary reference frame, rotor reference frame and synchronously rotating reference frames.

2.5 Park's Transformation, Rotor Reference Frame and Synchronous Machine Equivalent Circuit

A novel approach for the analysis of electrical machines was propounded by R.H. Park [31]. As hinted in Section 2.4, Park's transformation technique eliminates the rotor-position dependency of synchronous machine flux linkage equations. This technique helps to simplify electrical machine analysis. Specifically, Park's transformation transforms the stator winding variables to the rotor reference frame. The synchronous machine's rotor position-dependent inductances arise due to the relative motion and varying magnetic reluctance of the electric circuits. Therefore, Park's transformation eliminates the rotor-position dependency of the flux linkage equations, and the state variables of the machine equations become constant at steady state. The Park's equation are derived as follows:

$$\mathbf{v}_{qd0s}^r = \mathbf{r}_s \mathbf{i}_{qd0s}^r + \omega_r \lambda_{dqs}^r + p\lambda_{qd0s}^r \tag{2.19}$$

$$\mathbf{v}_{qdr}^{'} = \mathbf{r}_r^{'} \mathbf{i}_{qdr}^{'} + p\lambda_{qdr}^{'} \tag{2.20}$$

where

$$\lambda_{dqs}^r = \begin{bmatrix} \lambda_{ds}^r & -\lambda_{qs}^r & 0 \end{bmatrix}^{\mathrm{T}} \tag{2.21}$$

14

where from (2.7), the flux linkage equation in the rotor reference frame may be obtained as

$$
\begin{bmatrix} \lambda_{qd0s}^{r} \\ \lambda_{qdr}^{'} \end{bmatrix} = \begin{bmatrix} \mathbf{K}_{s}^{r}\mathbf{L}_{s}(\mathbf{K}_{s}^{r})^{-1} & \mathbf{K}_{s}^{r}\mathbf{L}_{sr}^{'} \\ \frac{2}{3}(\mathbf{L}_{sr}^{'})^{T}(\mathbf{K}_{s})^{-1} & \mathbf{L}_{r}^{'} \end{bmatrix} \begin{bmatrix} \mathbf{i}_{qd0s}^{r} \\ \mathbf{i}_{qdr}^{'} \end{bmatrix}
\tag{2.22}
$$

$$
\mathbf{K}_{s}^{r}\mathbf{L}_{s}(\mathbf{K}_{s}^{r})^{-1} = \begin{bmatrix} L_{ls} + L_{mq} & 0 & 0 \\ 0 & L_{ls} + L_{md} & 0 \\ 0 & 0 & L_{ls} \end{bmatrix}
\tag{2.23}
$$

$$
\mathbf{K}_{s}^{r}\mathbf{L}_{sr}^{'} = \begin{bmatrix} L_{mq} & L_{mq} & 0 & 0 \\ 0 & 0 & L_{md} & L_{md} \\ 0 & 0 & 0 & 0 \end{bmatrix}
\tag{2.24}
$$

$$
\frac{2}{3}(\mathbf{L}_{sr}^{'})^{T}(\mathbf{K}_{s}^{r})^{-1} = \begin{bmatrix} L_{mq} & 0 & 0 \\ L_{mq} & 0 & 0 \\ 0 & L_{md} & 0 \\ 0 & L_{md} & 0 \end{bmatrix}
\tag{2.25}
$$

It is observed that the machine's inductances become constant upon transformation.

The synchronous machine equivalent circuit is shown in Figure 2.2. It is worthy of note that superscript r indicates the rotor frame of reference.

Therefore, expanding equations (2.19) and (2.20), we get:

$$v_{qs}^r = r_s i_{qs}^r + \omega_r \lambda_{ds}^r + p\lambda_{qs}^r \tag{2.26}$$

$$v_{ds}^r = r_s i_{ds}^r - \omega_r \lambda_{qs}^r + p\lambda_{ds}^r \tag{2.27}$$

$$v_{0s} = r_s i_{0s}' + p\lambda_{0s} \tag{2.28}$$

$$v_{kq1}^{'r} = r_{kq1}' i_{kq1}^{'r} + p\lambda_{kq1}^{'r} \tag{2.29}$$

$$v_{kq2}^{'r} = r_{kq2}' i_{kq2}^{'r} + p\lambda_{kq2}^{'r} \tag{2.30}$$

$$v_{fd}^{'r} = r_{fd}' i_{fd}^{'r} + p\lambda_{fd}^{'r} \tag{2.31}$$

$$v_{kd}^{'r} = r_{kd}' i_{kd}^{'r} + p\lambda_{kd}^{'r} \tag{2.32}$$

Substituting (2.23)-(2.25) and (2.16) into (2.22), the flux linkage equations in expanded form may be expressed as follows:

$$\lambda_{qs}^r = L_{ls} i_{qs}^r + L_{mq}(i_{qs}^r + i_{kq1}^{'r} + i_{kq2}^{'r}) \tag{2.33}$$

$$\lambda_{ds}^r = L_{ls} i_{ds}^r + L_{md}(i_{ds}^r + i_{fd}^{'r} + i_{kd}^{'r}) \tag{2.34}$$

$$\lambda_{0s} = L_{ls} i_{0s} \tag{2.35}$$

$$\lambda_{kq1}^{'r} = L_{lkq1}' i_{kq1}^{'r} + L_{mq}(i_{qs}^r + i_{kq1}^{'r} + i_{kq2}^{'r}) \tag{2.36}$$

$$\lambda_{kq2}^{'r} = L_{lkq2}' i_{kq2}^{'r} + L_{mq}(i_{qs}^r + i_{kq1}^{'r} + i_{kq2}^{'r}) \tag{2.37}$$

$$\lambda_{fd}^{'r} = L_{lfd}' i_{fd}^{'r} + L_{md}(i_{ds}^r + i_{fd}^{'r} + i_{kd}^{'r}) \tag{2.38}$$

$$\lambda_{kd}^{'r} = L_{lkd}' i_{kd}^{'r} + L_{md}(i_{ds}^r + i_{fd}^{'r} + i_{kd}^{'r}) \tag{2.39}$$

2.6   Rectifier

A rectifier is a device that converts an ac signal to dc. It may undergo this process using diodes. Rectifiers and many other power converters could be thought of as a switch matrix and functions of switching [36]. Shown below in Figure 2.3 is an ac-dc

switch matrix converter capable of ac to dc rectification. Many of the discussions about rectifiers presented in this section are adapted from [36].

To avoid violating Kirchhoff voltage and current laws, the switch configuration is such that

$$q_{11} + q_{21} = 1 \tag{2.40}$$

$$q_{12} + q_{22} = 1 \tag{2.41}$$

If diodes replace these switches, the classical single phase rectifier circuit or rectifier bridge is obtained. The single phase rectifier bridge arrangement is shown in Figure 2.4.

When diode 1,1 and diode 2,2 are conducting (i.e. ON), $v_{out} = v_{in}$, and the arrangement for this condition is shown in Figure 2.5. Whereas when diodes 1,2 and 2,1 are conducting(i.e. ON), $v_{out} = -v_{in}$, and the arrangement for this condition is shown in Figure 2.6

Let

$$v_{in} = \sqrt{2}E \cos \omega t \tag{2.42}$$

where v_{rms} is the rms voltage, and for the interval $\frac{-\pi}{2} \leq \omega t \leq \frac{\pi}{2}$, the output voltage may be defined as follows:

$$v_{out} = v_{in} = \sqrt{2}v_{rms}cos\omega t \tag{2.43}$$

But for interval $\frac{\pi}{2} \leq \omega t \leq \frac{3\pi}{2}$,

17

$$v_{out} = -v_{in} = -\sqrt{2}v_{rms}\cos\omega t \tag{2.44}$$

For every one period of input voltage, two equal periods of output voltage is achieved. Therefore, the average output voltage may be expressed as:

$$\bar{v}_{out} = V_{d0} = \frac{1}{\pi}\int_{\frac{-\pi}{2}}^{\frac{\pi}{2}} \sqrt{2}v_{rms}\cos\omega t d(\omega t) = \frac{2}{\pi}(\sqrt{2}v_{rms}) \tag{2.45}$$

2.7 Three Phase Rectifiers

Three phase rectifier are commonly used for the conversion of ac power to dc power for heavy loads [37]. A balanced three-phase voltage source serves as the input to the diode rectifier shown in Figure 6.1. A three-phase diode rectifier is considered in this research. The rectifier is made up of three-phase diode bridge, with diodes D_1 to D_6 [38, 39].

As highlighted in [37], around any path of the circuit in Figure 6.1, the Kirchoff's voltage law indicates that only one diode per time may conduct at the top half of the bridge i.e D_1, D_3 or D_5. Same arguement goes for the bottom half of the bridge; in that only one diode (D_2, D_4 or D_6) may conduct at one time. Therefore, it is not practicable for D_1 and D_4 to conduct at the same time. Neither can D_3 and D_6 conduct simultaneously. In addition, D_2 and D_5 cannot undergoe simultaneous conduction.

2.8 Voltage Behind Reactance Formulation of Synchronous Machine Equations

Alternative synchronous machine model formulations are useful for special purposes. One of such purposes is in interfacing synchronous machine models with power electronic circuits, e.g. machine-converter systems. As noted in [1], reference frame theory can be utilized for the elimination of rotor-dependent inductances from the synchronous machines. It is difficult to apply a transformation to power electronic circuit models. Hence, coupling the qd model of the machine to the abc variable model of the power electronic circuit would require creation of a qd to abc interface.

A common alternative which is utilized herein, is the detailed physical variable voltage behind reactance (PVVBR) model formulation of the synchronous machine. This enables coupling of the synchronous machine to the power electronic circuit model (e.g. rectifier), and can be conveniently implemented in both state-variable-based solvers (e.g. MATLAB/Simulink, etc.) and electromagnetic transient programs (EMTP) e.g. PSCAD/EMTDC. The derivation of the PVVBR of the synchronous machine is described below.

The q- and d- axes magnetizing flux linkages for a machine with M damper windings in the q-axis and N damper windings in the d-axis for instance are defined as:

$$\lambda_{mq} = L_{mq}^{''} i_{qs}^{''} + \lambda_q^{''} \tag{2.46}$$

$$\lambda_{md} = L_{md}^{''} i_{ds}^{''} + \lambda_d^{''} \tag{2.47}$$

where the subtransient magnetizing inductances of the q- and d- axes are given in equations (2.48) and (2.49) respectively.

$$L''_{mq} = \left(\frac{1}{L_{mq}} + \sum_{j=1}^{M} \frac{1}{L_{lkqj}} \right)^{-1} \tag{2.48}$$

$$L''_{md} = \left(\frac{1}{L_{md}} + \frac{1}{L_{lfd}} + \sum_{j=1}^{N} \frac{1}{L_{lkdj}} \right)^{-1}. \tag{2.49}$$

The subtransient dynamic flux linkages in the q- and d-axes may be expressed in equations (2.50) and (2.51) respectively.

$$\lambda''_q = L''_{mq} \left(\sum_{j=1}^{M} \frac{\lambda_{kqj}}{L_{lkqj}} \right) \tag{2.50}$$

$$\lambda''_d = L''_{md} \left(\frac{\lambda_{fd}}{L_{lfd}} + \sum_{j=1}^{N} \frac{\lambda_{kdj}}{L_{lkdj}} \right) \tag{2.51}$$

The voltage equations of the stator are then derived as:

$$v^r_{qs} = r''_q i^r_{qs} + \omega_r L''_d i^r_{ds} + p L''_q i^r_{qs} + e''_q \tag{2.52}$$

$$v^r_{ds} = r''_d i^r_{ds} - \omega_r L''_q i^r_{qs} + p L''_d i^r_{ds} + e''_d \tag{2.53}$$

where

$$r''_q = r_s + L''^2_{mq} \left(\sum_{j=1}^{M} \frac{r_{kqj}}{L^2_{lkqj}} \right) \tag{2.54}$$

$$r''_d = r_s + L''^2_{md} \frac{r_{fd}}{L^2_{lfd}} + L''^2_{md} \left(\sum_{j=1}^{M} \frac{r_{kdj}}{L^2_{lkdj}} \right). \tag{2.55}$$

The subtransient voltages e''_q and e'''_d which represents the effects of the rotor

circuits:

$$e_q'' = \omega_r \lambda_d'' + \sum_{j=1}^{M} \left(\frac{L_{mq}'' r_{kqj}}{L_{lkqj}^2} \left(\lambda_q'' - \lambda_{kqj} \right) \right) \tag{2.56}$$

$$e_d'' = -\omega_r \lambda_q'' + \sum_{j=1}^{N} \left(\frac{L_{md}'' r_{kdj}}{L_{lkdj}^2} \left(\lambda_d'' - \lambda_{kdj} \right) \right) + \frac{L_{md}''}{L_{lfd}} v_{fd} + \frac{L_{md}'' r_{fd}}{L_{lfd}^2} \left(\lambda_d'' - \lambda_{fd} \right) \tag{2.57}$$

with

$$p\lambda_{kqj} = -\frac{r_{kqj}}{L_{lkqj}} \left(\lambda_{kqj} - \lambda_{mq} \right) \tag{2.58}$$

$$p\lambda_{kdj} = -\frac{r_{kdj}}{L_{lkdj}} \left(\lambda_{kdj} - \lambda_{md} \right) \tag{2.59}$$

$$p\lambda_{fd} = -\frac{r_{fd}}{L_{lfd}} \left(\lambda_{fd} - \lambda_{md} \right) + v_{fd}. \tag{2.60}$$

The equations (2.46)-(2.60) represent the VBR formulations used herein to implement the detailed model of the synchronous machine connected to the three phase rectifier model.

2.9 Literature Review

Features such as simplicity, low cost, and high efficiency explain the popularity of line commutated rectifiers (e.g. diode rectifiers) in many applications [40]. Particularly, synchronous machine-rectifier systems are found in such applications as brushless excitation of synchronous generators [41, 42], shipboard power systems [43–49], aircraft power systems [50, 51], HVDC transmission [52], and in the electrical subsystem of electric vehicles [2]. Furthermore, the high penetration of power electronic-based devices due to renewable energy integration into the traditional power grid will continue to involve the use of line commutated converters/rectifiers [40].

Efficient and accurate models of machine-rectifier systems are of utmost importance, as the simulation studies for the aforementioned applications may involve con-

sideration of many design alternatives (i.e., different parameter sets), long simulation run times, and systems with many machines and high complexity (e.g. [53,54]). Furthermore, prior to a system's physical implementation, modeling and simulation can be useful in analyzing and studying the system's performance, predicting its behavior and response during transient and steady state scenarios. This procedure is also applicable post-hardware implementation, in a process referred to as digital twin; commonly employed in many industries, e.g. automotive, utility, etc.

Different techniques and approaches exist for the modeling and simulation of synchronous machine-rectifier systems, and simulations can be performed in either state-variable-based (e.g. MATLAB/Simulink [55], PLECS [56], SimPowerSystems [57]) or nodal-analysis-based environments (e.g. PSCAD/EMTDC [58], MicroTran [59]). The conventional detailed model approach is able to represent the details of each diode's repeated switching, providing very accurate waveform predictions [60]. However, the downside of this approach is its long simulation run times and significant computational expense: accurate modeling of the switching events involves explicit zero-crossing detection [61] and time-step adjustment [62], thereby requiring relatively small simulation time steps. Thus, the detailed switching models may not be desirable in situations where multiple simulations are required for design evaluation and optimization purposes and for systems with many components [63]. Likewise, detailed switching models are not as useful for tasks based on operating point linearization like control design because the waveforms continue to switch in steady state.

To overcome these challenges, the development of the AVM became a necessity. According to [61] and [64], the AVM helps to reduce the computational cost of detailed model by avoiding or averaging fast switching effects over an interval of switching. There are two broad categories under which the rectifier AVMs are classified: analytical and parametric. The analytical AVM (AAVM) method (e.g., [41,65–71]) provides

a technique in which the rectifier ac and dc variables relations are obtained analytically and based on certain assumptions. For instance, initial AAVM approaches are predicated upon the presumption of a consistent commutating reactance and idealized ac system [65,66]. The work in [68] established the synchronous machine's d-axis subtransient reactance as the effective ac commutating reactance. This approach is improved upon in [69], wherein the ac commutating reactance is determined as a function of d- and q-axes reactances and the firing angle of the converter. Generally, AAVMs are most useful in limited operating modes of the rectifier (i.e., those corresponding with the analysis used to establish the model) and can require implicit solutions to nonlinear equations to achieve high accuracy, adversely affecting computational efficiency [30].

The numerical or parametric average-value model (PAVM) (e.g., [2, 40, 72–79]) provides an alternative to the AAVM. It affords the simplicity of AVMs by utilizing numerical solutions directly in the development stage of the PAVM by incorporating the results of simulation of a detailed switching model to determine the parameters of the PAVM. Early work in this area [72] represented the rectifier averaged behavior using parameters that are constant and independent of the dynamic operating conditions of the system. Later it was proposed that the model would be more accurate by using dynamic parameters varying with respect to the loading conditions [2]. The PAVM has been extended in various ways. For instance, the concept was explored in the modeling of line-commutated/thyristor-controlled rectifiers in [40, 75, 80], resulting in parametric relations that are functions of multiple variables. The fundamental approach of PAVMs is the same: the PAVM is based on establishing the rectifier ac and dc variable relationships by averaging the results of detailed simulations.

Anecdotally, it has been observed that there are situations in which PAVMs yield less accurate results despite their widely successfully use. Specifically, situations in which machines with significant subtransient saliency experience highly dynamic

loading were observed to result in lower accuracy. In [69,81], it is found that subtransient saliency can influence the behavior of synchronous machine-rectifier systems. In [2], the parametric relationships are based on loading condition, but this does not appear to be sufficient in all situations. Therefore, a saliency-sensitive parametric average-value model (SSPAVM) of the synchronous machine-rectifier system is proposed herein. The proposed SSPAVM is based on both the loading condition (as in [2]) and the instantaneous operating angle of the machine, which can result in differences when there is deviation from the steady-state operating angle for a given loading condition.

An important step in the development of the PAVM is the establishment of the nonlinear numerical or algebraic functions required to represent the rectifier behavior. These functions are extracted from the detailed model simulation. In doing so, the authors in [72], established a PAVM using a set of fixed coefficients obtained from the detailed model's steady-state solutions. The results from this model are shown to be inaccurate in certain simulation scenarios studied in [2]. Therein, multiple steady-state simulations were used in extracting the rectifier numerical functions, and it was also established that these nonlinear parametric functions are dependent upon the loading condition of the system. An alternative "fast procedure" was proposed for extracting these relationships in [30]. Therein, a transient simulation study which involved an exponential increase in the rectifier dc load was employed for obtaining the model parameters required to develop the PAVM. The authors therein indicate that this scenario is able to span or cover the various rectifier operational modes. Various other characterization techniques have been used for PAVMs, including approaches based on nested loops.
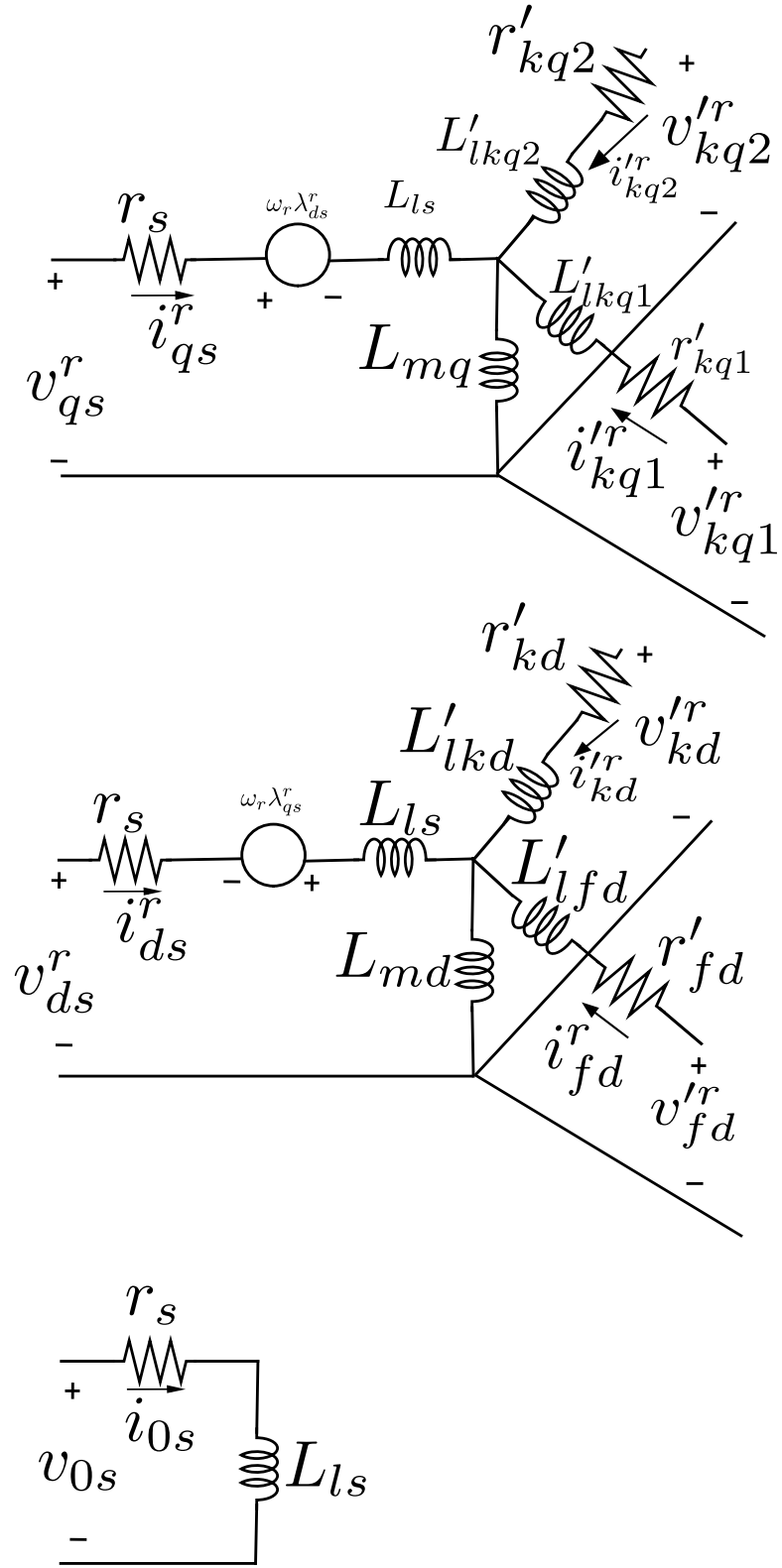
Figure 2.2: Three-phase synchronous machine equivalent circuit in the rotor reference frame [1]
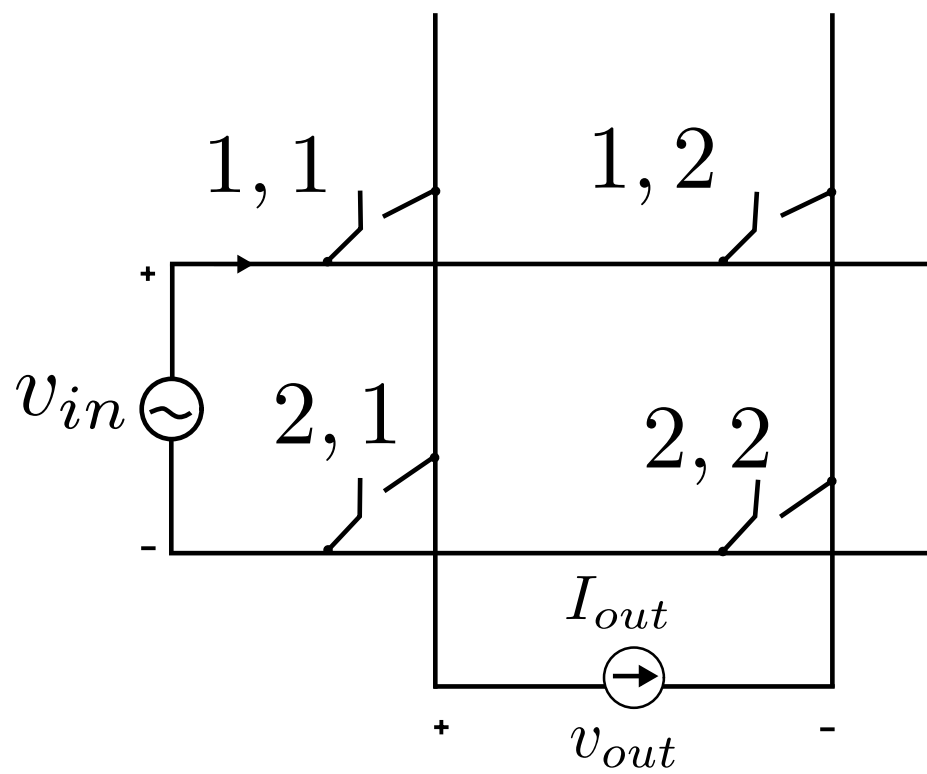
Figure 2.3: AC-DC switch matrix converter
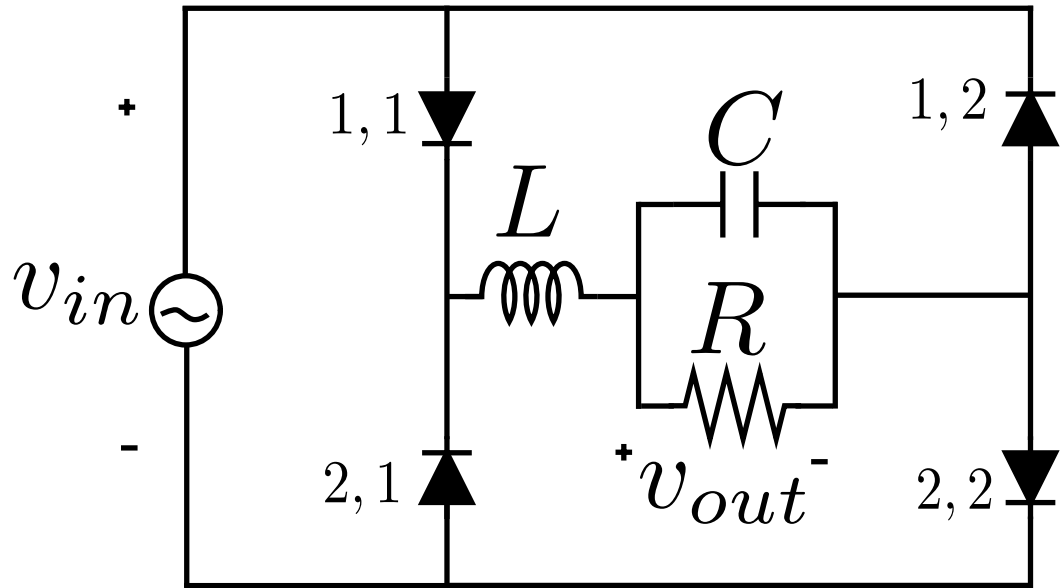
Figure 2.4: A simple rectifier bridge
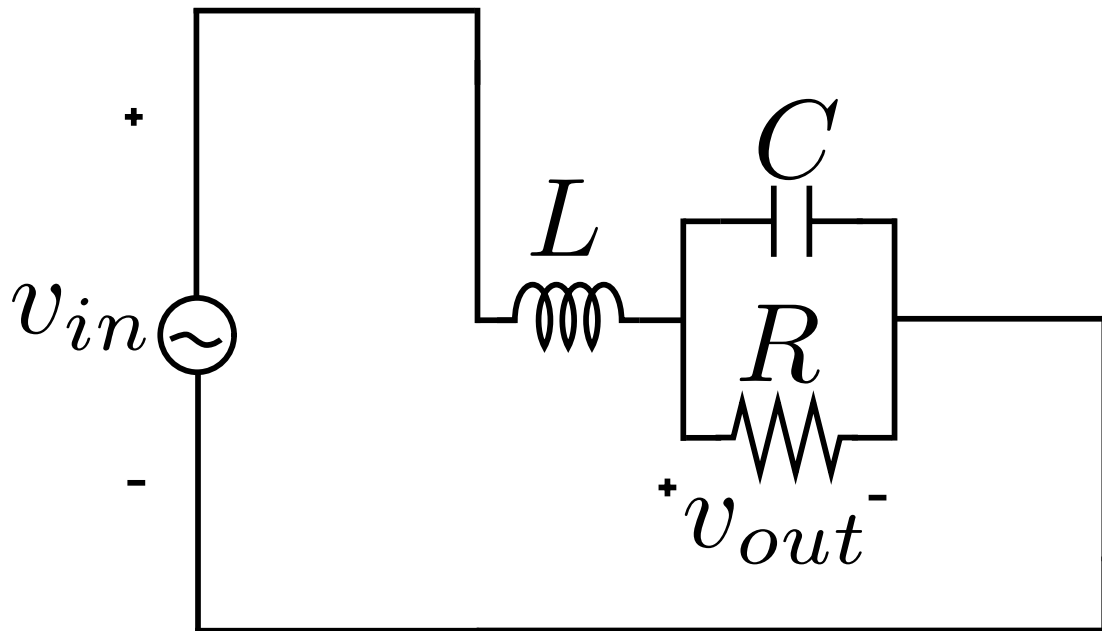
Figure 2.5: Conduction configuration for diodes 1,1 and 2,2 conducting
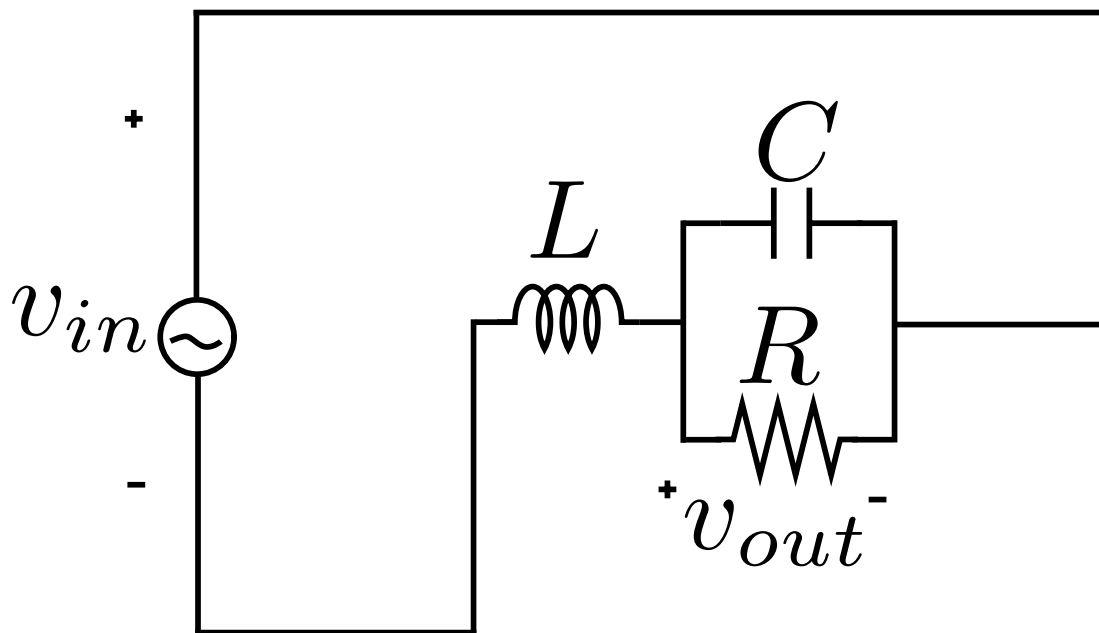
Figure 2.6: Conduction configuration for diodes 1,2 and 2,1 conducting

Chapter 3 Parametric Average-Value Modeling of Salient Machine-Rectifier Systems

3.1 Preamble

There are many techniques for modeling and simulation of synchronous machine-rectifier systems. The more common approaches are the detailed and average-value modeling techniques. The detailed simulation technique takes into account the details of the diode switching and is both very accurate and very expensive in terms of computational resources. To alleviate this disadvantage, the average-value modeling technique is often utilized. In this approach, the details of diode switching are neglected or averaged. In that light, the work presented herein explores a unique saliency-sensitive parametric average-value model (SSPAVM) of the synchronous machine-rectifier system. This model extends existing parametric average-value models to include the angle of the current as an input to the parameterized rectifier relationships. The performance of the proposed SSPAVM is compared with both detailed simulation and prior AVM in steady and transient state scenarios. The proposed SSPAVM more accurately predicts the detailed model waveforms in comparison to the existing AVM, while retaining the extensive computational cost savings associated with average-value models. The procedure for obtaining the essential parametric functions required to develop the proposed SSPAVM is presented in Chapter 4.

The main contributions of this chapter are:

1. Establishing a two-dimensional SSPAVM of synchronous machine-rectifier systems, utilizing the rectifier dynamic impedance and the current angle as the inputs to the model's parametric relationships.

2. Validating the proposed SSPAVM against a detailed switching model and com-

paring with the previous PAVM.

3. Demonstrating that the proposed SSPAVM can provide significant accuracy improvements with respect to the previous PAVM while retaining comparable computational efficiency.

The remainder of this chapter is organised as follows. Section 3.2 explains the general concepts of PAVMs and establishes the proposed SSPAVM. A variety of simulation studies for two different systems are presented for model validation in Section 3.3. This chapter is based on [82]. Preprints are also available on TechRxiv [83].

3.2 Parametric Average-Value Models of Machine-Rectifier Systems

All AVMs are fundamentally based upon the assumption that all the ac and dc variables may be replaced by their fast averages over a protypical switching interval (when the ac variables are transformed to a suitable reference frame). However, PAVMs are further based on the approximation that the relationship between averaged ac and dc voltages and currents can be represented using functions that are parametrized based on operating conditions. The notational conventions used herein are described in Subsection 3.2.1.

3.2.1 Notation

Vectors and matrices are in bold font. The stator variables of the synchronous machine are expressed as $\mathbf{f}_{abcs} = \begin{bmatrix} f_{as} & f_{bs} & f_{cs} \end{bmatrix}^{\mathrm{T}}$, where f may represent current i or voltage v. The stator variables may then be transformed to the rotor reference frame as

$$\mathbf{f}_{qd0s} = \mathbf{K}_s \mathbf{f}_{abcs}, \tag{3.1}$$

where

$$\mathbf{K}_s = \frac{2}{3} \begin{bmatrix} \cos\theta_r & \cos\left(\theta_r - \frac{2\pi}{3}\right) & \cos\left(\theta_r + \frac{2\pi}{3}\right) \\ \sin\theta_r & \sin\left(\theta_r - \frac{2\pi}{3}\right) & \sin\left(\theta_r + \frac{2\pi}{3}\right) \\ \frac{1}{2} & \frac{1}{2} & \frac{1}{2} \end{bmatrix} \tag{3.2}$$

and $\mathbf{f}_{qd0s} = \begin{bmatrix} f_{qs} & f_{ds} & f_{0s} \end{bmatrix}^T$ are the q- and d-axis and zero-sequence components of the three-phase variable, respectively. Herein, the zero-sequence component is always equal to zero. Using the space phasor notation employed herein $\vec{f} = f_{qs} - jf_{ds}$.

The mathematical relationship between the electrical angular velocity ω_r and the mechanical angular velocity ω_{rm} of the machine is defined as

$$\omega_r = \frac{P}{2}\omega_{rm}, \tag{3.3}$$

where P is the number of magnetic poles of the machine. Likewise, the electrical angular position θ_r is related to the mechanical angular position θ_{rm} of the machine:

$$\theta_r = \frac{P}{2}\theta_{rm}. \tag{3.4}$$

3.2.2 Parametric Average-Value Model Rectifier Relationships

In the previous PAVM established in [2], the behavior of the rectifier shown in Figure 3.1 is described using the following relationships:

$$|\vec{v}| = \alpha(\cdot)v_{dc} \tag{3.5}$$

$$i_{dc} = \beta(\cdot)|\vec{i}| \tag{3.6}$$

$$\angle\vec{v} = \angle\vec{i} + \phi(\cdot) + \pi, \tag{3.7}$$

where the space phasor form of the synchronous machine stator voltages and currents in the rotor reference frame are $\vec{v}$ and $\vec{i}$, respectively. The numerical functions are
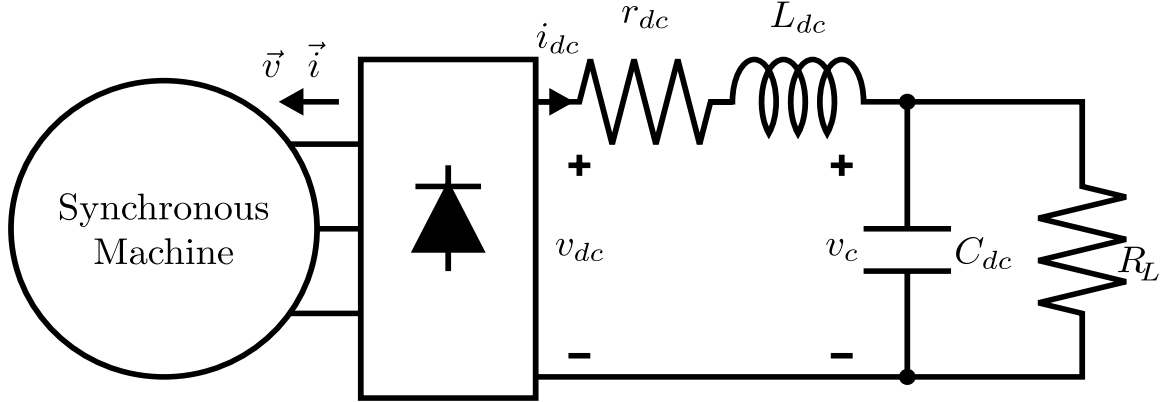
Figure 3.1: Machine-rectifier system

$\alpha(\cdot)$, $\beta(\cdot)$ and $\phi(\cdot)$, and the phase offset π is a consequence of positive current $\vec{i}$ into the synchronous machine. In [2], the numerical functions are characterized by a "convenient" dynamic impedance z, described mathematically as

$$z = \frac{v_c}{|\vec{i}|}, \tag{3.8}$$

where v_c is the LC filter's capacitor voltage. Because v_c is a natural state variable, z can be used for this purpose without introducing an algebraic loop in state-variable-based simulation environments.

3.2.3 Parametric Average-Value Model Formulation

Models of the synchronous machine on the ac side and the LC filter on the dc side have a natural voltage-in, current-out formulation, where the input of each of these models is voltage and the output is current. This would require a formulation of the rectifier model where the input is currents and the output is voltages, a formulation proposed in [77], but it has also been shown that such formulations can create numerical stiffness in certain situations [84]. A practical approximation is introduced in [2] that transforms the LC filter dynamics into a proper state model with a current-in, voltage-out formulation. In this approximation, which is used herein, the dc voltage

is approximated as

$$v_{dc} = v_c + r_{dc}i_{dc} + L_{dc}\frac{d\hat{i}_{dc}}{dt} \tag{3.9}$$

where

$$\frac{d\hat{i}_{dc}}{dt} = \frac{i_{dc} - \hat{i}_{dc}}{\tau} \tag{3.10}$$

and τ is a time constant that is small relative to the switching frequency. The capacitor voltage is a state variable modeled using

$$\frac{dv_c}{dt} = \frac{i_{dc} - v_c/R_L}{C_{dc}}. \tag{3.11}$$

The dynamics of the synchronous machine can be expressed in the rotor reference frame using a standard model [1].

3.2.4 Saliency-Sensitive Parametric Average-Value Model Rectifier Relationships

The fundamental contribution of this work is that the rectifier numerical functions α, β, and ϕ are functions of the dynamic impedance z and the angle of the ac current $\angle\vec{i}$. This is based on the observation that during transient events with machines with high substransient saliency, the dynamic impedance alone is insufficient to represent the operating condition of the system as demonstrated herein. Therefore, the proposed SSPAVM represents the rectifier relationships as follows:

$$|\vec{v}| = \alpha(z, \angle\vec{i})v_{dc} \tag{3.12}$$

$$i_{dc} = \beta(z, \angle\vec{i})|\vec{i}| \tag{3.13}$$

$$\angle\vec{v} = \angle\vec{i} + \phi(z, \angle\vec{i}) + \pi. \tag{3.14}$$

Hence, the previous PAVM of the synchronous machine-rectifier system in [2] is modified herein such that z and $\angle\vec{i}$ serve as lookup tables' input, forming the proposed

SSPAVM.

3.2.5 Saliency-Sensitive Parametric Average-Value Model Summary

The SSPAVM is sumarized in Figure 3.2. Specifically, the dc model provides access to the capacitor voltage v_c as a state variable and the synchronous machine model provides the stator currents (while not state variables, they can be calculated independently of the rectifier's behavior). These values are used to calculate the dynamic impedance z and the current angle $\angle \vec{i}$. Using two-dimensional lookup tables, the values of $\alpha(\cdot)$, $\beta(\cdot)$, and $\phi(\cdot)$ are calculated. These values are used with (3.12)–(3.14) to determine $\vec{v}$ and i_{dc}. The dc voltage v_{dc} is calculated from the model of the dc system as modified using (3.9)–(3.10).

3.3 Simulation Studies

In this section, the proposed SSPAVM is validated using the detailed switching model and compared with a previous PAVM formulation. A voltage-behind-reactance formulation of the machine (e.g., [1]) and the detailed representation of the rectifier are employed in the detailed model simulations, whereas the standard formulation in the rotor reference frame is used with both the previous PAVM and the proposed SSPAVM. For both PAVM models, the approximation of the inductor current derivative described in (3.9)–(3.10) is used to transform the LC filter into a current-in, voltage-out formulation, and the value $\tau = 10$ µs is used herein, as in [2]. All simulations are performed in MATLAB R2021b Simulink with the following settings: ode23tb algorithm, relative tolerance of 10^{-4}, maximum step size of 0.02 s, and absolute tolerance set to its default value. The detailed switching model of the rectifier is implemented using Stateflow. For both detailed switched model and both PAVMs, the field voltage and the initial state variables are initially zero. The machine rotates at constant rated speed. The excitation voltage is linearly ramped over 1 s from zero
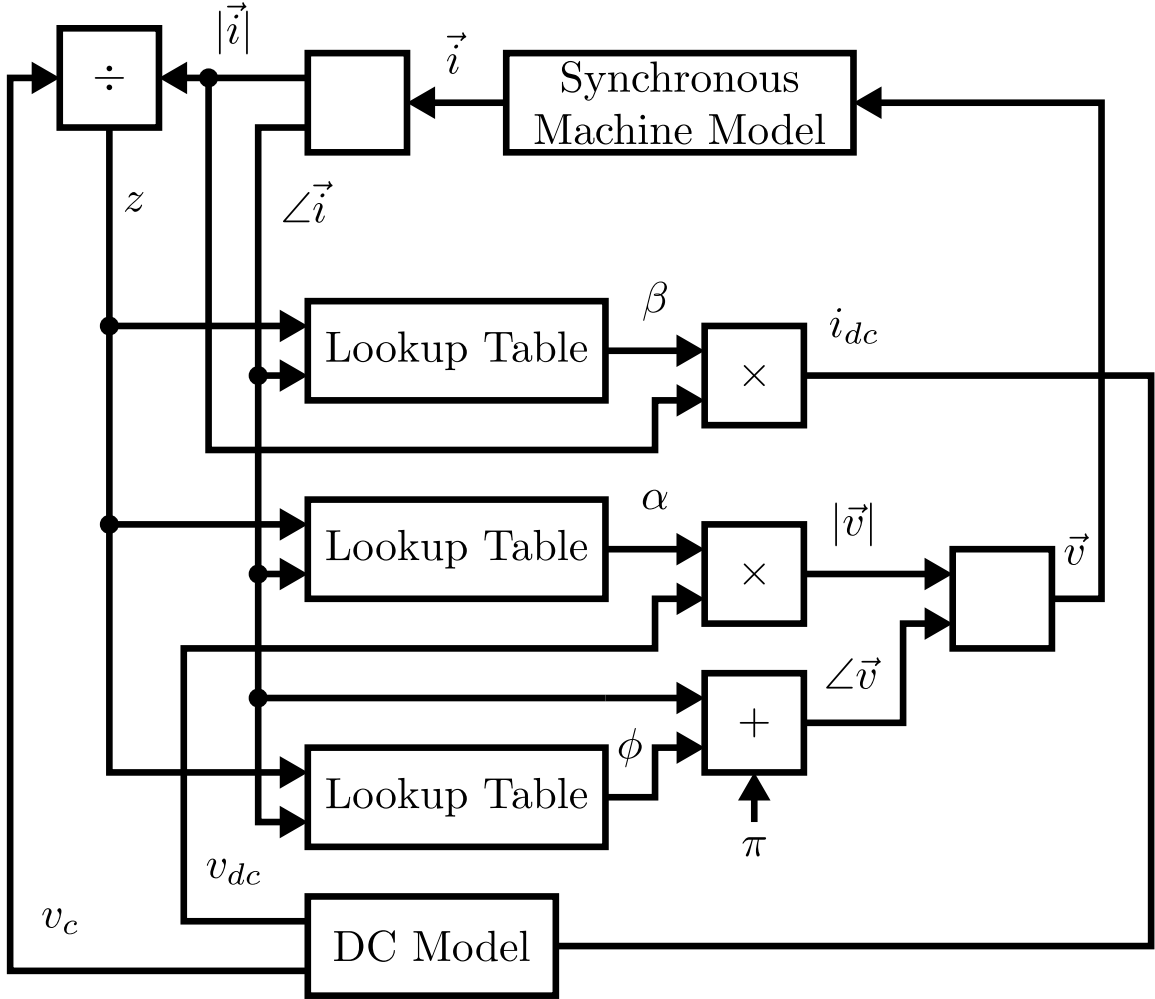
Figure 3.2: Summary of model formulation

to a value which under open circuit conditions, would yield machine rated voltage. The models are then further simulated for 8 s to attain steady state. Simulation results for the last 2 s (120 cycles) are obtained, with a transient event happening at 1 s. The lookup tables in the PAVM models are implemented using cubic spline interpolation with clipping for values outside of the support points. All simulations are performed using an Intel(R) Core(TM) i7-8750H CPU (2.20GHz and 16 GB of RAM). The average values of the waveforms associated with the detailed model are calculated as described below in Subsection 3.3.1.

3.3.1 Averaging of Detailed Model Waveforms

The waveforms of the detailed model are averaged as follows. The simulation period is divided into intervals corresponding to the period of the rectifier switching period (1/360 s). At the boundaries of each interval, a boundary point is established using linear interpolation. Within each interval, the average value of each waveform is calculated using trapezoidal rule numerical integration. The calculated average value is used to represent the average of the detailed model within that interval, and the average of the detailed model is piecewise constant within each interval. This process is used to compare the results of the detailed model with the results of the AVMs and is shown in Figure 3.3.
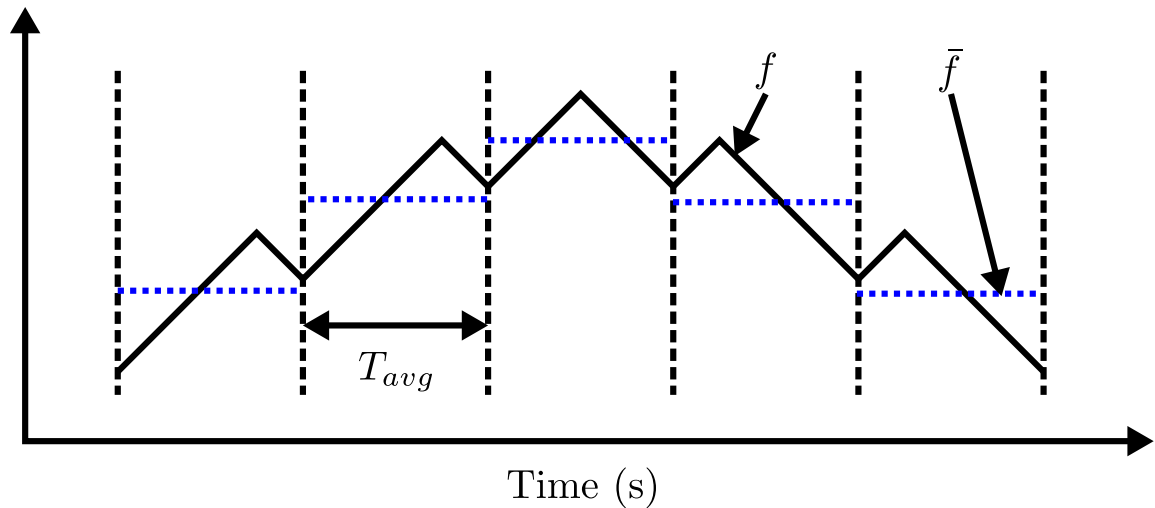
Figure 3.3: Method of averaging detailed model waveforms

3.3.2 Base Machine and Rectifier with Step Load

In the first series of studies, a base machine (selected to correspond with that studied in [2] to facilitate comparison) is simulated with a representative rectifier and LC filter. The parameters of this system are given in Table 3.2. Each of these studies involves stepping the dc load resistance to observe the transient response to these load

changes. The synchronous machine field winding is excited by a voltage of 1.42 V (referred), the value that would produce rated terminal voltage if the machine were unloaded. The five step load changes considered are shown in Table 3.1 and are selected to represent a wide range of changes in operating condition.

Table 3.1: Accuracy Improvement of Proposed SSPAVM over Previous PAVM for Base Machine and Rectifier With Step Load

Step Load	Variable	Improvement (%)
30 Ω to 10 Ω	v_{qs}^r	0.64
	v_{ds}^r	1.57
	i_{qs}^r	0.06
	i_{ds}^r	3.97
	v_{dc}	4.36
	i_{dc}	2.35
10 Ω to 30 Ω	v_{qs}^r	-0.72
	v_{ds}^r	5.67
	i_{qs}^r	2.05
	i_{ds}^r	2.63
	v_{dc}	10.47
	i_{dc}	2.97
15 Ω to 30 Ω	v_{qs}^r	4.13
	v_{ds}^r	10.02
	i_{qs}^r	2.84
	i_{ds}^r	2.85
	v_{dc}	14.28
	i_{dc}	3.63
15 Ω to 45 Ω	v_{qs}^r	3.13
	v_{ds}^r	8.03
	i_{qs}^r	2.02
	i_{ds}^r	1.33
	v_{dc}	11.44
	i_{dc}	2.08
15 Ω to 60 Ω	v_{qs}^r	2.72
	v_{ds}^r	6.33
	i_{qs}^r	1.44
	i_{ds}^r	0.80
	v_{dc}	8.20
	i_{dc}	1.41

For each of the simulations, the step load occurs at 1 s. The rms errors with respect to the average values of the waveforms from the detailed model during the

0.1 s following the step are calculated for the stator voltages v_{qs}^r and v_{ds}^r and currents i_{qs}^r and i_{ds}^r in the rotor reference frame and the dc voltage v_{dc} and current i_{dc}, and the reduction in error of the proposed SSPAVM relative to the previous PAVM in predicting the detailed model waveform is shown in Table 3.1.

Generally, there was close agreement of the waveforms over the simulation period. However, on zooming into the waveforms during the period immediately following the step change, certain differences become more apparent. Representative examples of these differences are shown in Figure 3.4 and Figure 3.5. In these figures, which are associated with a step increase in load and a step decrease, respectively, deviations between the previous PAVM and the detailed model can be observed, while the proposed SSPAVM follows the detailed model more accurately during the transient. The ultimate result of these differences is that the proposed SSPAVM demonstrates meaningful improvements in accuracy in nearly all cases and waveforms, with the only exception being the q-axis voltage during the 10-30 Ω step, where both models had comparably small errors.

3.3.3   System Parameters

The base synchronous machine studied herein is that described in [2], which facilitates comparison between models. It is a 5-hp, 60-Hz, 230-V machine with parameters given in Table 3.2.

A representative dc link filter with parameters $r_{dc} = 0.32$ Ω, $L_{dc} = 1.19$ mH, and $C_{dc} = 4.9$ mF is studied.

3.3.4   Salient Machine and Rectifier with Step Load

To obtain a more salient machine, the base machine (which is also salient) is modified by replacing the q-axis damper circuits with a single damper circuit with $L_{lkq1}^{'} = 15$ mH and $r_{kq1}^{'} = 1$ Ω. As before, an excitation voltage of 1.42 V (referred) is used

Table 3.2: Base Synchronous Machine Parameters

$\omega_b = 2\pi 60$ rad/s	$P = 4$
$r_s = 0.382$ Ω	$L_{ls} = 1.1$ mH
$L_{mq} = 24.9$ mH	$L_{md} = 39.3$ mH
$r'_{kq1} = 5.07$ Ω	$L'_{lkq1} = 3.5$ mH
$r'_{kq2} = 1.06$ Ω	$L'_{lkq2} = 3.5$ mH
$r'_{kq3} = 0.447$ Ω	$L'_{lkq3} = 26.2$ mH
$r'_{kd1} = 140$ Ω	$L'_{lkd1} = 9.9$ mH
$r'_{kd2} = 1.19$ Ω	$L'_{lkd2} = 4.9$ mH
$r'_{kd3} = 1.58$ Ω	$L'_{lkd3} = 4.5$ mH
$r'_{fd} = 0.112$ Ω	$L'_{lfd} = 1.5$ mH

for exciting the field winding of the salient synchronous machine, which produces rated machine voltage at no-load conditions.

To further validate the proposed SSPAVM, the series of studies (step load changes) performed in Subsection 3.3.2 are repeated for the salient synchronous machine-rectifier system. Representative results from these transient simulation scenarios, in the period immediately following the transition, are shown in Figure 3.6 and Figure 3.7. These zoomed-in figures indicate that the proposed SSPAVM's waveforms more accurately predict the detailed model's waveforms, in comparison with the previous PAVM's waveforms. While such differences were observed with the base machine system, they are more pronounced for the salient machine system.

In addition, the rms error is determined in the same manner as described in Subsection 3.3.2 to ascertain each AVM's accuracy in approximating the detailed model's waveform. As seen in the figures, it is notable that the proposed SSPAVM exhibits an even higher model accuracy with the salient synchronous machine as seen in Section 3.3 than it did with the base synchronous machine considered in Subsection 3.3.2 (and shown in Table 3.1). Both the waveforms and error calculations confirm the saliency sensitivity of the proposed SSPAVM.
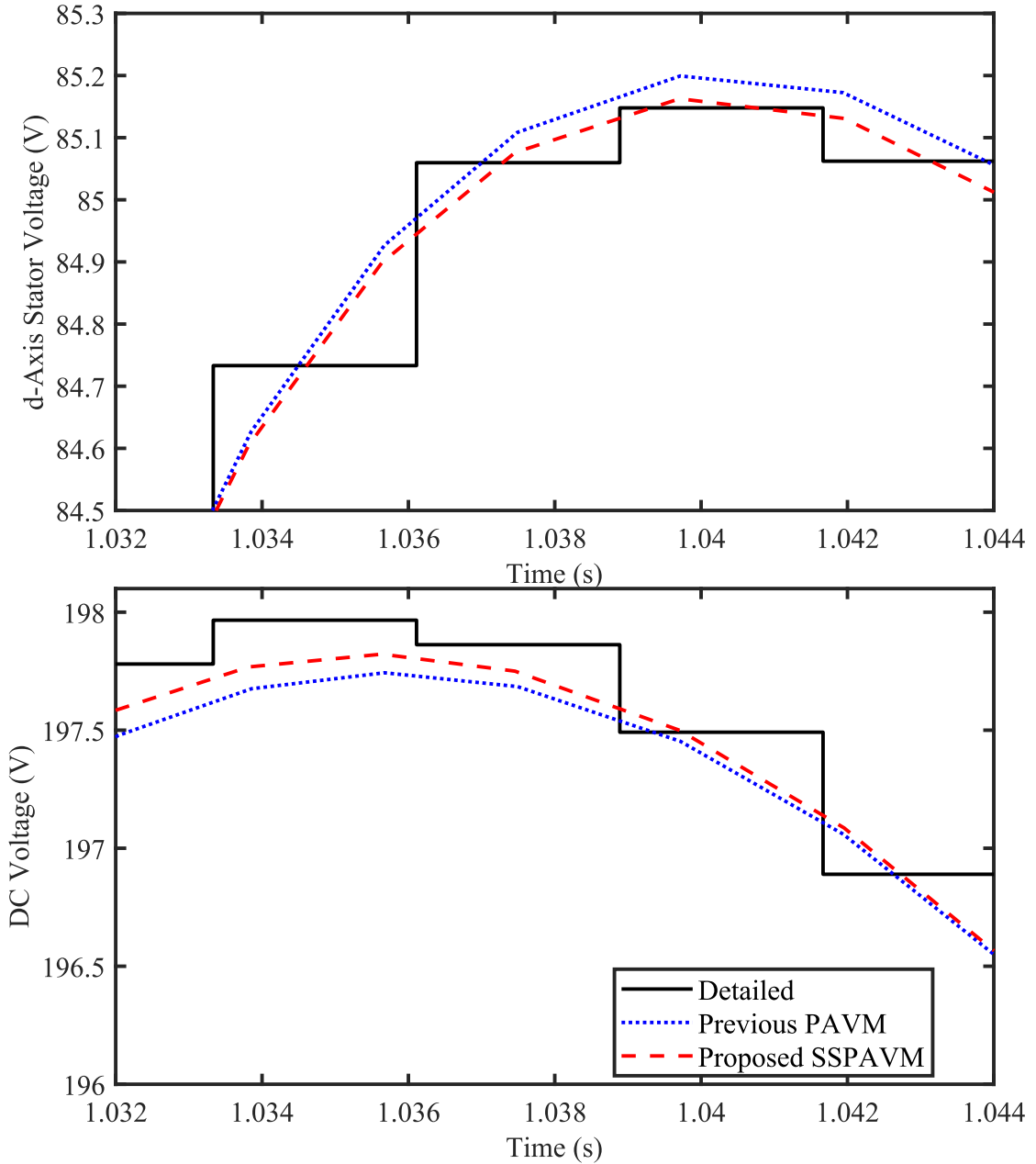
Figure 3.4: Base machine and rectifier with step load from 30 Ω to 10 Ω

3.3.5 Salient Machine and Rectifier Pulse Load

In this case study, the salient synchronous machine's field winding is excited by a voltage of 1.42 V (referred). The stator winding feeds a pulsed load via a rectifier and LC filter. The circuit representation of this study is shown in Figure 3.8. The

Table 3.3: Accuracy Improvement of Proposed SSPAVM over Previous PAVM for Salient Machine and Rectifier with Step Load

Step Load	Variables	Improvement (%)
30 Ω to 10 Ω	v_{qs}^r	3.12
	v_{ds}^r	6.13
	i_{qs}^r	13.44
	i_{ds}^r	14.86
	v_{dc}	14.97
	i_{dc}	14.46
10 Ω to 30 Ω	v_{qs}^r	19.34
	v_{ds}^r	24.98
	i_{qs}^r	28.92
	i_{ds}^r	22.84
	v_{dc}	32.83
	i_{dc}	24.51
15 Ω to 30 Ω	v_{qs}^r	27.73
	v_{ds}^r	29.98
	i_{qs}^r	33.61
	i_{ds}^r	28.39
	v_{dc}	41.58
	i_{dc}	30.33
15 Ω to 45 Ω	v_{qs}^r	17.27
	v_{ds}^r	23.59
	i_{qs}^r	23.44
	i_{ds}^r	14.45
	v_{dc}	28.38
	i_{dc}	19.00
15 Ω to 60 Ω	v_{qs}^r	15.12
	v_{ds}^r	18.83
	i_{qs}^r	16.88
	i_{ds}^r	6.68
	v_{dc}	19.72
	i_{dc}	11.86

pulses are repeated at a frequency of 15 Hz, R_{base} is 50 Ω, and P_{max} is 1000 W. The pulsed load scenario represents the charging/discharging cycle of an energy storage device (e.g. a capacitor) charged with constant current through a dc-dc converter and suddenly discharged. Such systems can be found in electric ship and aircraft systems (e.g., [85–87]).

The waveforms of the detailed model, previous PAVM, and proposed SSPAVM

shown in Figure 3.9 suggest that the proposed SSPAVM waveforms more acurately portrays the detailed model waveforms than the previous PAVM waveforms did. This is expected because the loading of the salient machine system rapidly transitions through different loading conditions (similar to the load steps described above). The percentage of accuracy improvement from the previous PAVM to the proposed SS-PAVM is displayed in Table 3.4. The table clearly shows that the proposed SSPAVM outperforms the previous PAVM in terms of accuracy for all the stator voltages, stator currents, dc voltage and dc current.

Table 3.4: Accuracy Improvement of Proposed SSPAVM over Previous PAVM for Salient Machine and Rectifier with Pulse Load

Case	Variables	Improvement (%)
Pulse Load	v_{qs}^r	11.27
	v_{ds}^r	27.02
	i_{qs}^r	23.58
	i_{ds}^r	9.23
	v_{dc}	24.60
	i_{dc}	19.11

3.3.6 Computational Performance

The computational cost of running each of the models, detailed model, previous PAVM, and proposed SSPAVM, for each case study considered herein is measured. To do so, both the number of time steps in each simulation and run times are recorded for each model (Table 3.5 and Table 3.6). The run times are averaged over 20 simulations (to account for stochastic variability in computer performance) for each case and for each model.

For the base machine-rectifier system, the results are reported in Table 3.5. It is observed that in all cases, both the proposed SSPAVM and previous PAVM require far fewer time steps and significantly less simulation run time than the detailed model. It is also observed in the table that both PAVMs have comparable time

steps and simulation run times. Specifically, the additional complexity of using a two-dimensional look-up table to represent the rectifier relationships does not carry a significant computational penalty.

Similarly, for the salient machine-rectifier system, the results are reported in Table 3.6. It is again observed that in all cases, both the proposed SSPAVM and the previous PAVM require fewer time steps and less simulation run time than the detailed model. In all studies of both the base and the salient machine/rectifier systems, both PAVMs saved at least 98% of the run time of the detailed model, and in all cases, these savings were comparable between the PAVMs.

Table 3.5: Computational Efficiency of Models for Base Machine-Rectifier System

Step Load	Simulation	Time steps	Run time (s)
	Detailed	21602	7.59
30 Ω to 10 Ω	Previous PAVM	151	0.10
	Proposed SSPAVM	153	0.11
	Detailed	21701	7.32
10 Ω to 30 Ω	Previous PAVM	149	0.09
	Proposed SSPAVM	153	0.10
	Detailed	22345	7.26
15 Ω to 30 Ω	Previous PAVM	147	0.10
	Proposed SSPAVM	152	0.11
	Detailed	22326	7.24
15 Ω to 45 Ω	Previous PAVM	157	0.10
	Proposed SSPAVM	154	0.11
	Detailed	22116	7.22
15 Ω to 60 Ω	Previous PAVM	153	0.09
	Proposed SSPAVM	156	0.10

Table 3.6: Computational Efficiency of Models for Salient Machine-Rectifier System

| Step/Pulse Load	Simulation	Time steps	Run time (s)
	Detailed	21339	7.13
30 Ω to 10 Ω	Previous PAVM	185	0.09
	Proposed SSPAVM	193	0.11
	Detailed	22631	7.29
10 Ω to 30 Ω	Previous PAVM	202	0.09
	Proposed SSPAVM	206	0.10
	Detailed	23898	7.54
15 Ω to 30 Ω	Previous PAVM	181	0.09
	Proposed SSPAVM	195	0.10
	Detailed	23306	7.69
15 Ω to 45 Ω	Previous PAVM	205	0.09
	Proposed SSPAVM	197	0.09
	Detailed	22779	7.41
15 Ω to 60 Ω	Previous PAVM	228	0.09
	Proposed SSPAVM	203	0.10
	Detailed	23306	7.68
Pulse Load	Previous PAVM	731	0.12
	Proposed SSPAVM	758	0.13
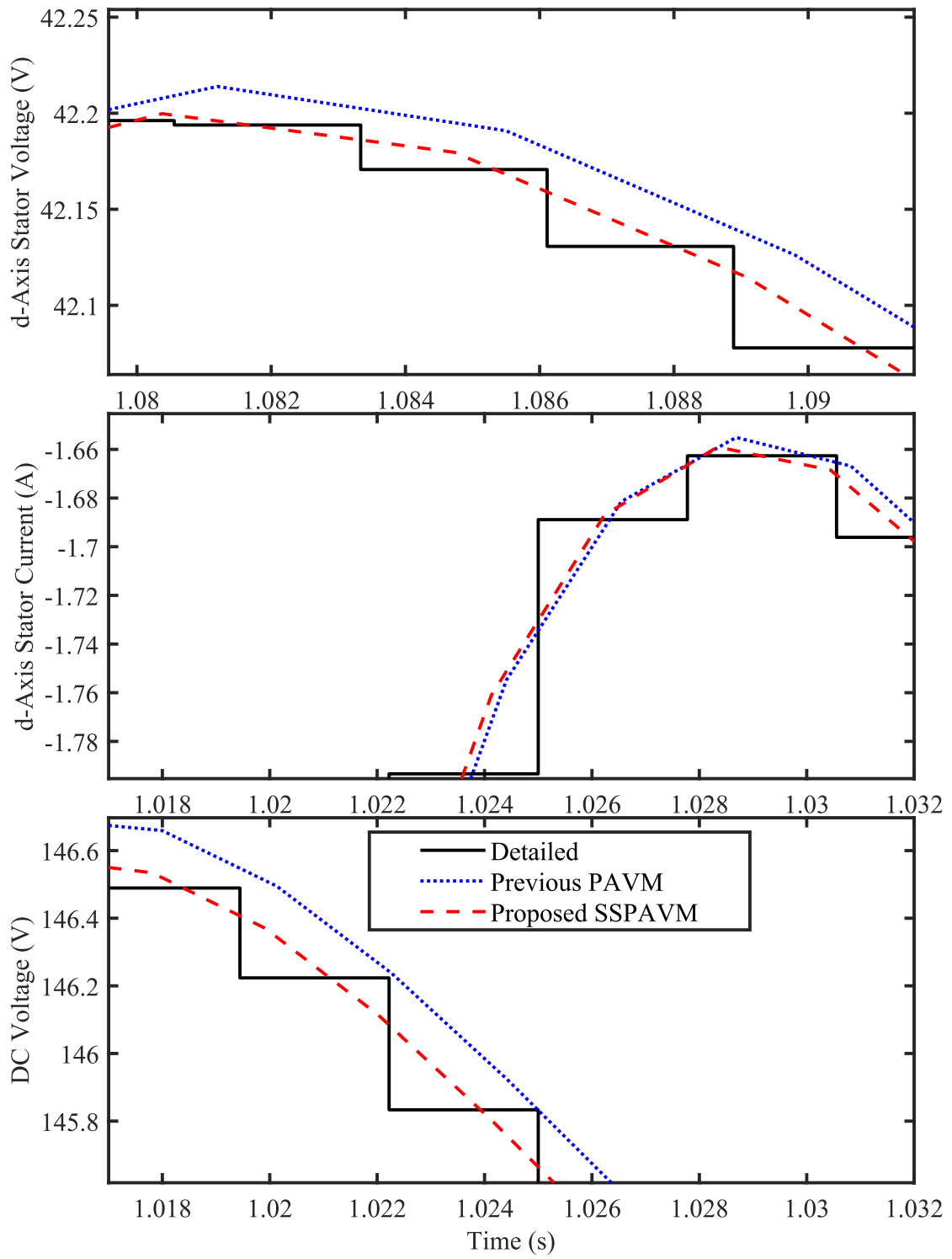
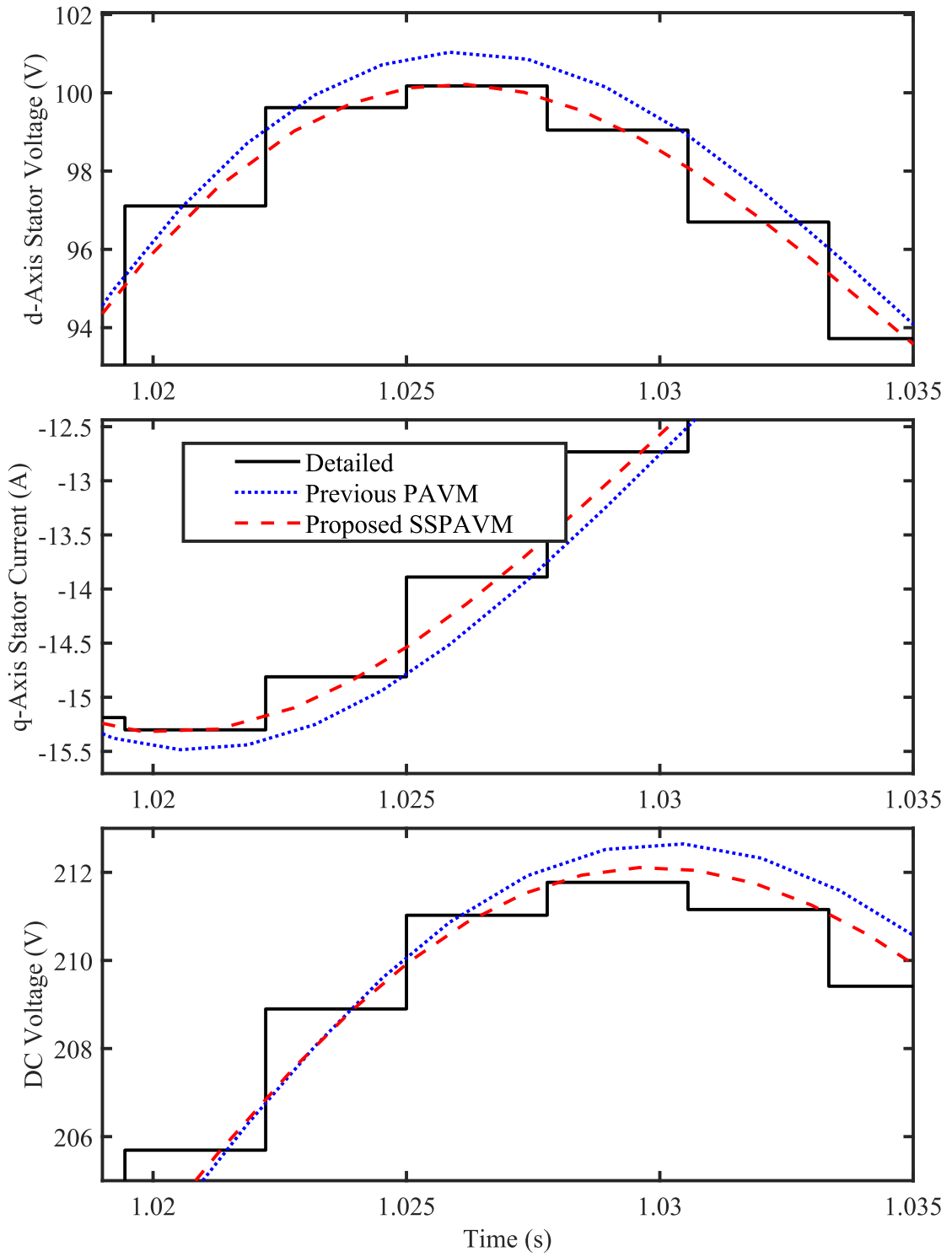Figure 3.5: Base machine and rectifier with step load from 15 Ω to 45 Ω

Figure 3.6: Salient machine and rectifier with step load from 30 Ω to 10 Ω
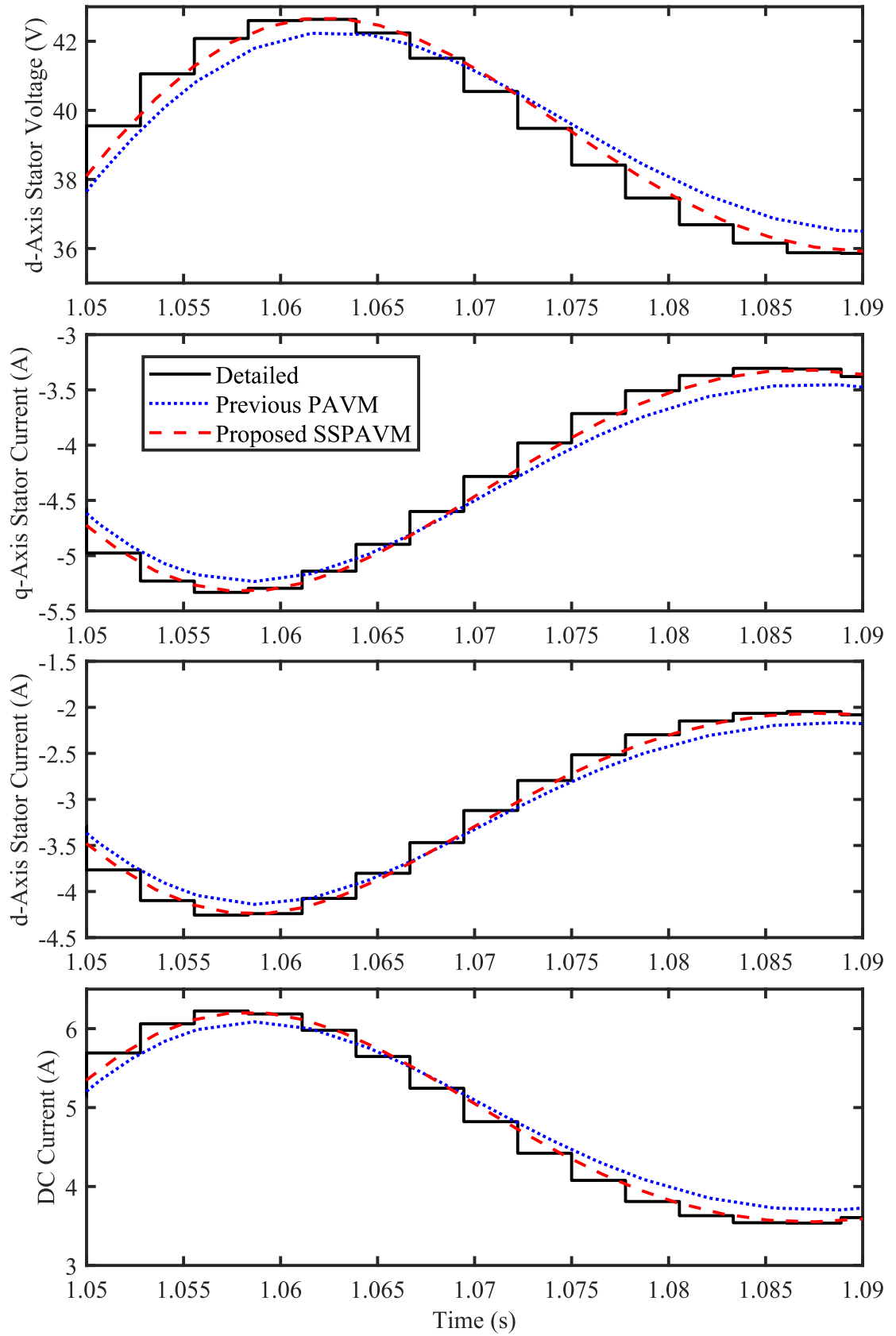
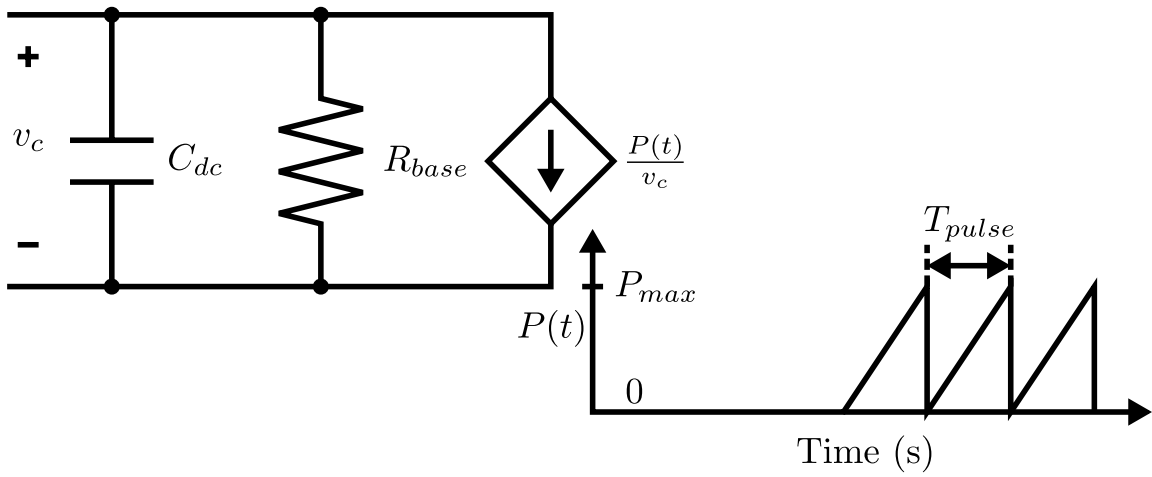Figure 3.7: Salient machine and rectifier with step load from 15 Ω to 45 Ω

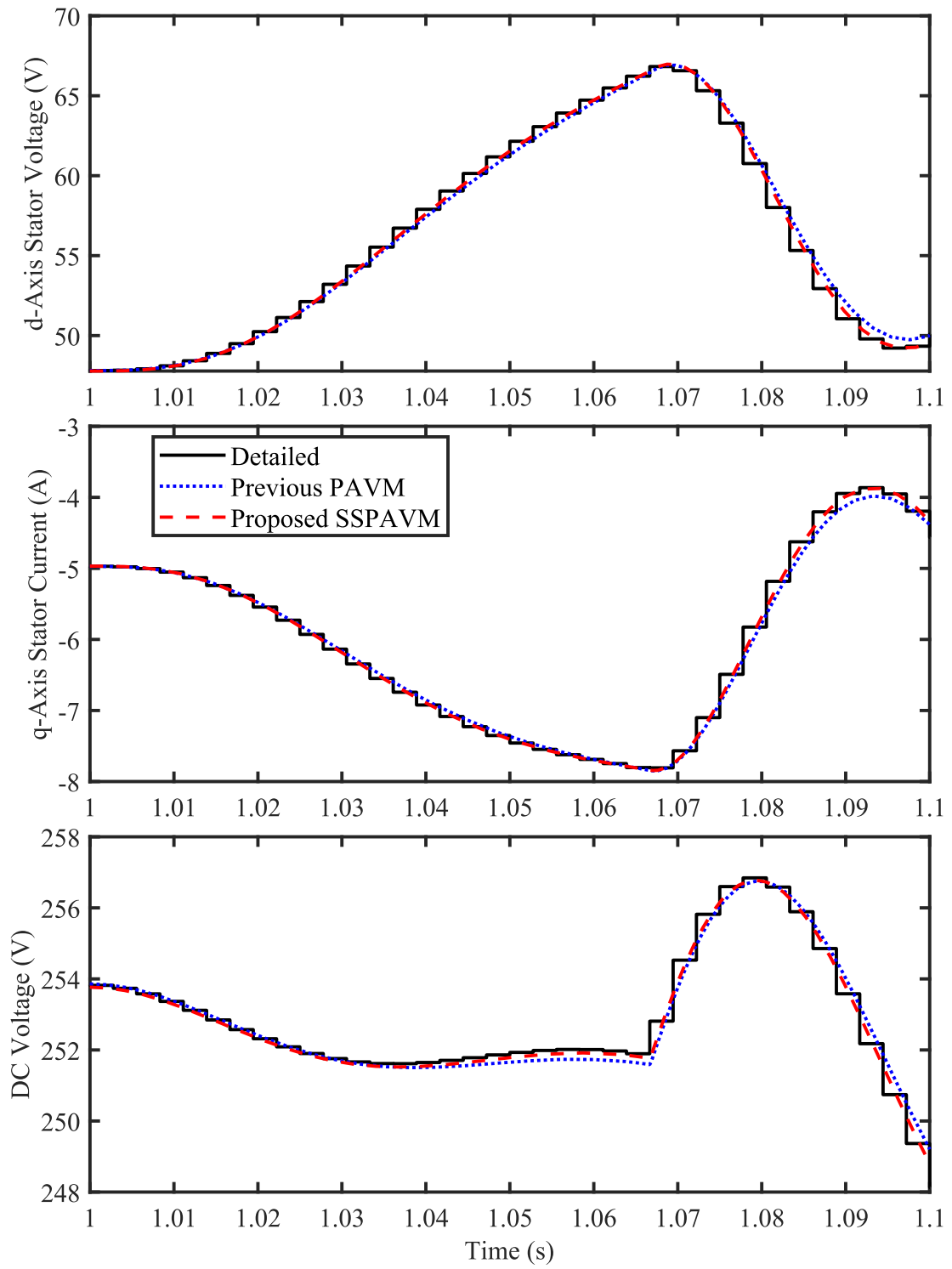Figure 3.8: Rectifier system loaded with dc pulse load

Figure 3.9: Pulse load scenario for a salient synchronous machine-rectifier system

Chapter 4 Multidimensional Characterization of Parametric Relationships for Salient Machine-Rectifier Systems

4.1 Preamble

Parametric average-value models (PAVMs) of synchronous machine-rectifier systems have proven to be very useful in studying the behavior of these systems. PAVMS are able to represent the system's dynamic characteristics in a computationally efficient manner. To develop a PAVM of the synchronous machine-rectifier system, the essential parametric functions are extracted once from the detailed model of the system. Existing PAVMs (starting with [2]) implicitly encode an assumption that the current angle of the machine under each loading condition is a function of that loading condition (represented by dynamic impedance). However, it is observed herein that during transient events with machines of high substransient saliency, the dynamic impedance alone may not be sufficient to represent the operating condition of the system. Thus, under certain circumstances, this implicit assumption upon which the previous PAVMs are based can be violated. Therefore, it is shown herein that the rectifier parametric functions can be represented as functions of both the dynamic loading condition of the rectifier and the current angle of the synchronous machine's ac currents, and a method of extracting these two-dimensional relationships is proposed. It is also shown that previous PAVMs are unable to represent the rectifier parametric functions during transient events, particularly for more salient synchronous machines. This approach is used in developing the saliency-sensitive PAVM (SSPAVM) of the machine-rectifier systems proposed in Chapter 3.

The fundamental contributions of this chapter are

1. to demonstrate that the rectifier parametric functions can be represented as

functions of both the dynamic impedance and the current angle,

2. to propose a method of extracting the two-dimensional lookup table values required to represent these functions, and

3. to show how previous PAVMs are unable to represent the rectifier parametric functions during transient events, particularly for more salient synchronous machines.

The organization of the rest of this chapter is as follows. Section 4.2 describes the mathematical modeling relationships for both the previous PAVM and the proposed SSPAVM. The procedure for extracting the multidimensional lookup table values needed for the proposed SSPAVM is proposed in Section 4.3. Section 4.4 demonstrates the characterization procedure results for two synchronous machine-rectifier systems and shows how the previous PAVM does not represent the recitifer parametric functions under certain conditions. This chapter is based on [88]. Preprints are also available on TechRxiv [89].

4.2 Modeling Relationships

The mathematical notation and conventions used herein are described in the appendix. The essential principle of PAVMs is that there is a condition-dependent parametric relationship between the average values of the ac voltages and currents and the dc voltages and currents for the machine-rectifier circuit in Figure 3.1. Specifically, the variables are related according to

$$|\bar{\vec{v}}| = \alpha(\cdot)\bar{v}_{dc} \tag{4.1}$$

$$\bar{i}_{dc} = \beta(\cdot)|\bar{\vec{i}}| \tag{4.2}$$

$$\phi(\cdot) = \angle\bar{\vec{v}} - \angle\bar{\vec{i}} - \pi. \tag{4.3}$$

51

In [72], these relationships are considered constant. Starting in [2], these relationships are represented as dependent on loading condition. The relationships have also been described as functions of other operating conditions such as frequency [80] and firing angle for thyristor-based rectifiers [75].

4.2.1 Previous Parametric Average-Value Model

In [2] and following works (e.g., [30, 76]), the relationships (4.1)–(4.3) are functions of a "conveniently defined" dynamic impedance:

$$z = \frac{\bar{v}_c}{|\vec{\bar{i}}|}. \tag{4.4}$$

This is a convenient dynamic indicator of rectifier loading because $\bar{v}_c$ would ordinarily be a state variable in state-variable-based simulation environments and could be used to determine these relationships without introducing algebraic loops. Likewise, $\bar{v}_c$ is algebraically related to $\bar{v}_{dc}$ and $\bar{i}_{dc}$ in steady state (even identical to $\bar{v}_{dc}$ if r_{dc} is neglected or incorporated within the parametric relationships). Herein, such a model is referred to as the previous PAVM.

4.2.2 Proposed Saliency-Sensitive Parametric Average-Value Model

Herein, the relationships (4.1)–(4.3) are functions of the dynamic impedance z, but they are also functions of the angle of the ac currents (i.e., $\angle \vec{\bar{i}}$). This representation is based on the authors' anecdotal observation that PAVMs based only on the dynamic impedance do not always represent the behavior of machines with significant subtransient saliency well in situations with highly dynamic loading. Herein, such a model is referred to as the proposed SSPAVM.

4.3 Characterization Procedures

Both models are characterized by simulating a detailed (i.e., switch level) model of the machine-rectifier system shown in Figure 3.1. The system is simulated with different fixed resistive dc loads to determine the governing rectifier relationships (i.e., (4.1)–(4.3)). The system is simulated using MATLAB/Simulink's ode23tb solver using default parameters and tolerances. The maximum time step is limited to 10 µs. The voltage-behind-reactance (VBR) model of the machine is given in [1], and the dc link dynamics are given by

$$L_{dc}\frac{di_{dc}}{dt} = v_{dc} - R_{dc}i_{dc} - v_c \tag{4.5}$$

$$C_{dc}\frac{dv_c}{dt} = i_{dc} - \frac{v_c}{R_L}. \tag{4.6}$$

The dynamics are simulated with a detailed ideal switching model of the three-phase rectifier implemented using Stateflow. The machine rotates at constant rated speed. The initial state variables and field voltage are zero. The excitation of the machine varies depending on which of the two procedures described below is used, but it is generally ramped from zero linearly over 1 s to a value that would produce rated machine voltage under open-circuit conditions. The system is then simulated 8 s to reach steady state. The average-values of v_{qs}^r, v_{ds}^r, i_{qs}^r, i_{ds}^r, v_{dc}, i_{dc}, and v_c are calculated during the last period of the simulation (the period of these variables is one sixth the fundamental period of the ac). These 'raw' values are used to establish the parametric relations (4.1)–(4.3). There are other approaches for establishing these data points (e.g., using a fast procedure [30]), but this seqence of steady-state simulations is used to avoid the possibility of introducing errors by exciting certain system dynamics.

4.3.1 Previous Parametric Average-Value Model Procedure

For the previous PAVM, the one-dimensional relationships are established by ramping the field voltage from zero linearly over 1 s to the value that would produce rated machine voltage V_{rated} (line-to-line, rms) under open-circuit conditions:

$$v'_{fd} = \frac{r'_{fd}\sqrt{\frac{2}{3}}V_{rated}}{\omega_b L_{md}}. \tag{4.7}$$

This simulation is conducted for different load resistances, which are logarithmically varied from 0.1 mΩ to 10 kΩ with 32 steps per decade. The lookup table values are determined using the least-squares spline approximation algorithm spap2 to select the 120 z knots that create the least error in approximating α, β, and ϕ using cubic spline interpolation. The value of 120 is intentionally selected as a large number to reduce the likelihood that undersampling contributes to the observed responses; practically, smaller numbers could be used (e.g., values of 10 and 23 are reported in [2] and [77], respectively).

4.3.2 Proposed Saliency-Sensitive Parametric Average-Value Model Procedure

The same machine-rectifier system shown in Figure 3.1 is simulated with different fixed resistive dc loads to determine the governing rectifier relationships (4.1)–(4.3) as above. The same simulation parameters and procedure are used with one exception. To adjust the angle of excitation of the machine to determine the two-dimensional relationships, the field winding is shorted, and biases are added to the q- and d-axis magnetizing flux linkages, being physically equivalent to a permanent magnet, the position of which on the rotor could be adjusted. These biases are ramped linearly from zero to their final values over 1 s, and the magnitude of these biases is related

to the field voltage applied in the one-dimensional case such that the final biases are

$$\lambda_{mq,bias} = \frac{\sqrt{\frac{2}{3}}V_{rated}\cos\delta_{bias}}{\omega_b} \tag{4.8}$$

$$\lambda_{md,bias} = -\frac{\sqrt{\frac{2}{3}}V_{rated}\sin\delta_{bias}}{\omega_b}, \tag{4.9}$$

where δ_{bias} is the angle of excitation.

As with the previous procedure, this simulation is conducted for different load resistances, which are logarithmically varied from 0.1 mΩ to 10 kΩ with 32 steps per decade. To facilitate the interpolation process described below, one extra step (using the same logarithmic spacing) is added above and below this range. The angles of excitation are varied from $-180°$ to $180°$ with steps of $15°$. There is a clear relationship between the load resistance and the resulting value of z, and a similar relationship exists between the angle of excitation and the resulting angle of the current space vector. However, it is not straightforward to select the load resistance and excitation angle to result in a specific combination of z and $\angle\vec{\vec{i}}$. Therefore, the resulting data is scattered rather than gridded as shown in Figure 4.1, which shows the resulting data when this procedure is applied to the base machine and rectifier system described below. This figure shows that gridded values of load resistance and excitation angle result in scattered values of dynamic impedance and current angle.

The spap2 algorithm requires gridded data for multivariate spline approximation. Gridded data in the z-$\angle\vec{\vec{i}}$ space is constructed from the scattered data using a Delaunay triangulation. To achieve this, MATLAB's scatteredInterpolant function is used with its natural interpolation method. The base-10 logarithm of the z data is used to avoid scaling problems, and the $\angle\vec{\vec{i}}$ data (in radians) is tiled $\pm2\pi$ to ensure periodicity. The scattered data is interpolated over a gridded range. The grid includes 2,561 z values (approximately 10 times the original number of load resistance values) that are logarithmically distributed from the minimum value associated with the lowest
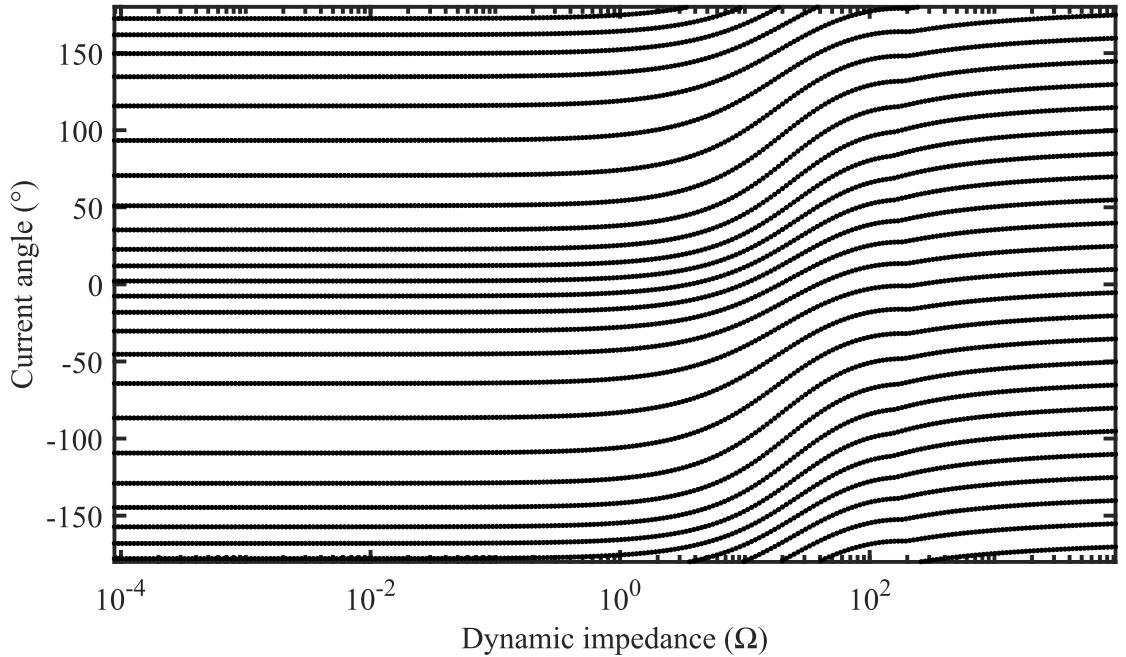
Figure 4.1: Scattered two-dimensional data sites from parameterization process for base machine and rectifier.

load resistance of 0.1 mΩ to the maximum value associated with the highest load resistance of 10 kΩ and 241 $\angle\vec{\vec{i}}$ values (approximately 10 times the original number of bias angle values) distributed from −180° to 180°. An illustration of this process for the base machine and rectifier system is shown in Figure 4.2. This figure shows that gridded data can be extracted by oversampling the scattered data from above.

With the gridded data, the lookup table values are determined using the least-squares spline approximation algorithm spap2 to select the 120 z knots and 25 $\angle\vec{\vec{i}}$ knots that create the least error in approximating α, β, and ϕ using cubic interpolation. As mentioned above, the value of 120 is intentionally selected as a large number to reduce the likelihood that undersampling contributes to the observed responses.
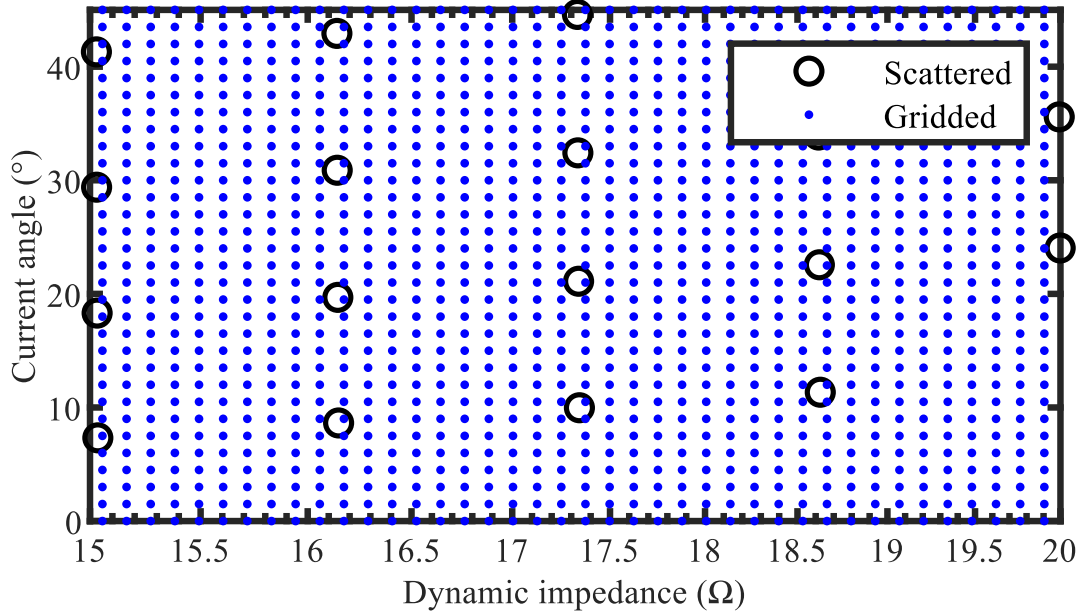
Figure 4.2: Extraction of gridded data sites from scattered data for base machine and rectifier.

4.4 Demonstration and Discussion

The procedures described above are completed for the two related systems with the parameters reported in Table 3.2. These systems are based on the parameters described in [2]. The first system has a relatively less salient machine (referred to as the base machine), with subtransient saliency represented by $L_q''/L_d'' \approx 1.36$. The second system has a modified machine (referred to as the salient machine), with its damper windings modified such that $L_q''/L_d'' \approx 5.38$.

The rectifier numerical functions for the base machine and salient machine are shown in Figure 4.3 and Figure 4.4, respectively. Both plots show 'raw' values of the parametric functions α, β, and ϕ versus dynamic impedance z, with the proposed SS-PAVM parametric functions projected onto the previous PAVM parametric functions. It can be seen that the PAVM results are contained within the SSPAVM results, but that the SSPAVM results predict different values of α, β, and ϕ under certain condi-

57

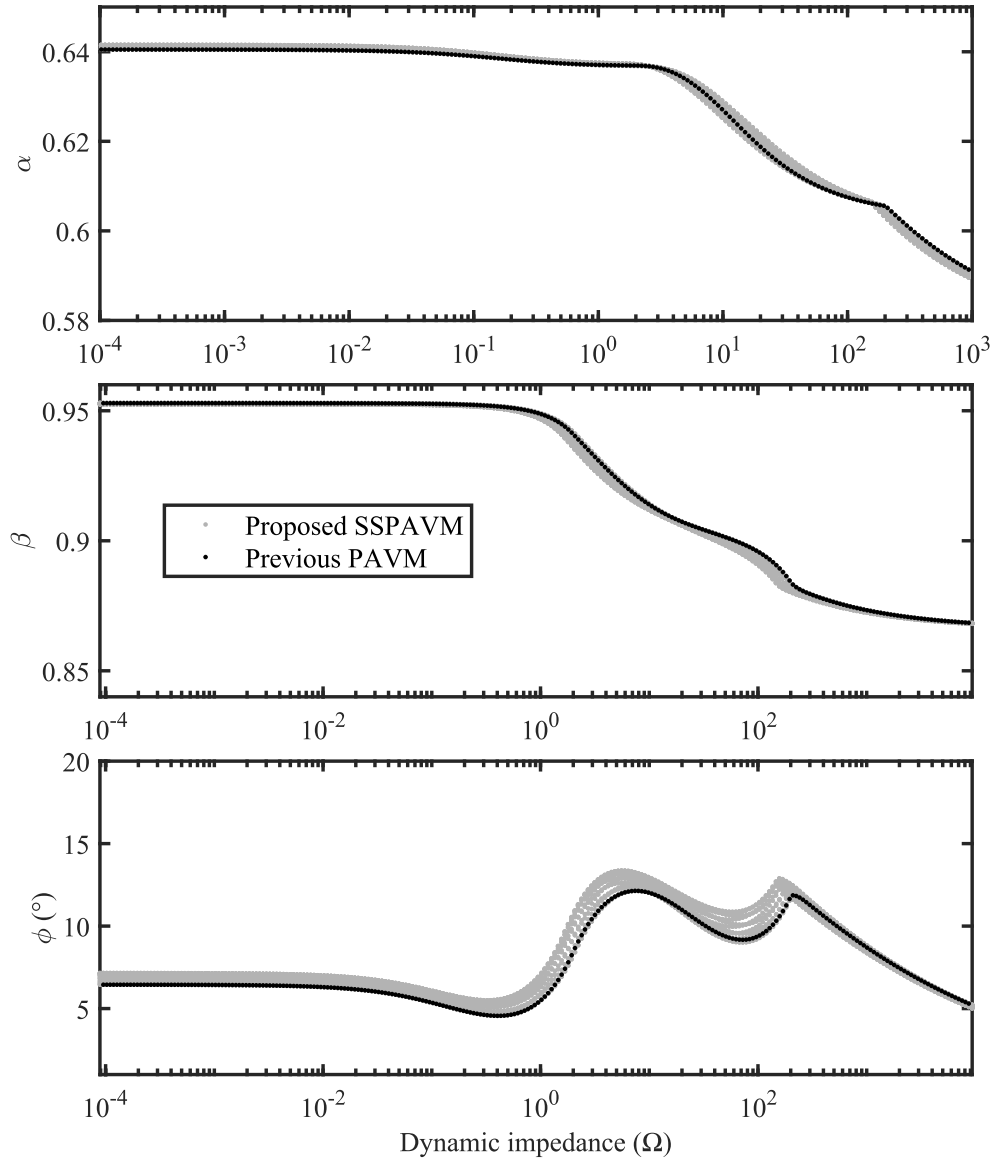Figure 4.3: Parametric functions for base machine with rectifier.

tions, and this is particularly pronounced for the salient machine-rectifier system as seen in Figure 4.4.

Furthermore, the PAVM lookup table values are extracted from the 'raw' data using the spap2 algorithm as described above and are shown in Figure 4.5 and Figure 4.6. The PAVM implicitly encodes an assumption that the current angle under
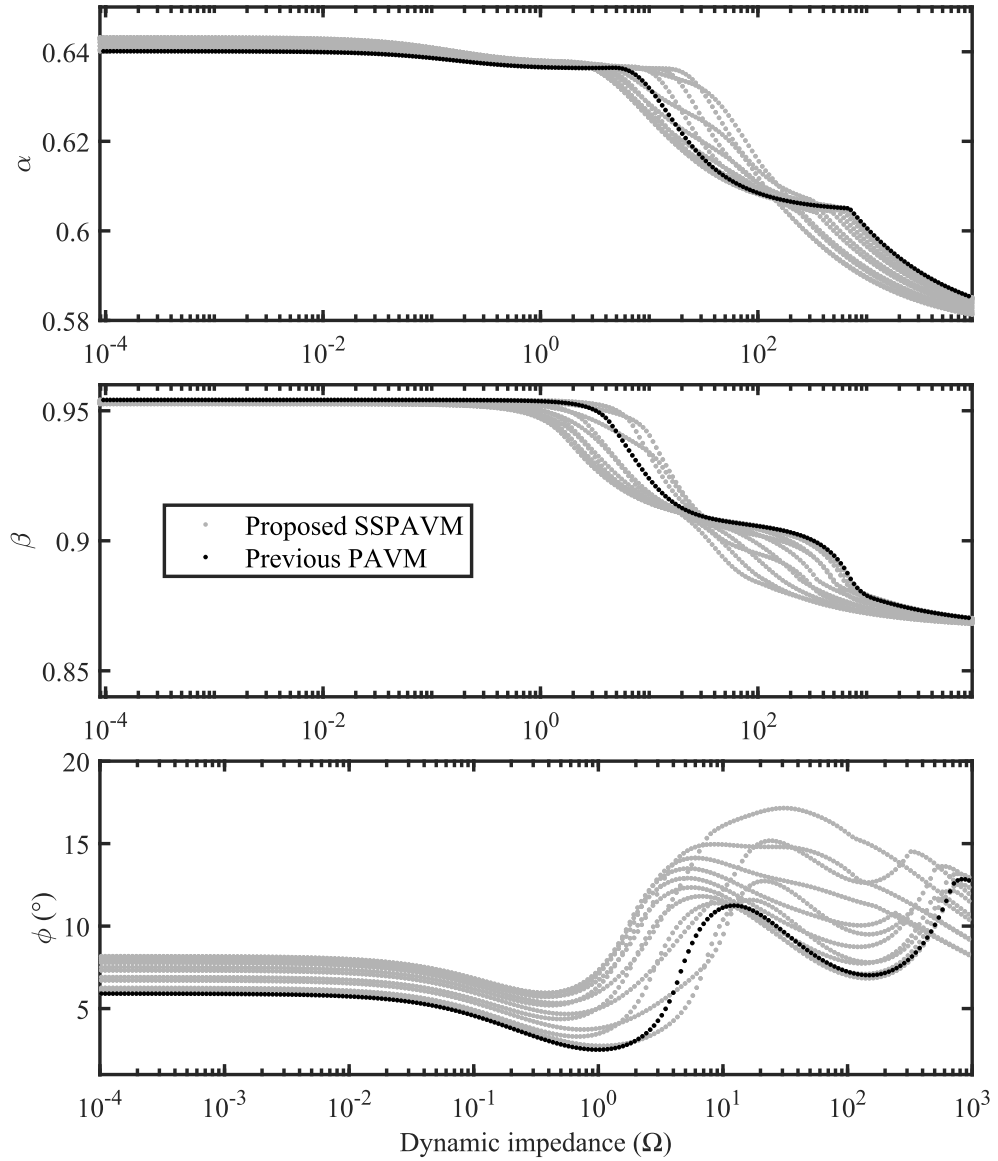
Figure 4.4: Parametric functions for salient machine with rectifier.

each loading condition is a function of that loading condition, i.e. $\angle \vec{i}$ is a function of z. This function is also shown for each system in Figure 4.5 and Figure 4.6. If this assumption holds, it is not necessary to consider the deviations observed in the SSPAVM data compared with the PAVM data in Figure 4.3 and Figure 4.4.

To consider whether this assumption holds, the detailed model is simulated for a

step change in resistive load from 10 Ω to 30 Ω for both systems. The average value of each of the waveforms v_{qs}^r, v_{ds}^r, i_{qs}^r, i_{ds}^r, v_{dc}, i_{dc}, and v_c is calculated over each $\frac{1}{360}$ s window and used to calculate values of $\bar{z}$, $\bar{\alpha}$, $\bar{\beta}$, $\bar{\phi}$ and $\angle\bar{\vec{i}}$. The observed current angles are compared with the current angles predicted as a function of z in Figure 4.7 and Figure 4.8. While the current angle matches the predicted current angle during steady state conditions, there are significant discrepancies during the transient and these are exaggerated for the salient machine-rectifier system (in Figure 4.8). Therefore, the implicit assumption upon which the previous PAVM is based is violated during these circumstances.

The consequence of this assumption being violated can be seen in Figure 4.9 and Figure 4.10, where the observed values of α, β, and ϕ, the fundamental relationships underlying PAVMs, are compared with the values predicted as a function of dynamic impedance z. As expected, the parametric functions match during steady-state conditions, but they deviate significantly during the transient, and this is again more pronounced for the salient machine-rectifier system.

The lookup table values for the proposed SSPAVM are extracted from the gridded data using spap2 as described above, and these table values are shown for the base machine and salient machine in Figure 4.11 and Figure 4.12, respectively. In addition, the lookup table values for the previous PAVM are superimposed at the current angle corresponding to each dynamic impedance. As expected, the previous PAVM parametric functions are coincident with the proposed SSPAVM parametric functions at the current angles on which they are based. These multidimensional parametric functions can serve as the basis for a SSPAVM [82] that, from the results presented herein, can be expected to perform more accurately in dynamic situations, particularly for more salient machine-rectifier systems.
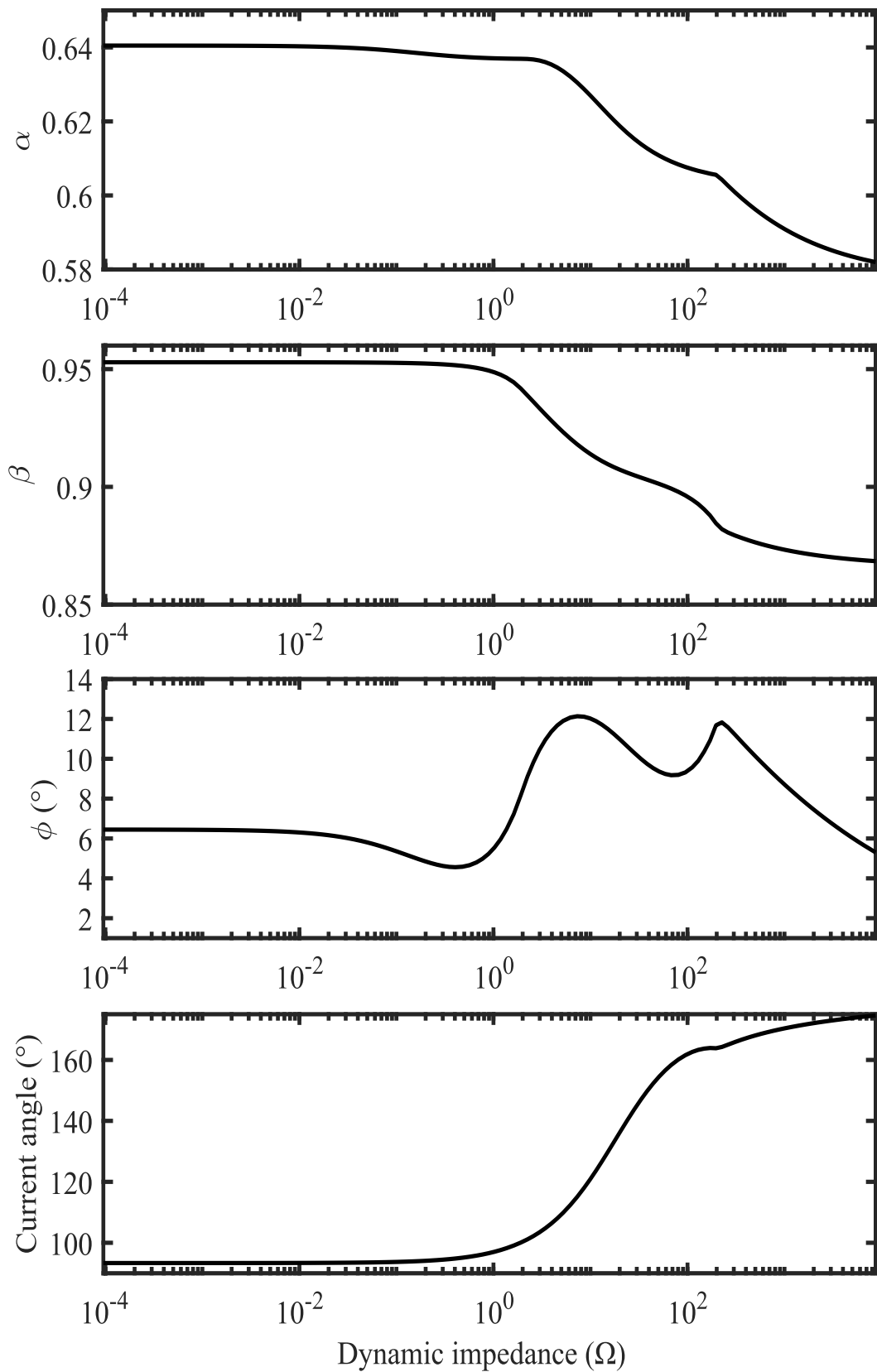
Figure 4.5: Previous PAVM parametric functions and current angle table values for base machine with rectifier.
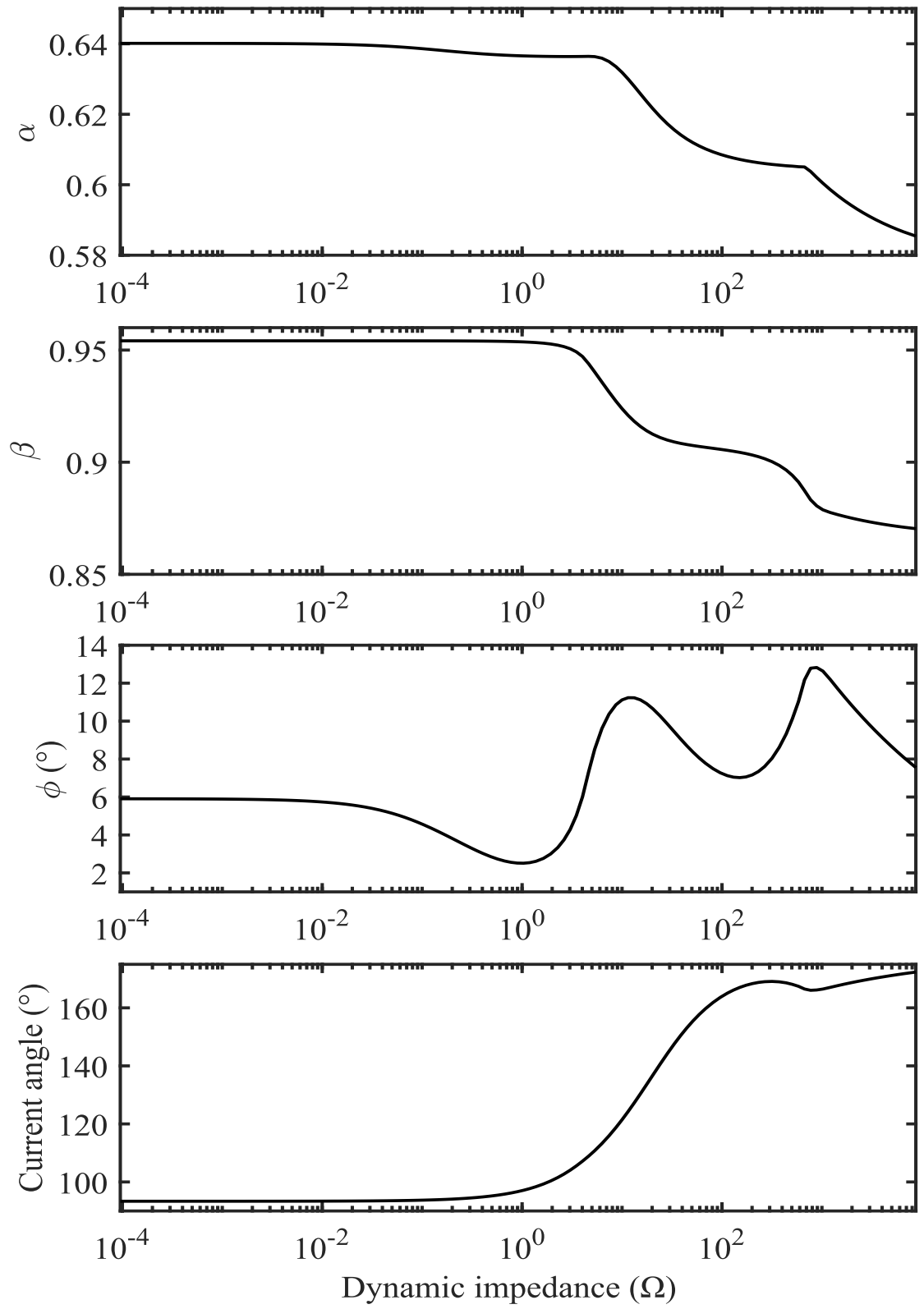
Figure 4.6: Previous PAVM parametric functions and current angle table values for salient machine with rectifier.
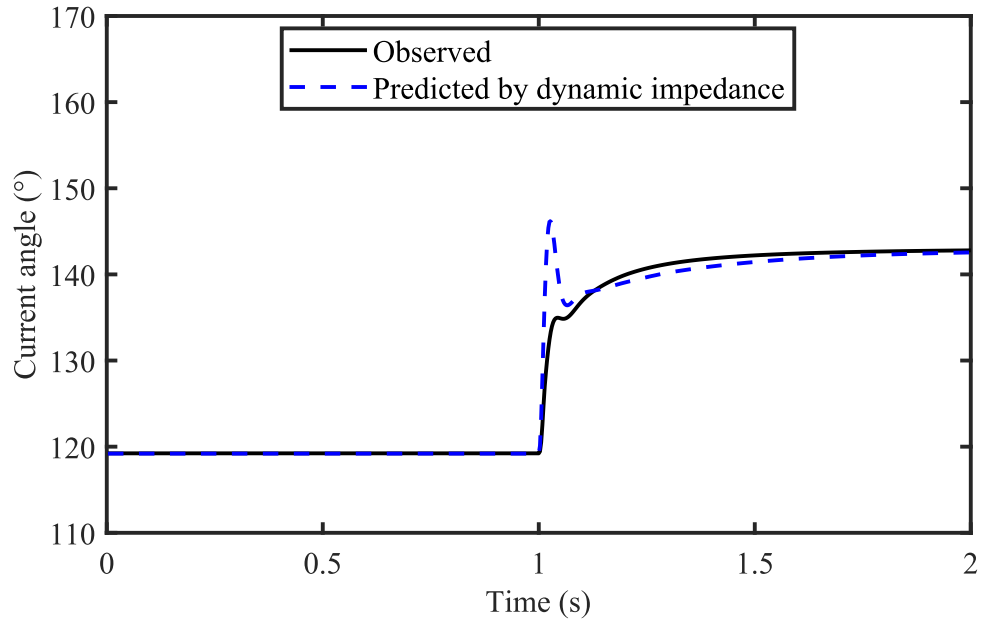
Figure 4.7: Observed and predicted current angle from detailed simulation of base machine with rectifier and step load from 10 Ωto 30 Ω.
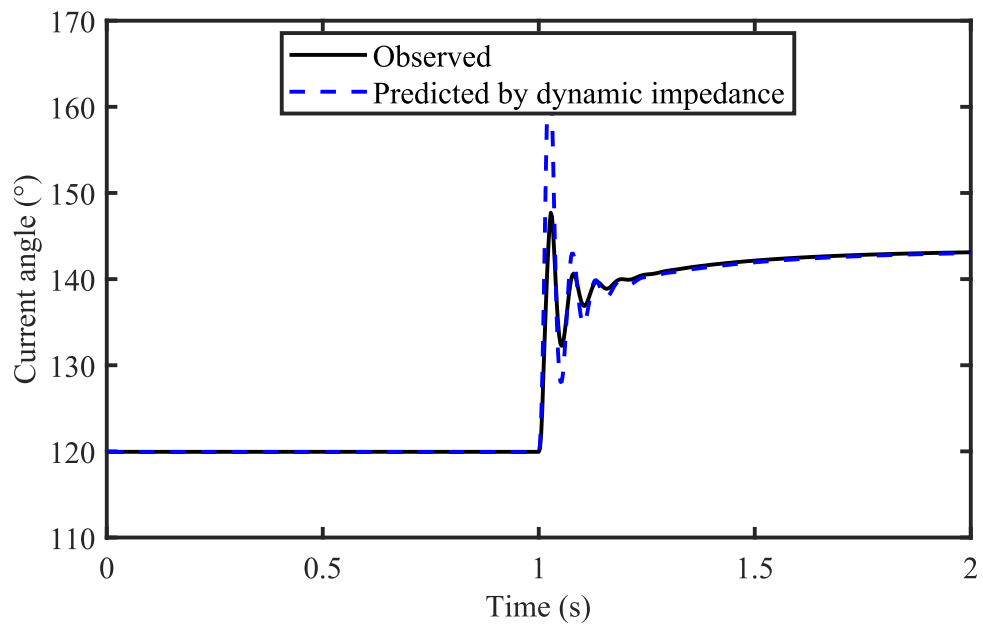
Figure 4.8: Observed and predicted current angle from detailed simulation of salient machine with rectifier and step load from 10 Ωto 30 Ω.

63
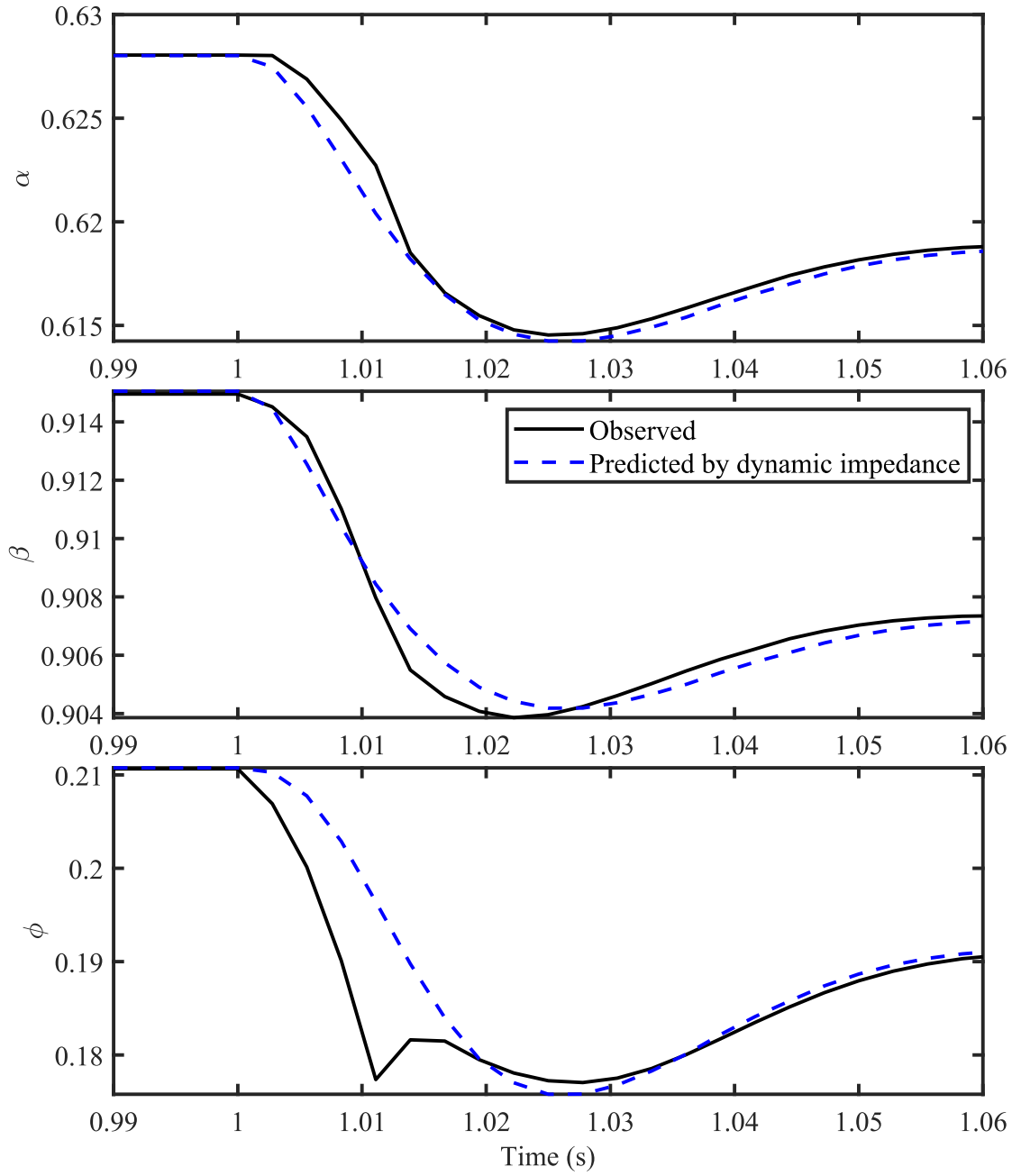
Figure 4.9: Observed and predicted parametric functions from detailed simulation of base machine with rectifier and step load from 10 Ω to 30 Ω.
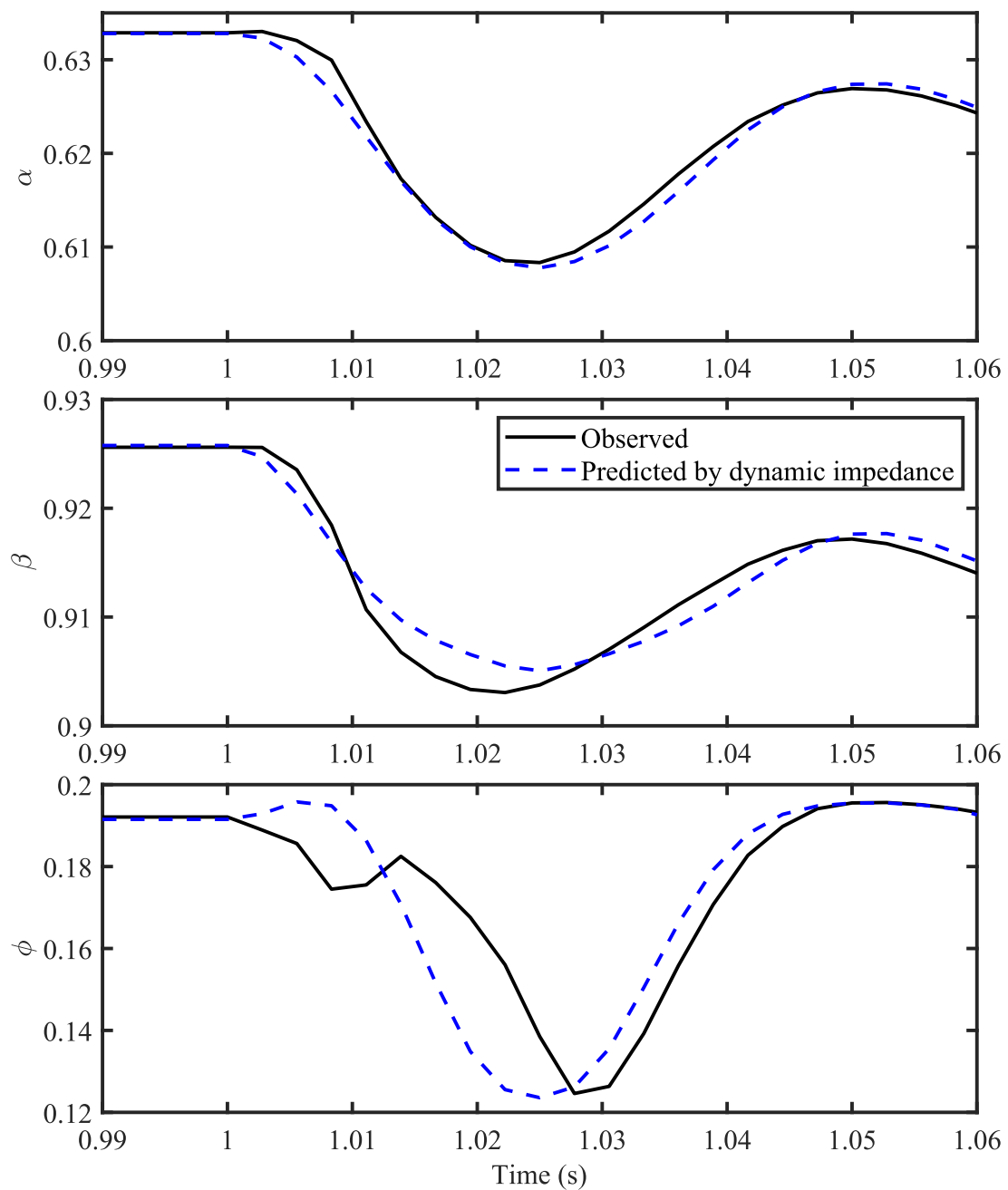
Figure 4.10: Observed and predicted parametric functions from detailed simulation of salient machine with rectifier and step load from 10 Ω to 30 Ω.
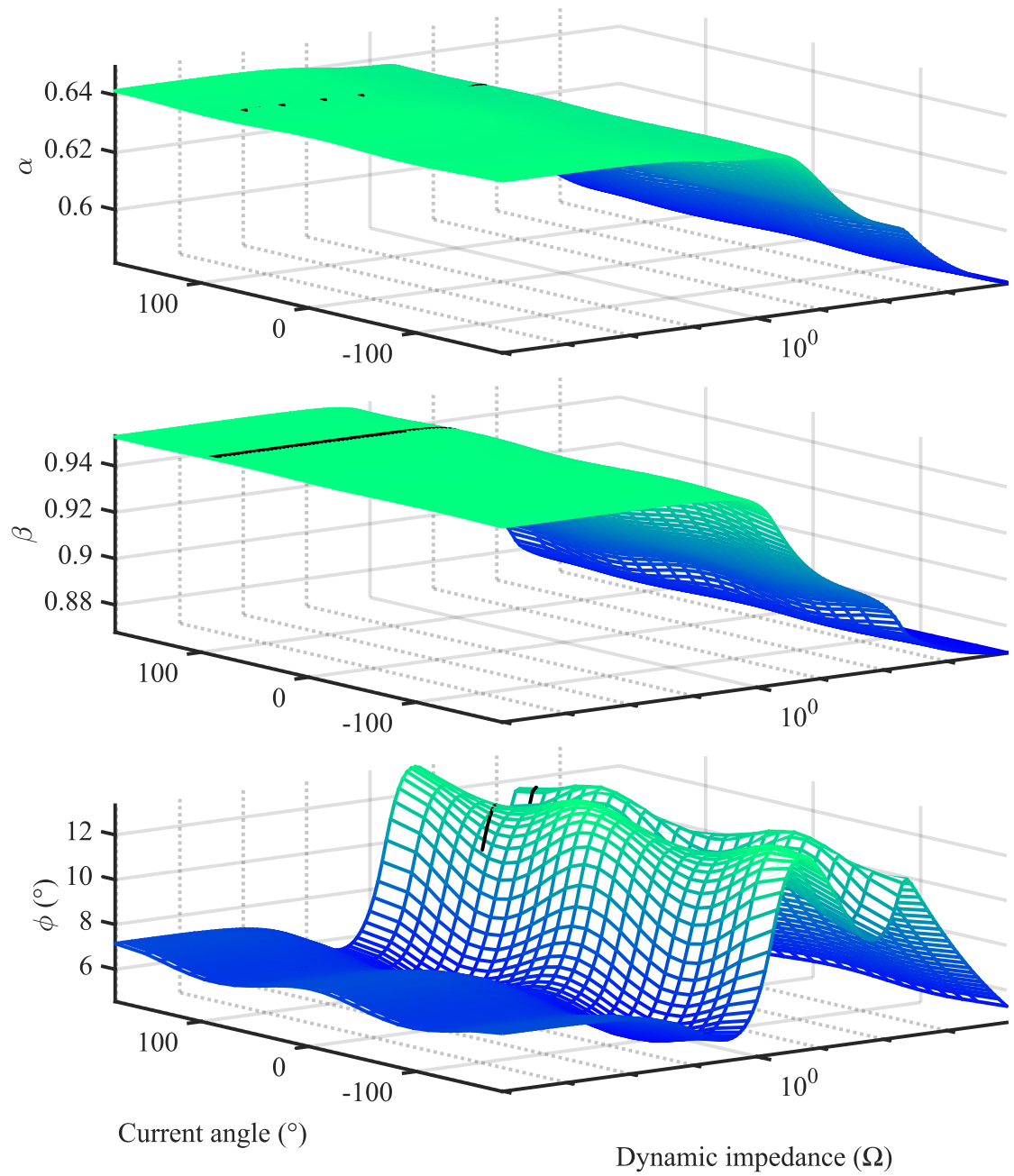
Figure 4.11: Proposed SSPAVM parametric functions table values for base machine with rectifier. The previous PAVM parametric functions and current angle table values are superimposed.
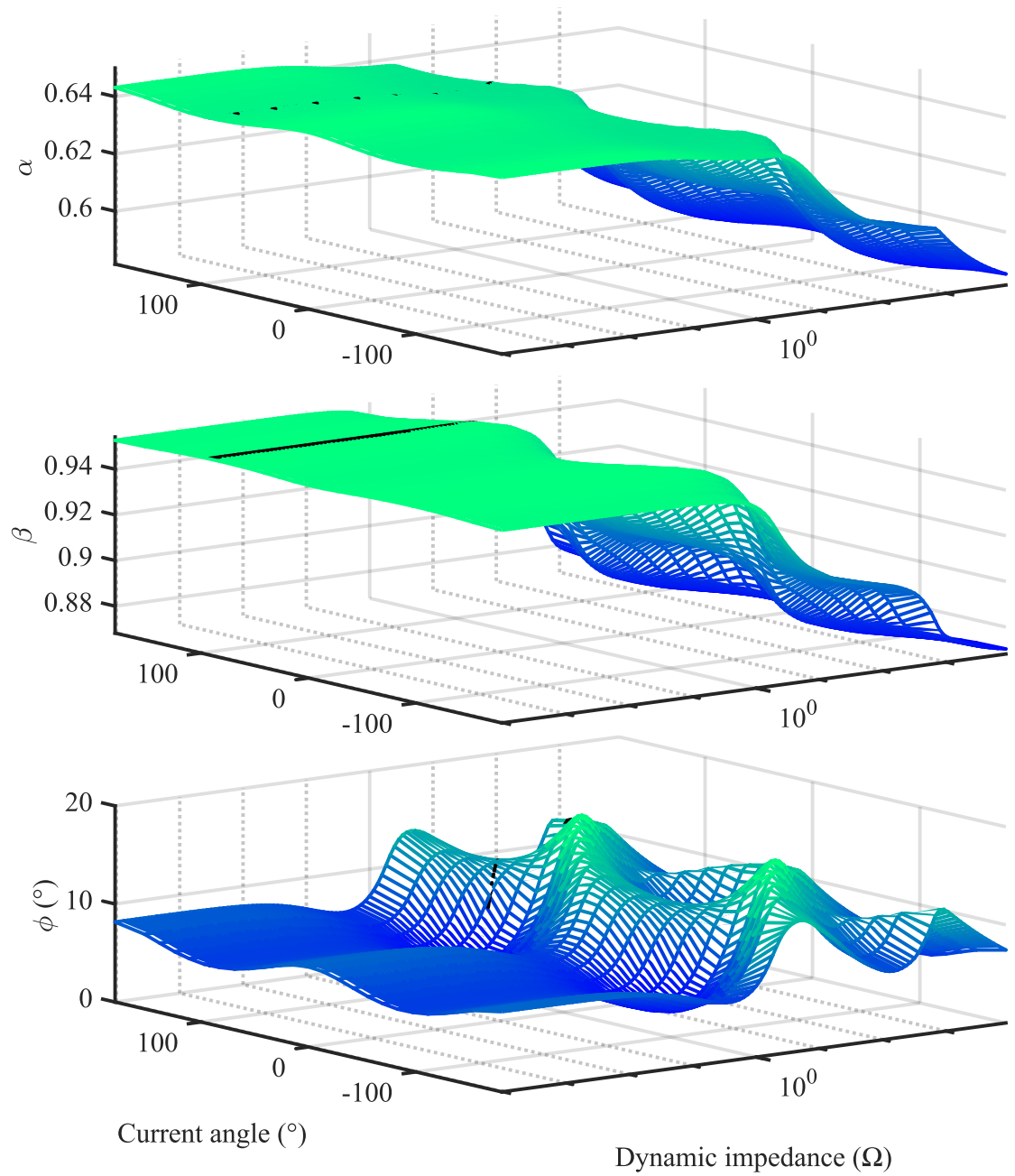
Figure 4.12: Proposed SSPAVM parametric functions table values for salient machine with rectifier. The previous PAVM parametric functions and current angle table values are superimposed.

Chapter 5 Multidimensional Fast Procedure for Extracting Parametric Functions for Salient Machine-Rectifier Systems

5.1   Preamble

AAVM method establishes an approach wherein the relationship between the ac and dc variables of the rectifier are analytically derived; with certain assumptions. Deriving the analytical model of the synchronous machine-rectifier system is generally arduous, and may only rely on a single rectifier operating mode. This necessitates the search for a method which can allow for numerical solutions early at the model development stage. Thus, the PAVM was established. To develop the PAVM, the essential AVM parameters are obtained from the detailed model simulations. Certain approaches have been advanced for extracting this much needed parametric functions from the detailed model simulations. For instance, multiple steady state simulation approach was advanced in [2], and these numerical functions were considered to be dependent on the dynamic loading of the system (z). This dynamic impedance served as the lookup table input for implementing the PAVM therein. This idea is further extended in [88] (Chapter 4) to include the machine's angle of current, $\vec{\angle i}$ as an additional variable (using multidimensional characterization approach) upon which the parametric functions would depend. This is due to the observation that during certain transient conditions, especially with machines of high subtransient saliency, z only is incapable of representing the system's operating conditions. Therefore in [82] (Chapter 3), these two variables (z and $\vec{\angle i}$) were utilized as lookup table inputs for developing the SSPAVM.

However, the drawback/consequence of the multiple steady state simulations in [2] and [88] is the high computational expense associated with running them. Hence the work in [30] seeks to reduce the computational burden associated with the approach

used in [2] by implementing a 'fast procedure' to extract the numerical functions required to develop the parametric average-value model of the synchronous machine-rectifier systems. The simulation run time was significantly reduced. Since then, some other works (for instance, [90–92]) have adopted this method. In the same vein, the work herein seeks to reduce the computational burden associated with the approach in [88] by implementing a multidimensional fast procedure characterization approach for extracting the required parametric functions using the detailed model simulations. These functions would be required to develop the SSPAVM of the synchronous machine-rectifier systems. This approach also ensures that several dynamic operating conditions that may not have been covered by the one-dimensional fast procedure in [30] and other works, are covered herein.

The main ideas of this chapter are

1. To present an alternative method for multidimensional characterization of parametric average-value model of the synchronous machine-rectifier systems.

2. To show that this approach beats the previous approach in terms of computational efficiency.

3. To demonstrate that both methods yield identical results. Hence, the faster approach presented herein should be prioritized.

This chapter is being compiled in a manuscript [93]

5.2 Proposed Multidimensional Fast Characterization Procedure

The detailed model of the machine-rectifier system depicted in Figure 3.1 is simulated in a similar process described in Section 4.3.2. However, instead of performing multiple steady state simulations using different fixed values of dc load resistances, a straightforward and faster approach is to perform a single simulation with exponentially increasing dc load resistances. Specifically, in this procedure, the load resistance

69

is exponentially increased from 10 $\mu\Omega$ to 1 MΩ. By doing this, it is possible to cover the entire rectifier operation range. The machine excitation angle is adjusted, and biases (which are ramped linearly from 0 over 1s to their required values) are added to the magnetizing flux inductances with the winding of the rotor shorted as described in Section 4.3.2. The magnitude of these biases have been defined in (4.8)–(4.9). The system is simulated using MATLAB/Simulink's ode23tb solver using the default tolerances and tolerances, and one simulation is for each machine angle. The maximum time step is set to 10 μ s.

The VBR model of the machine desribed in [1] and the dc link dynamics defined in (4.5)–(4.6) are simulated with an exact detailed switching model of the rectifier in Stateflow (rectifier model is described in Chapter 6). The system is simulated for 10 s. Average values of ac and dc voltages and currents (i.e. v_{qs}^r, v_{ds}^r, i_{qs}^r, i_{ds}^r, v_{dc}, i_{dc}, and v_c) are calculated, and subsequently used for calculating z, α, β, and ϕ. Some results from this method are shown in Figure 5.1. The plot shows the q-axis stator currents and voltages. It can be seen that they (currents and voltages) can be different for different angles of current (and machine angles by extension); the same cannot be inferred from the one-dimensional procedure advanced in [30]. These averaged values are then used in establishing the numerical relationships in (4.1)–(4.3).

5.3   Comparison of the multidimensional Fast and Slow Procedures

Results from the slow procedure in the previous chapter and the fast procedure herein are compared. They are essentially nearly the same, and will be shown in the figures in the course of the discussion in this section. Similar to the multidimensional slow procedure, the data obtained from the fast procedure herein is scattered as seen in Figure 5.2 and Figure 5.3. Therefore, gridded data required by MATLAB's spap2 algorithm for approximation must be obtained from this scattered data. The same process is employed for obtaining this gridded data in the z-$\angle\vec{i}$ space. However, to
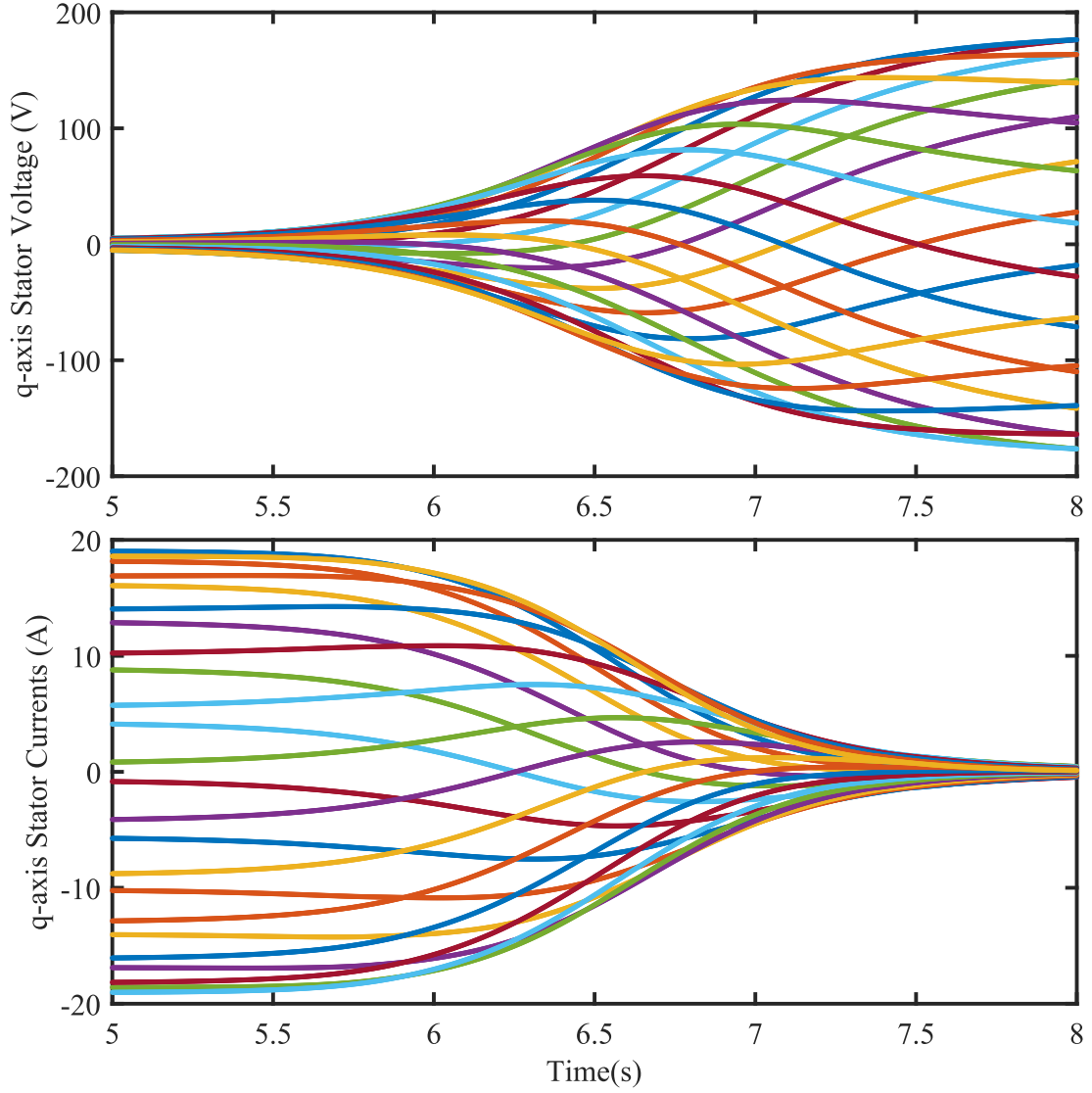
Figure 5.1: q-axis stator currents and voltages obtained from multidimensional fast procedure.

compare results from both procedures, identical grids are used for both procedures. Herein, it includes 2,386 z values that are logarithmically distributed from the minimum value of about 0.95 $\mu\Omega$ to the maximum value of 8.5 kΩ and 241 $\angle\vec{\vec{i}}$ values (approximately 10 times the original number of bias angle values) distributed from -180 ° to 180 ° with steps of 15 °. (More data points in the fast procedure is accounted for by the longer simulation time but has no effect on the results).

The lookup table for building an SSPAVM can then be determined from the gridded data using spap2 function in selecting 120 z knots and 25 $\angle\vec{\vec{i}}$ knots that best approximate (with least error) α, β, and ϕ using cubic interpolation. The problems of undersampling having an effect on the observed responses are resolved intentionally by selecting this large number of 120.

Figure 5.2: Scattered data sites from parameterization process using the two-dimensional fast procedure for base machine and rectifier.

The process is illustrated with both procedures for both the base machine-rectifier system and salient machine-rectifier systems described in Section 4.4. The fast and slow procedures are shown for the base machine with rectifier systems in Figure 5.4 and Figure 5.5, respectively, while the process for salient machine with rectifier systems is shown in Figure 5.6 and Figure 5.7. These figures show that gridded data can be extracted by oversampling the scattered data (angle values in this case) from above.

The explained procedures are carried out on both the salient and base-machine rectifier systems. The rectifier numerical functions from both the fast and slow pro-
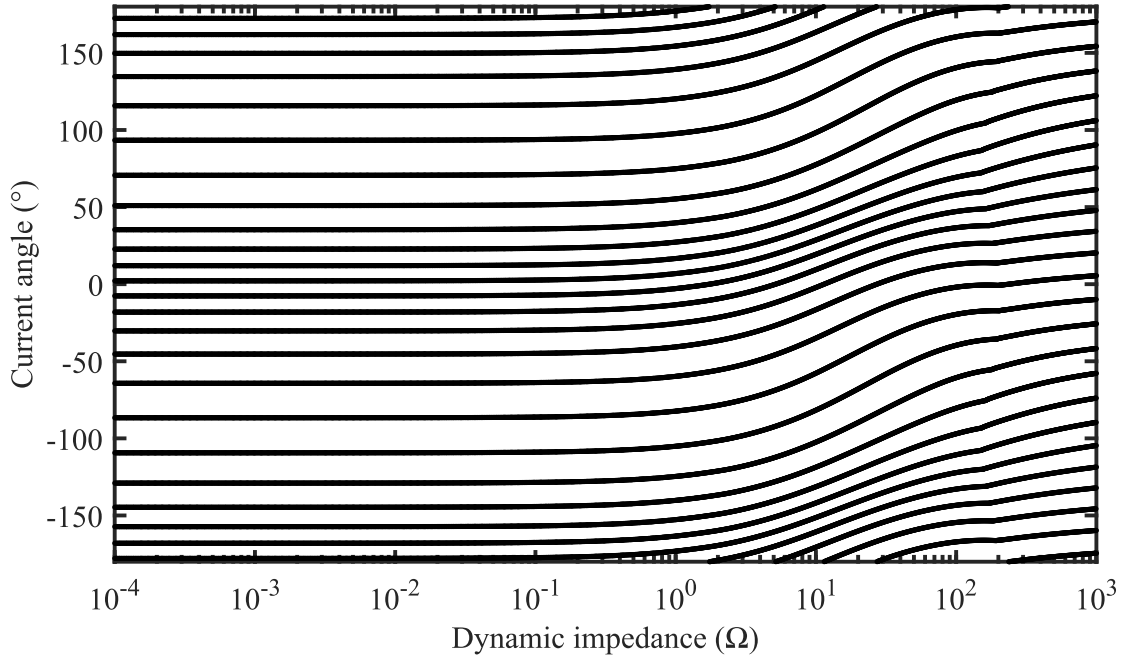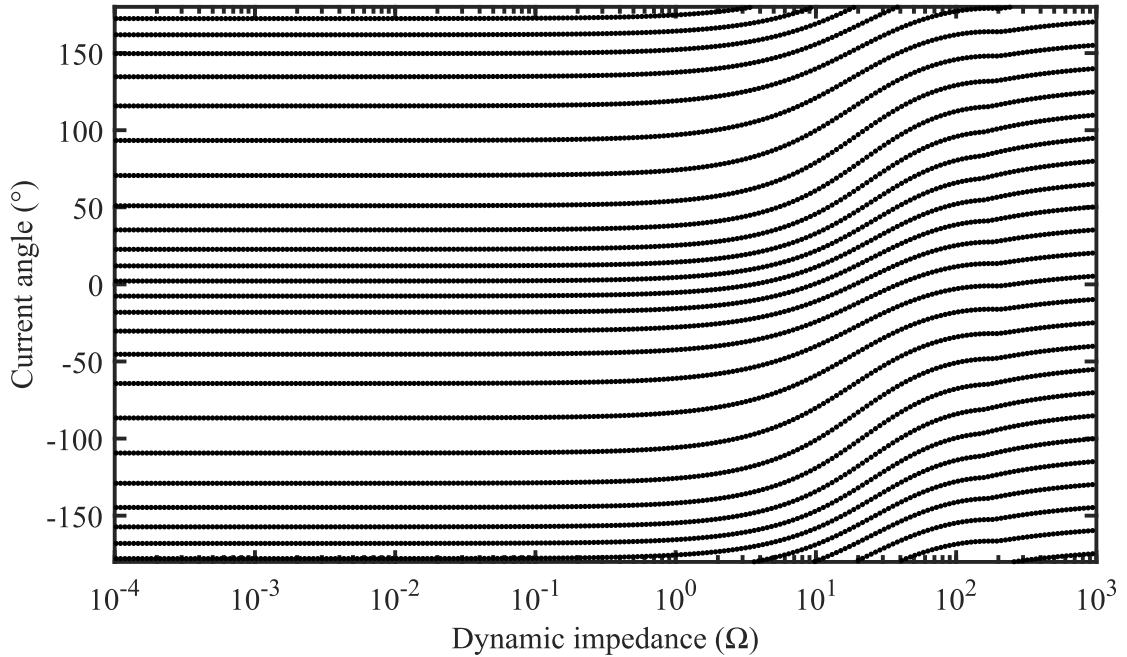
Figure 5.3: Scattered data sites from parameterization process using the two-dimensional 'slow' procedure for base machine and rectifier.

cedures for the base machine rectifier-systems are shown in Figure 5.8 and Figure 5.9, respectively.

Also, the rectifier numerical functions from both the fast and slow procedures for the salient machine rectifier-systems are shown in Figure 5.10 and Figure 5.11, respectively. These figures portray the raw values of the the functions α, β, and ϕ plotted vs the dynmaic impedance of the rectifier, z. From the figures, it can be seen that under some conditions, different values of α, β, and ϕ are predicted, and this is more obvious with the salient machine-rectifier system.

The extracted lookup table values using spap2 function as described above, are shown in the following figures. The lookup table values for the base machine-rectifier system using the fast and slow procedures are shown in Figure 5.12 and Figure 5.13, respectively.

Furthermore, the lookup table values for the salient machine-rectifier system using the fast and slow procedures are shown in Figure 5.14 and Figure 5.15, respectively.

Figure 5.4: Extraction of gridded data sites from scattered data for base machine and rectifier using the fast procedure.

These values of the multidimensional functions can be used for the development of an SSPAVM that will exhibit superior performance compared to previous PAVMs in dynamic conditions, particularly for salient machines with rectifiers.

5.3.1 Computation Time Comparison

To compare simulation times, the elapsed time between the start and end of simulation is measured. The time it takes to run the detailed model simulations using the fast procedure is about 1 hour, whereas it takes a simulation time of about 3 days to complete the detailed model simulations using the slow procedure to extract the parametric functions. This means there's a saving of more than 90% in terms of computational time, if the fast procedure is adopted rather than the slow procedure. The simulations are done using an Intel(R) Core(TM) i7-8750H CPU (2.20GHz and 16 GB of RAM).
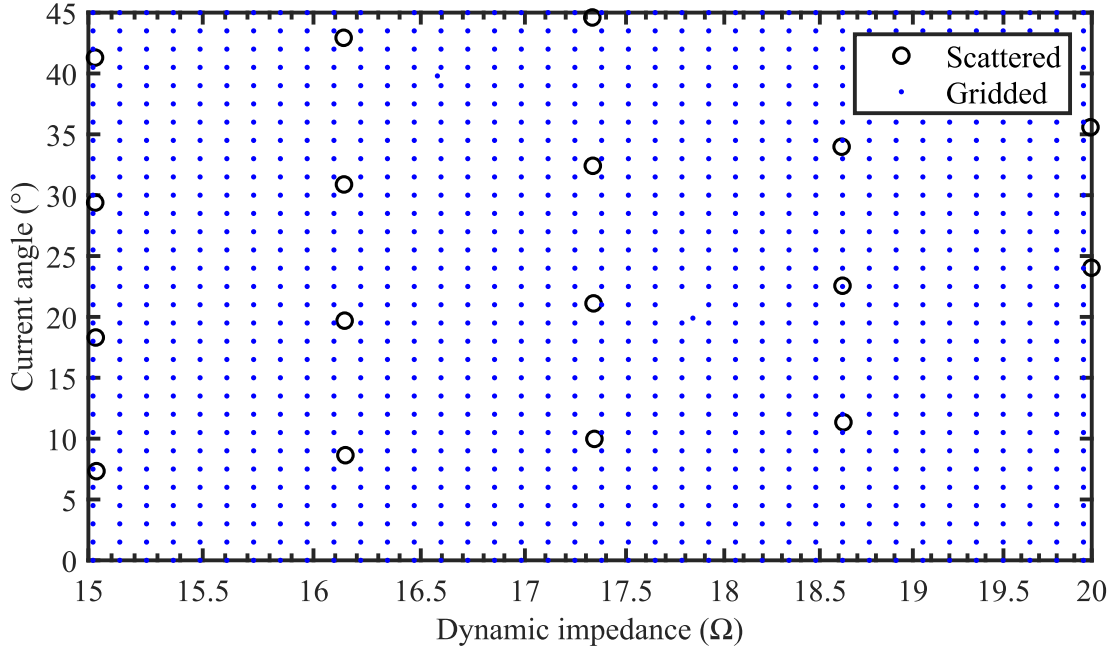
Figure 5.5: Extraction of gridded data sites from scattered data for base machine and rectifier using the slow procedure.

5.4 Approximation Error

The root mean squared error calculated by comparing the lookup table values obtained using spap2 algorithm with the raw values gotten from the slow and fast procedure simulations are tabulated in Table 5.1.

Table 5.1: Lookup Table Values Approximation Error

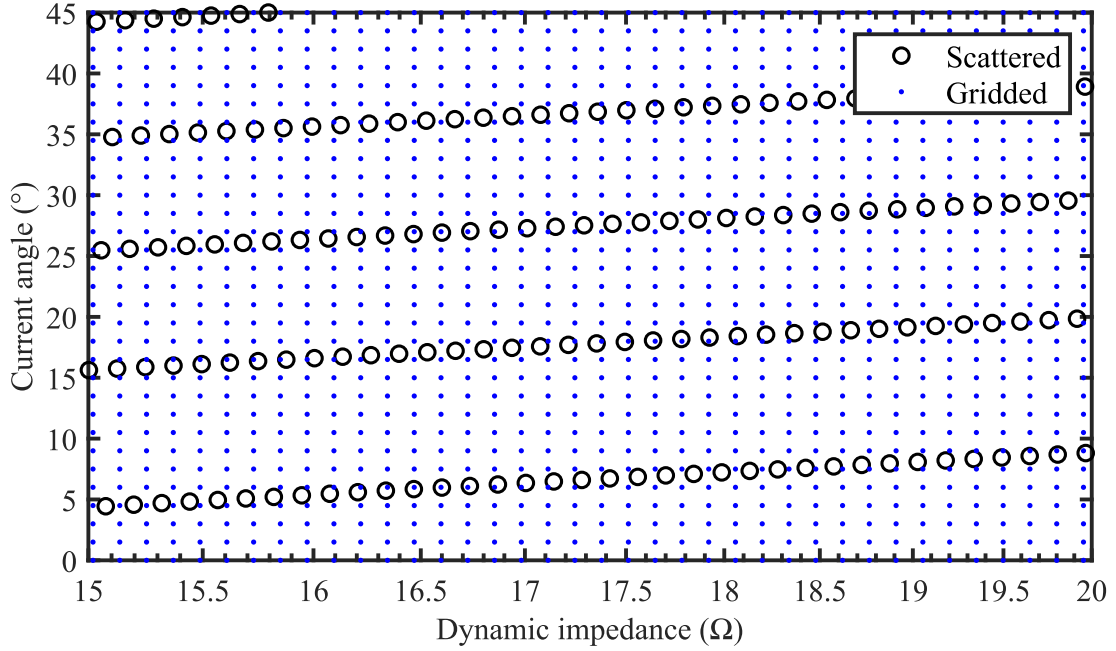| Machine	Functions	Fast Procedure	Slow Procedure
	α	0.0156	0.0066
Base Machine	β	0.0084	0.0121
	ϕ	0.1458	0.000757
	α	0.1712	0.0046
Salient Machine	β	0.0816	0.0091
	ϕ	1.6780	0.0029
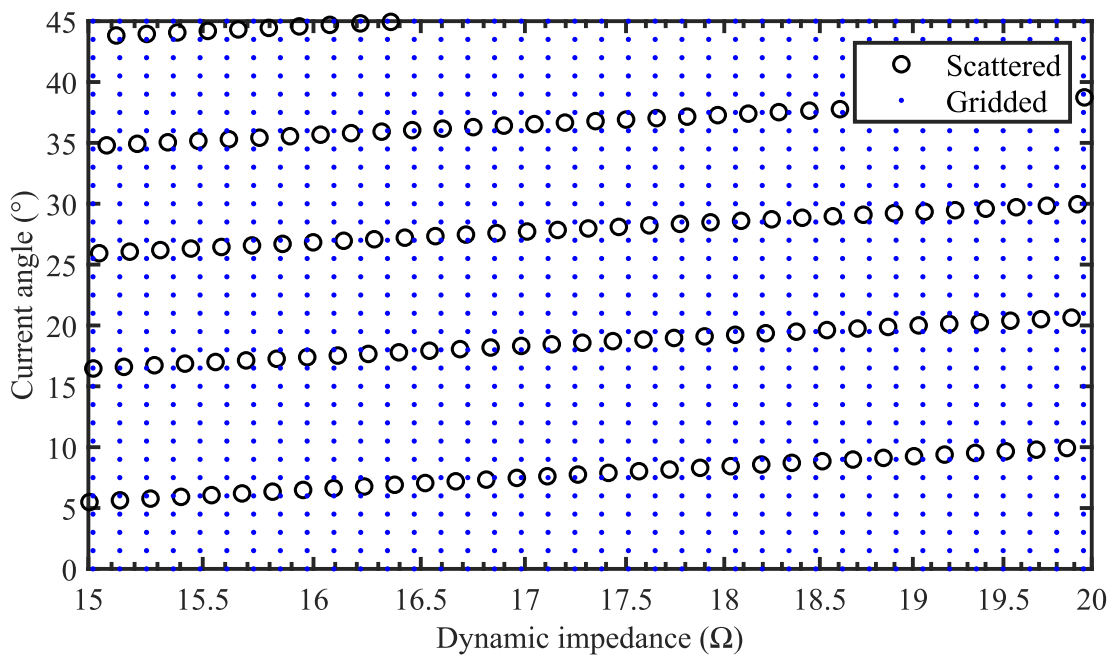
Figure 5.6: Extraction of gridded data sites from scattered data for salient machine and rectifier using the fast procedure.
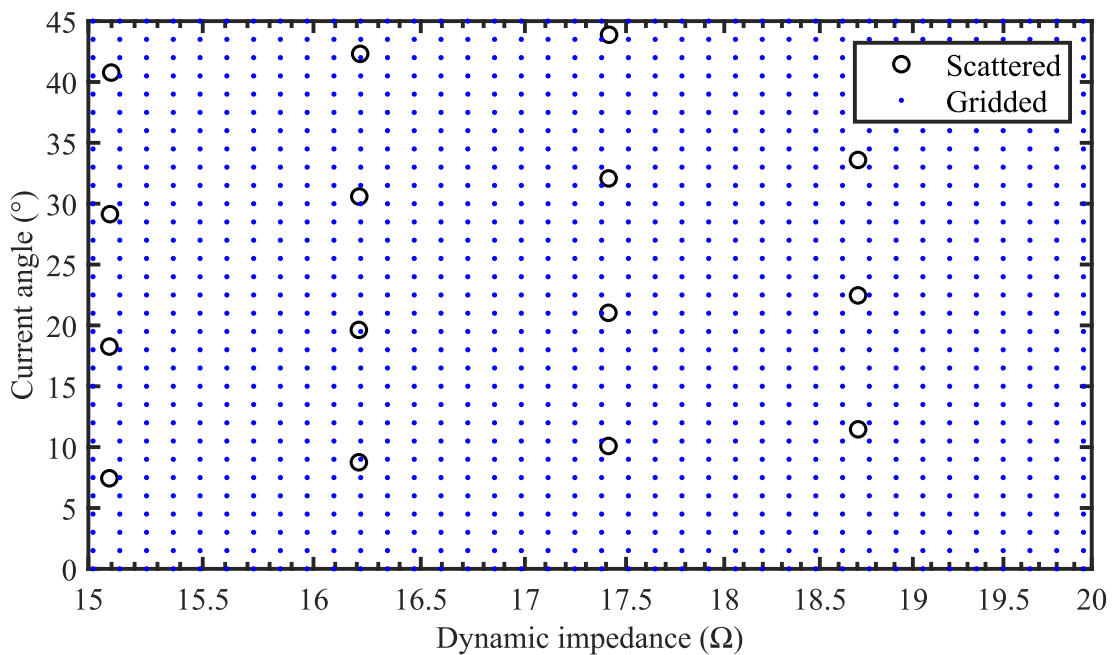
Figure 5.7: Extraction of gridded data sites from scattered data for salient machine and rectifier using the slow procedure.
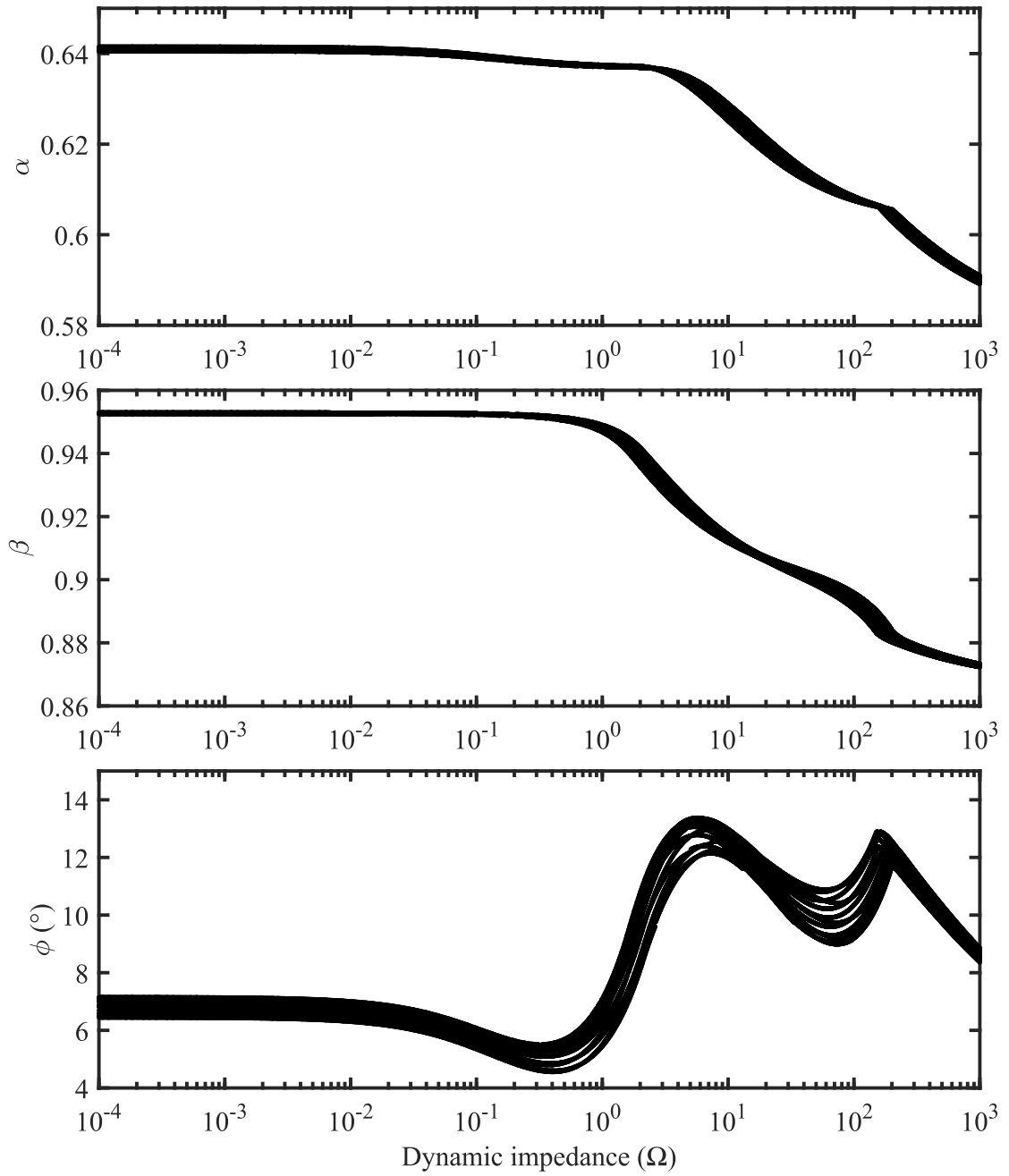
Figure 5.8: Parametric functions extracted from fast procedure for base machine with rectifier.
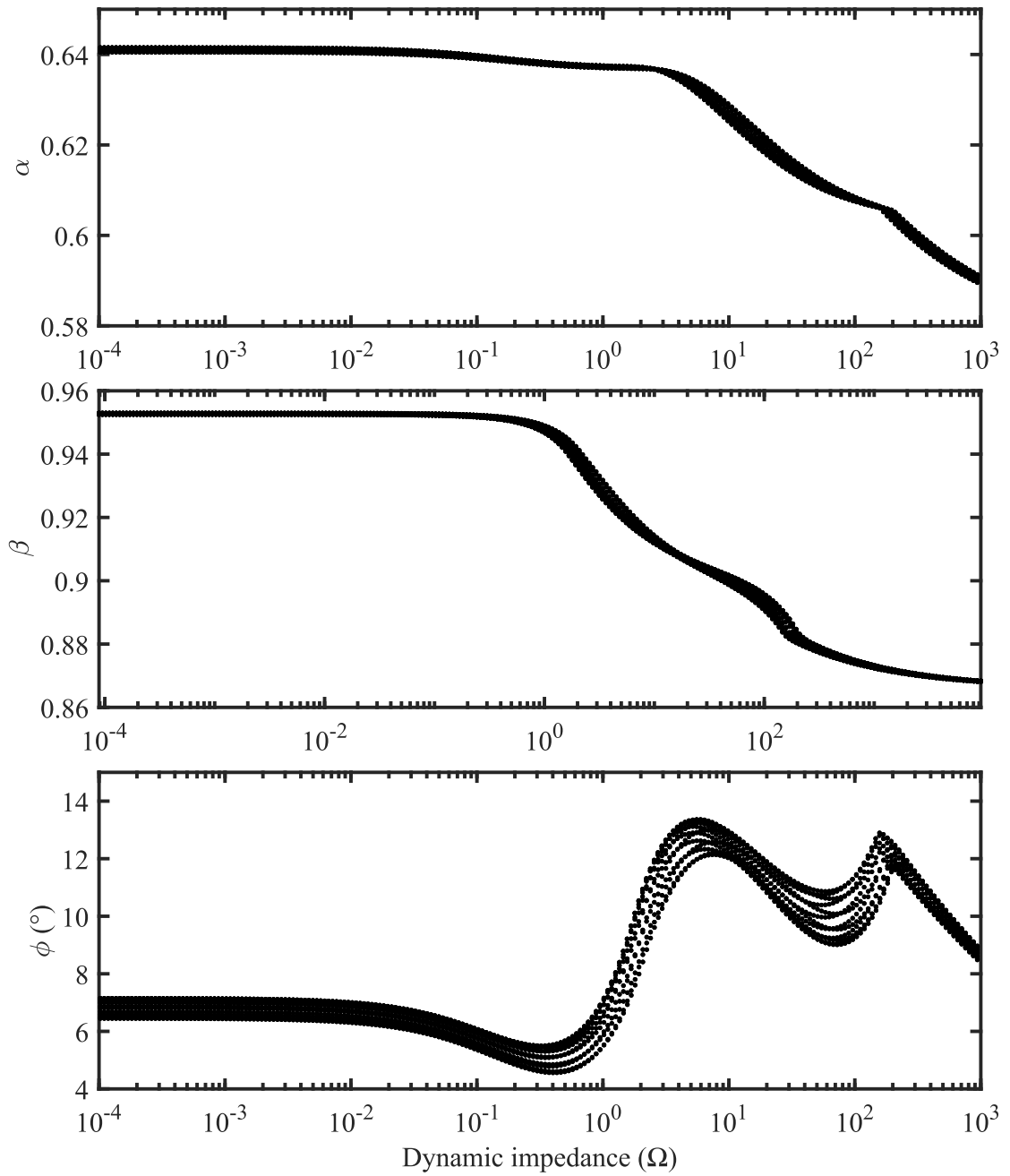
Figure 5.9: Parametric functions extracted from slow procedure for base machine with rectifier.
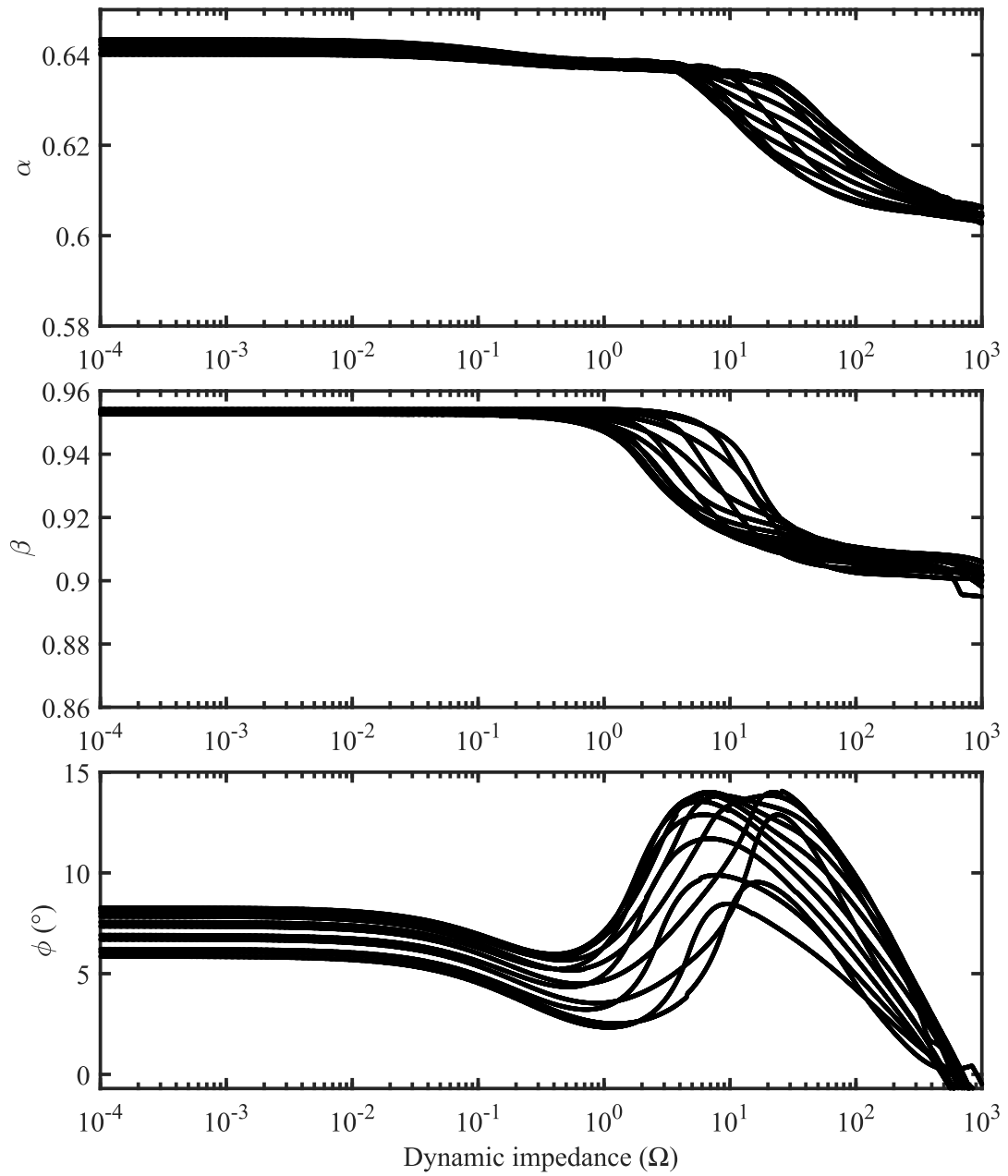
Figure 5.10: Parametric functions extracted from fast procedure for salient machine with rectifier. Fig will be be fixed
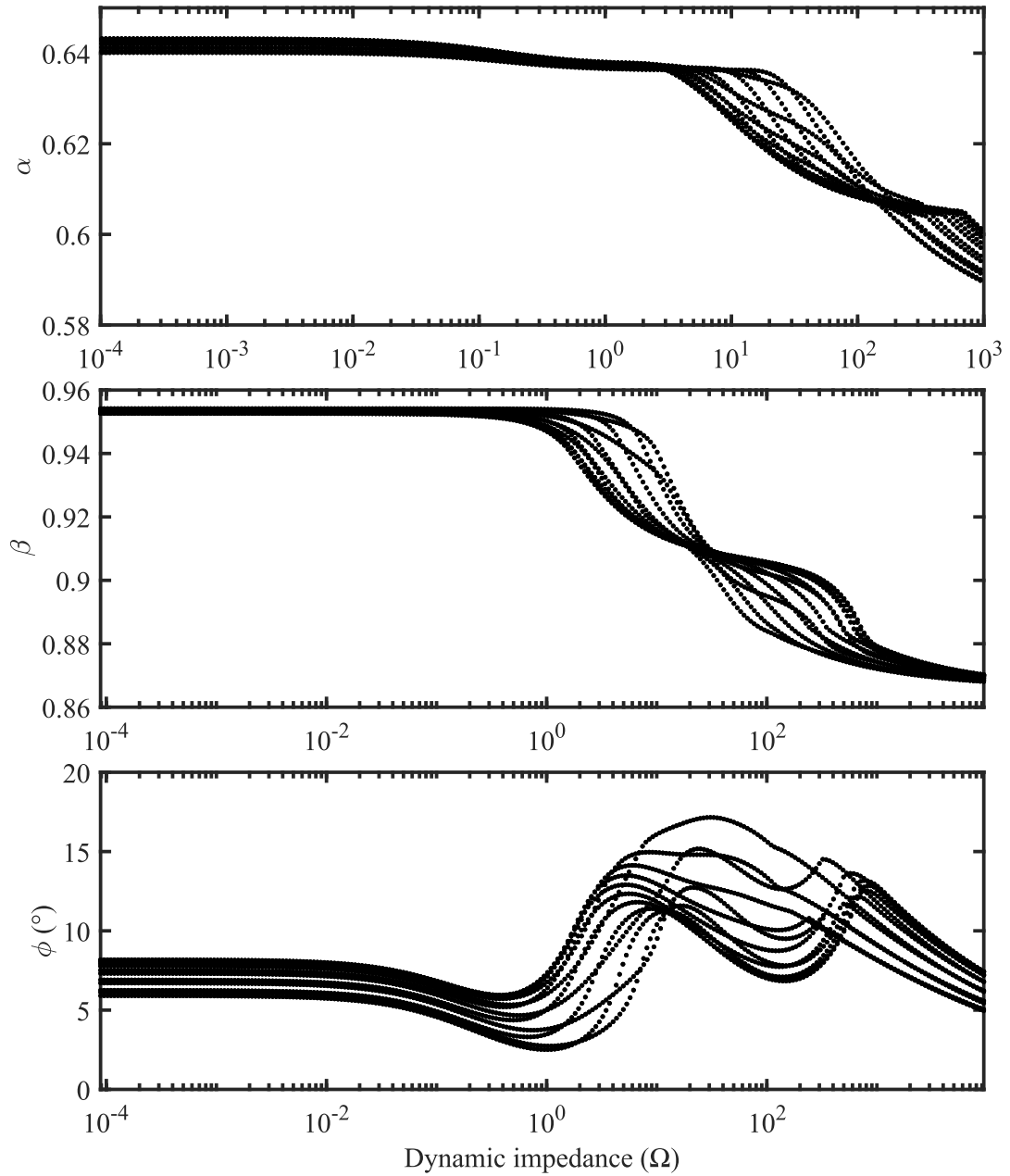
Figure 5.11: Parametric functions extracted from slow procedure for salient machine with rectifier.
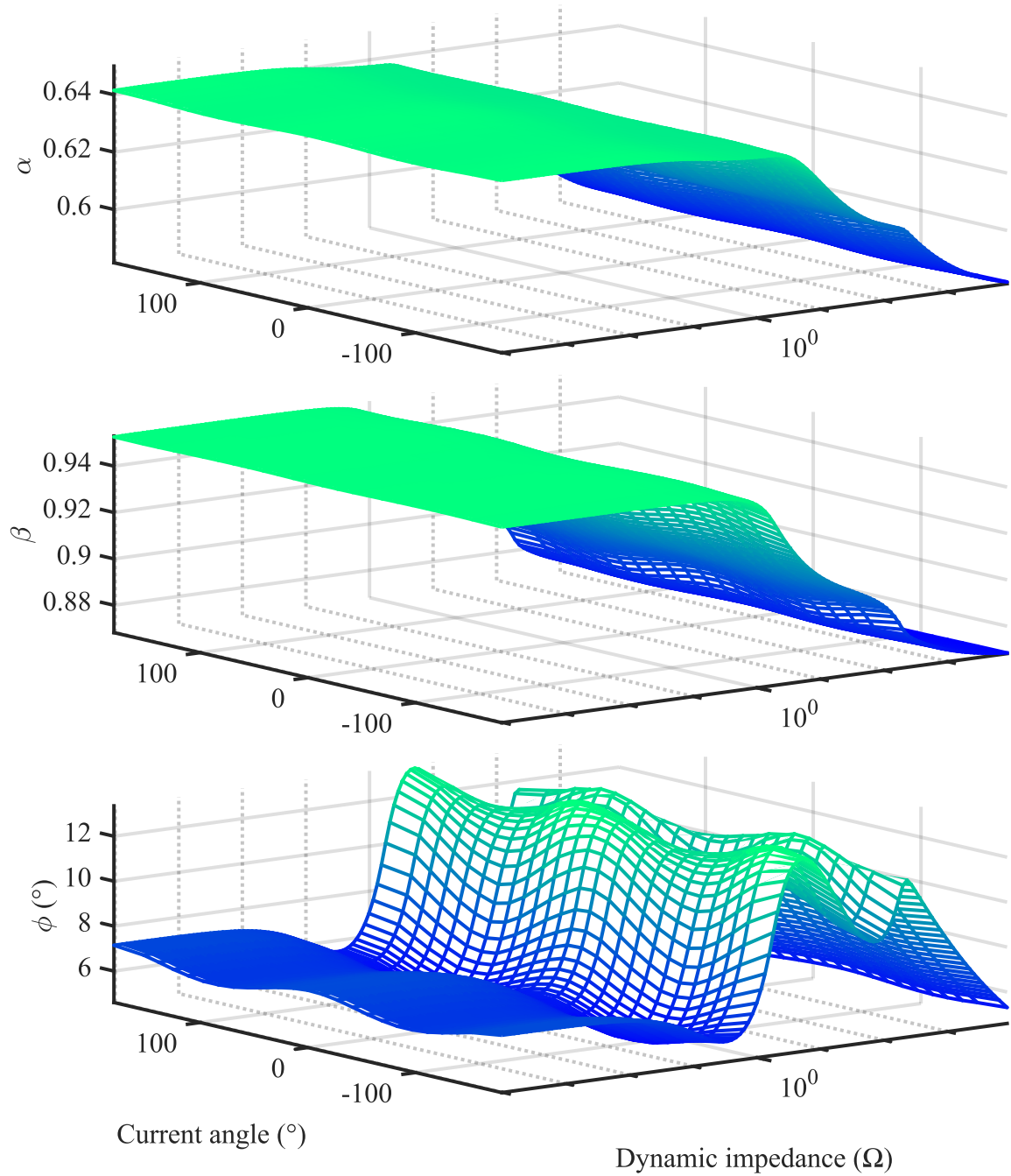
Figure 5.12: Proposed SSPAVM parametric functions table values extracted using fast procedure for base machine with rectifier.
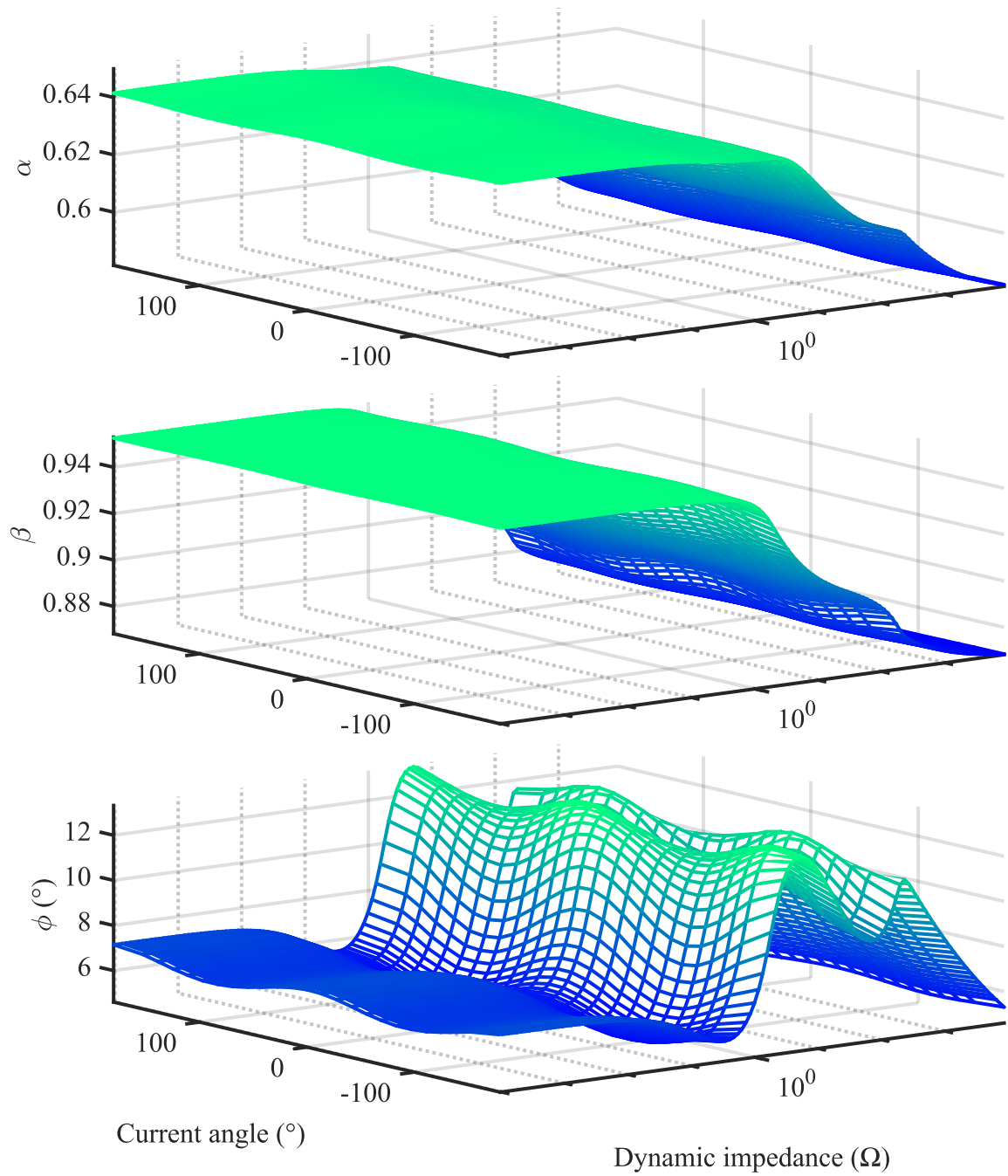
Figure 5.13: Proposed SSPAVM parametric functions extracted using slow procedure table values for base machine with rectifier.
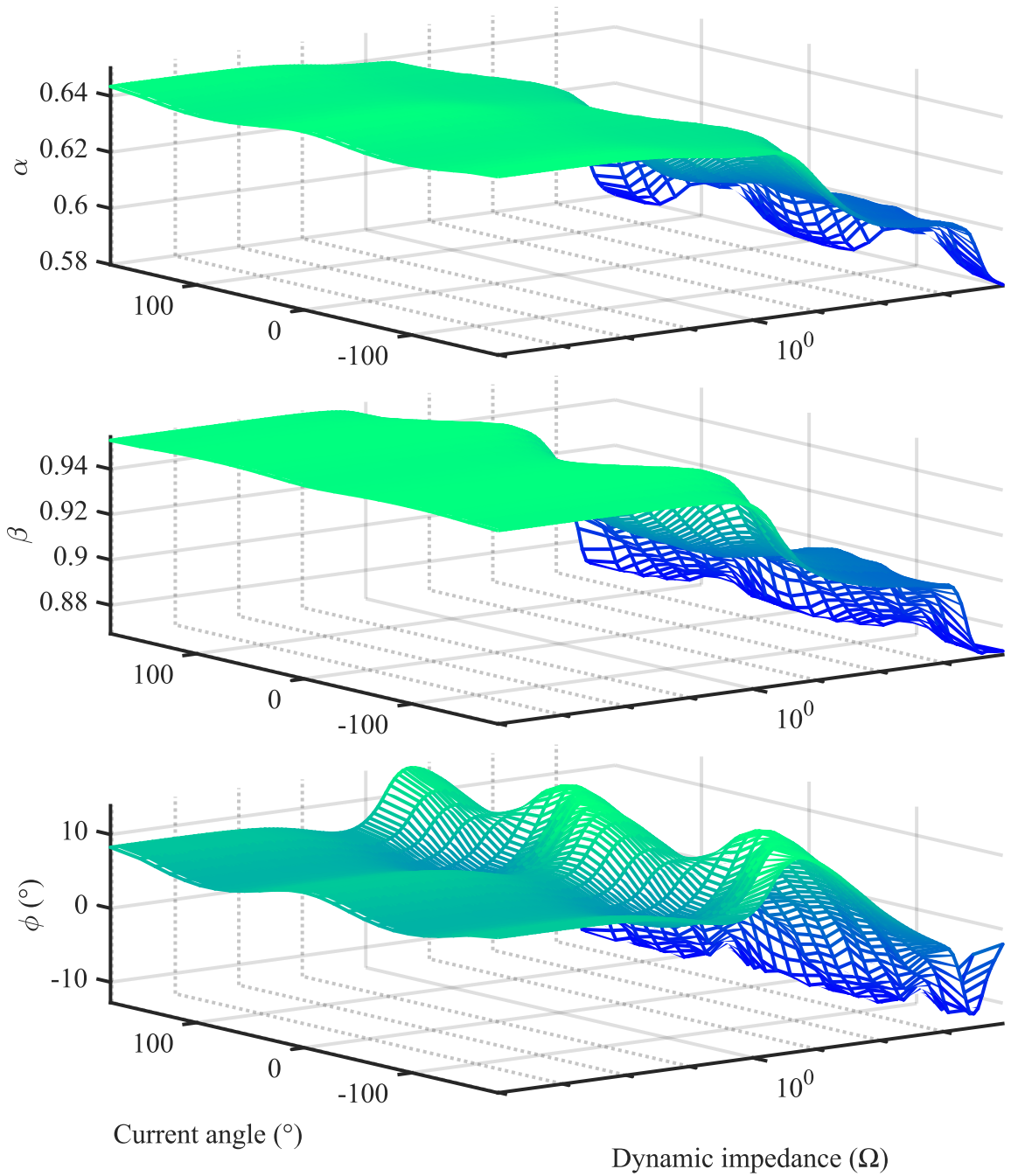
Figure 5.14: Proposed SSPAVM parametric functions table values extracted using fast procedure for salient machine with rectifier.
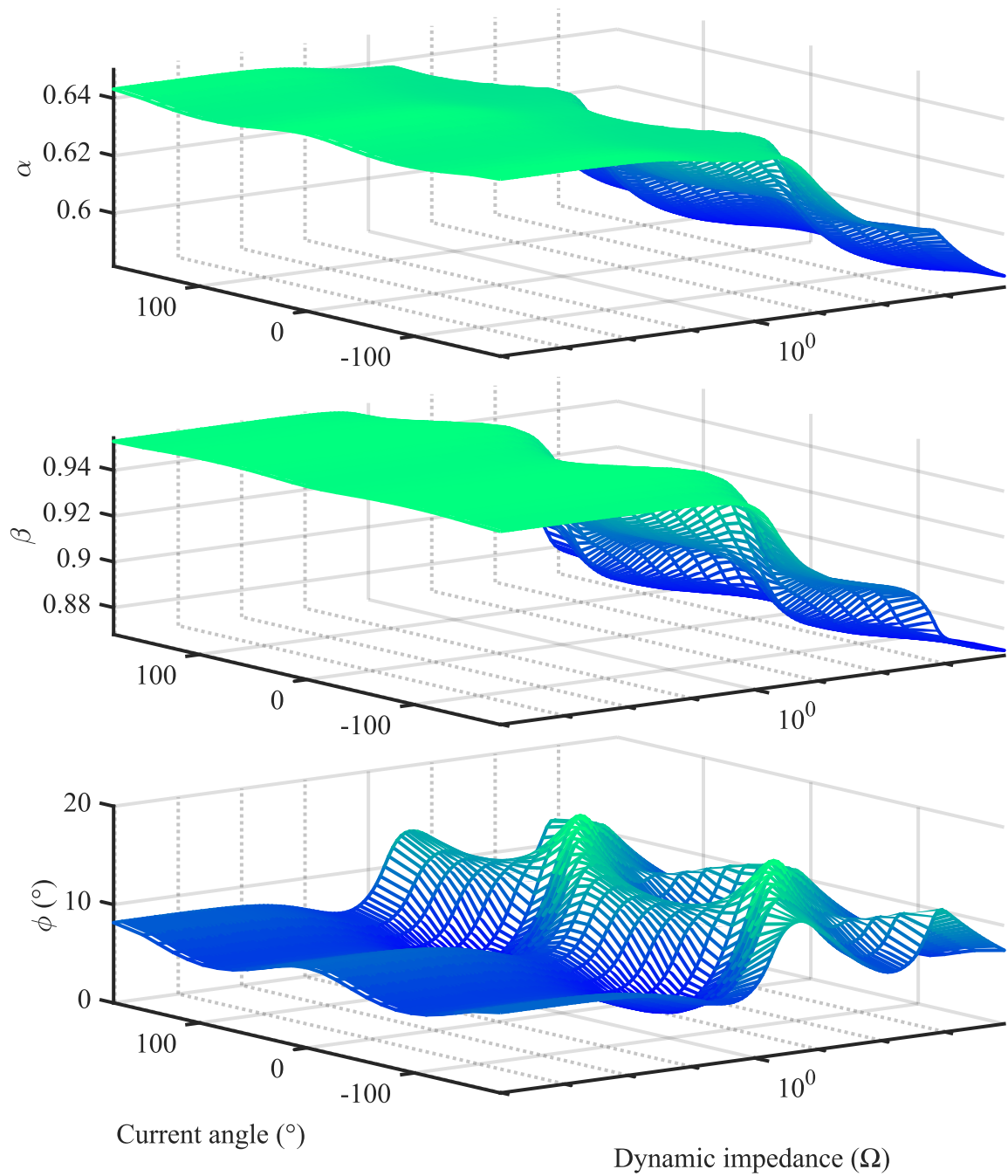
Figure 5.15: Proposed SSPAVM parametric functions table values extracted using slow procedure for salient machine with rectifier.

Chapter 6 Exact Detailed Rectifier Modeling as Hybrid System

6.1 Preamble

The conventional six-pulse diode rectifier are useful for power rectification (converting ac to dc) and operates in different modes. These operating or switching modes are determined by the conduction pattern of the diode, which futher depends on the loading condition of the rectifier. This loading condition therefore determines which and how many diodes may be ON or OFF at a time. The dc voltage waveform of the rectifier contains six pulses at every supply frequency cycle, hence the rectifier is commonly referred to as six-pulse rectifier [94]. A simplified diagram of the six-pulse diode rectifier is shown in Figure 6.1.
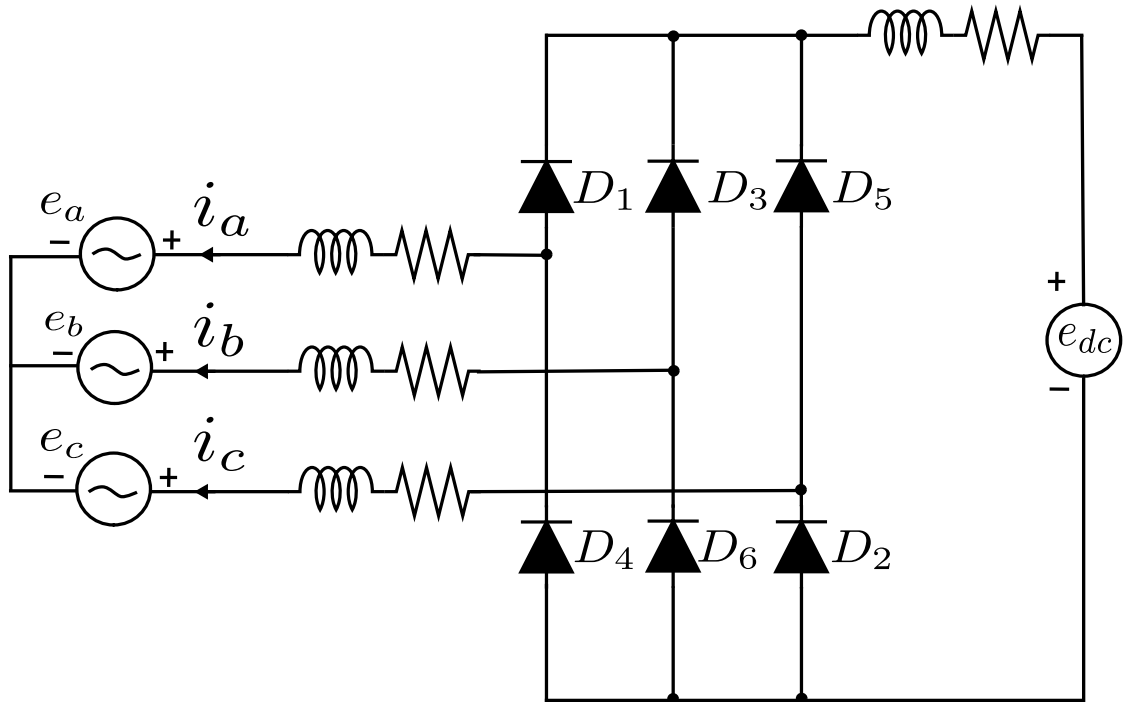
Figure 6.1: Six-pulse diode rectifier

6.2 Implementation as Hybrid System

To implement the rectifier model in Stateflow, the conduction pattern, rectifier transition conditions from one mode to another, and the interfacing governing differential equations (synchronous machine VBR model and the voltage across dc link inductor dynamics) at each state are considered.

$$v_{qs}^r = r_q'' i_{qs}^r + \omega_r L_d'' i_{ds}^r + pL_q'' i_{qs}^r + e_q'' \tag{6.1}$$

$$v_{ds}^r = r_d'' i_{ds}^r - \omega_r L_q'' i_{qs}^r + pL_d'' i_{ds}^r + e_d'' \tag{6.2}$$

$$v_{dc} = r_{dc} i_{dc} + L_{dc}\frac{di_{dc}}{dt} + e_{dc} \tag{6.3}$$

6.3 Simulation Variables

The important variables required for exact detailed modeling of the six-pulse diode rectifier are the input variables, output variables and the state variables. The input variables are e_{qd}'', e_{dc}, θ_r and ω_r. The output variables are v_{qds}^r, i_{qds}^r, v_{dc} and i_{dc}. There are essentially a maximum of three (3) continuous state variables. The number of state variables in a state can range from 0 to 3, depending on the conduction state.

Furthermore, the systematic modeling approach adopted herein considers the following diode conduction possibilities (or states):

1. No diode conducting (zero diode conduction).

2. Two (2) diodes conducting.

3. Three (3) conducting diodes (with two (2) diodes at the top).

4. Three (3) conducting diodes (with two (2) diodes at the bottom).

5. All six (6) diodes conducting.

These five (5) defined rectifier conduction possibilities are represented in State-flow environment as discrete states (with their respective nomenclatures herein given as 'Zero', 'Two', 'ThreeTwoUp', 'ThreeTwoDown', and 'All'). Each state has corresponding state actions which the stateflow model (the rectifier) must perform while that state is active. These actions are basically governing equations that calculates the voltage and current values at each state. Also, certain conditions must be met before a transition from one state to another can occur. The state actions, transition conditions, and transition actions are written in MATLAB language inside the matlab function block within the Stateflow environment.

6.4   Rectifier Conduction States

The block diagram of the rectifier model is shown in Figure 6.2. Each state is defined by a block, and the transitions between states are indicated by arrows to and fro the blocks.

6.4.1   The 'Zero' State

This is the default active state of the rectifier model at the start of simulation. In this state, There are no devices conducting, no voltage drop because there's no current. Hence, $v_{qds}^r = e_{qd}''$ and $v_{dc} = e_{dc}$. Also, there are no state variables as there are no changes in inductor currents with time. Therefore, the ac currents and dc currents are 0 ($i_{qds}^r = 0$ and $i_{dc} = 0$ respectively). Consequently, the current derivatives (pi_{dc}) are 0. The condition that must be **true** for a transition from this state to 'Two' state to occur, is that the line-to-line ac supply voltages at the rectifier ac side between any two phase must be greater than the dc voltage of the rectifier. That is, $|v_{ab}|$ or $|v_{ac}|$ or $|v_{bc}|$ must be greater than v_{dc}. If any of these conditions becomes **true**, two diodes become forward biased; then the system transitions to two diodes conducting (i.e. transition into the so called 'Two' state) with active diodes selected according to
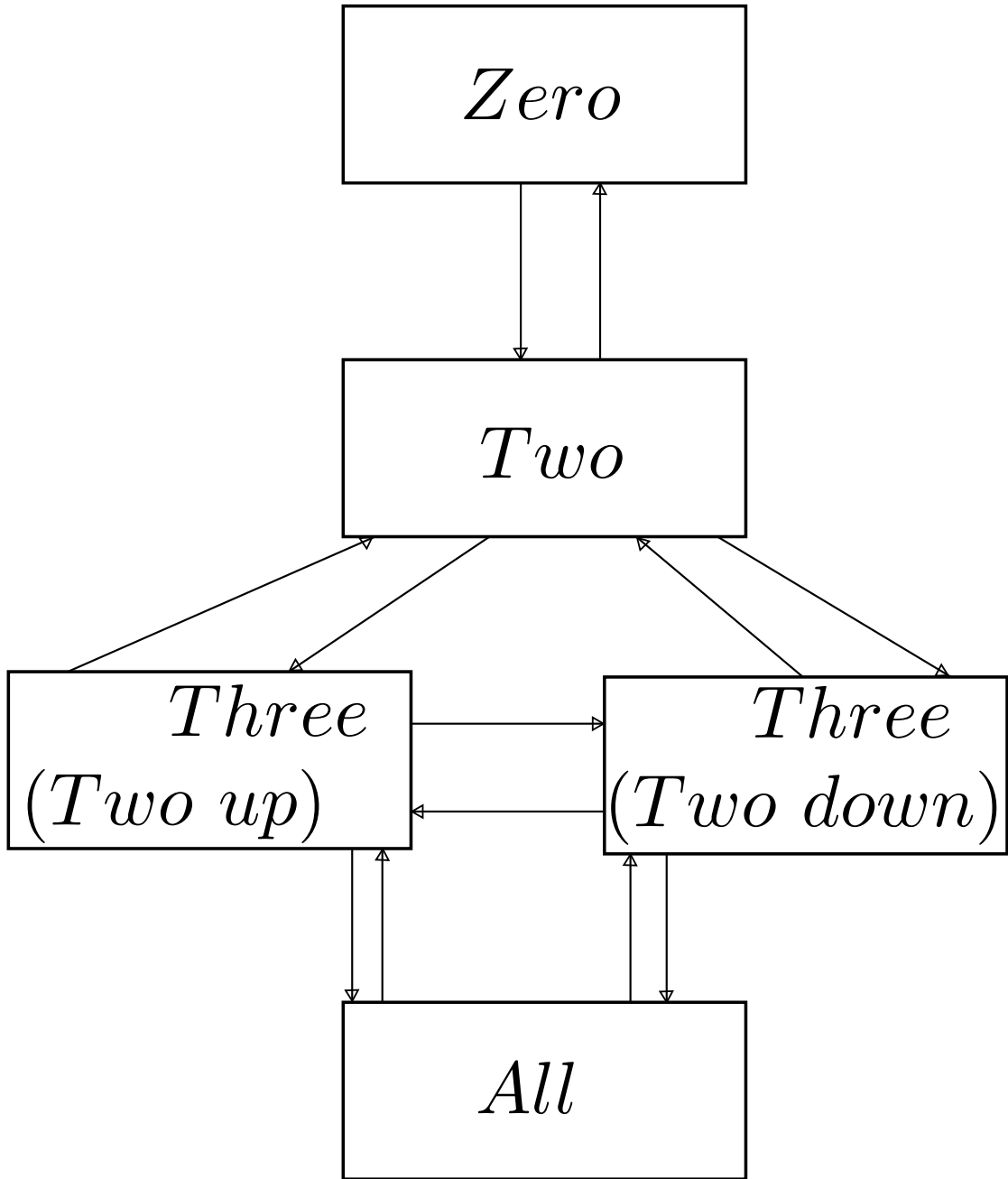
Figure 6.2: Rectifier conduction states

which of the ac phase voltages is greater than the dc voltage. The ac phase voltages are calculated as follows:

$$\mathbf{v_{abcs}} = \mathbf{K_s} \mathbf{v_{qds}^r} \tag{6.4}$$

$\mathbf{K_s}$ is Park's transformation defined in the Appendix.

If v_{ab} is greater than v_{dc} with v_a greater than v_b, then the conducting branches are in phases a and b, with upper conducting diode as D_1 and the lower conducting diode as D_6, and the nonconducting branch is phase c.

If v_{ab} is greater than v_{dc} with v_b greater than v_a, then the conducting branches are in phases a and b, with upper conducting diode as D_3 and the lower conducting diode as D_4, and the nonconducting branch is phase c.

If v_{ac} is greater than v_{dc} with v_a greater than v_c, then the condu cting branches are in phases a and c, with upper conducting diode as D_1 and the lower conducting diode as D_2, and the nonconducting branch is phase b.

If v_{ac} is greater than v_{dc} with v_c greater than v_a, then the conducting branches are in phases a and c, with upper conducting diode as D_5 and the lower conducting diode as D_4, and the nonconducting branch is phase b.

If v_{bc} is greater than v_{dc} with v_b greater than v_c, then the conducting branches are in phases b and c, with upper conducting diode as D_3 and the lower conducting diode as D_2, and the nonconducting branch is phase a.

If v_{bc} is greater than v_{dc} with v_c greater than v_b, then the conducting branches are in phases b and c, with upper conducting diode as D_5 and the lower conducting diode as D_6, and the nonconducting branch is phase a.

6.4.2 The 'Two' State

In this state, there are two diodes conducting (which maybe Diodes D_1 and D_6, D_1 and D_2, etc.). The state variable is the dc current, i_{dc}. The current and voltage selector matrices is used to assign values to the conducting and nonconducting diodes. That is, the selector matrices select values based on diode conditions. The current selector matrix assigns a value which may be (-1,0,1) to the diodes. These values mainly indicate whether the diode is conducting or not, and the sign (+ or -) indicate

the direction of the flow of current. For instance, the upper diode is assigned the value of -1; indicating that

1. It is an active (conducting) diode, and

2. The flow of current is in the reverse direction away from the rectifier into the machine.

The lower conducting diode is assigned a value of 1 indicating that:

1. It is an active (conducting) diode, and

2. Current flow is in the direction toward the rectifier.

Through the voltage selector matrix $\mathbf{P_v}$, a value of 1 is assigned to each of the conducting branches. Selector matrices are defined such that

$$\mathbf{i_{abcs}} = \mathbf{P_i} i_{dc} \tag{6.5}$$

$$\mathbf{v_{abcg}} = \mathbf{P_v} \begin{bmatrix} v_{dc} \\ v_{ng} \end{bmatrix} \tag{6.6}$$

(6.1)–(6.3) are then solved to obtain values for the unknown variables such as dc voltage; v_{dc}, voltage across the 'n-branch' (non-conducting diode terminal in the zero state) v_{ng}, and the derivative of the state variable- dc current; pi_{dc}. Consequently, the value of the ac currents and voltages in the $q-d$ axis are calculated thus:

$$\mathbf{i^r_{qds}} = \mathbf{K_s} \mathbf{P_i} i_{dc} \tag{6.7}$$

$$\mathbf{v^r_{qds}} = \mathbf{K_s} \mathbf{P_v} \begin{bmatrix} v_{dc} \\ v_{ng} \end{bmatrix} \tag{6.8}$$

90

$\mathbf{P_i}$ is the current selector matrix. Depending on which transition condition is met, there are three (3) transition possibilities from this state;

(i) 'TwoZero' transition (indicating a transition from two diodes conducting to no diode conducting). For 'TwoZero' transition to occur, the condition that must be **true** is that the rectifier dc current and its derivative must be less than or equal to zero (i.e. $i_{dc} \leq 0$ and $pi_{dc} \leq 0$).The diodes become reverse biased. The ac current becomes 0 and the transition occurs.

(ii) 'TwoThreeTwoUp' transition (indicating a transition from **Two** diodes conducting to **Three** diodes conducting, with two of the three conducting diodes at the top of the diode rectifier configuration).

For 'TwoThreeTwoUp' (with two of the three conducting diodes at the top) transition to occur, $v_{ng} \geq v_{dc}$. If this condition holds **true**, then the state variable (current) becomes 0, and the transition occurs.

(iii) 'TwoThreeTwoDown' transition (indicating a transition from **Two** diodes conducting to **Three** diodes conducting, with two of the three conducting diodes at the bottom of the diode rectifier configuration).

For 'TwoThreeTwoDown' (with two of the three conducting diodes at the bottom) transition to occur, $v_{ng} \leq 0$. If this condition holds **true**, then the state variable (current) becomes 0, and the transition occurs.

6.4.3 The 'ThreeTwoUp' State

This state is so named to naturally represent number of conducting diodes and their location in the diode rectifier configuration. In this state, there are three diodes conducting (with two upper diodes conducting including phase n). The two state variables are the dc currents, i_{dc} and i_{ns} through the conducting diodes. The current and voltage selector matrices are used to assign values to the conducting and

nonconducting diodes. That is, the selector matrices selects values based on diode conditions. The current selector matrix assigns a value which may be (-1,0,1) to the diodes. These values mainly indicate whether the diode is conducting or not, and the sign (+ or -) indicate the direction of the flow of current. For instance, a value value of -1 to diodes indicate that:

1. They are actively conducting

2. The current flow is in the reverse direction away from the rectifier into the machine.

A value of 1 to indicate that a diode

1. is actively conducting

2. The current flows into the rectifier.

Through the voltage selector matrix, a value of 1 is assigned to each of the conducting diodes. $\mathbf{P_i}$ and $\mathbf{P_v}$ are defined such that

$$\mathbf{i_{abcs}} = \mathbf{P_i} \begin{bmatrix} i_{dc} \\ i_{ns} \end{bmatrix} \tag{6.9}$$

$$\mathbf{v_{abcg}} = \mathbf{P_v} v_{dc} \tag{6.10}$$

(6.1) –(6.3) are then solved to obtain values for the unknown variables such as dc voltage; v_{dc}, and the derivative of the state variables (currents); pi_{dc} and pi_{ns}. The value of the ac currents and voltages in the $q - d$ axis is then calculated using

$$\mathbf{i_{qds}^r} = \mathbf{K_s P_i} \begin{bmatrix} i_{dc} \\ i_{ns} \end{bmatrix} \tag{6.11}$$

$$\mathbf{v_{qds}^r} = \mathbf{K_s P_v} v_{dc} \tag{6.12}$$

92

If one of the two upper conducting diode's current (and derivatives) become non-positive, that diode will become reverse biased and stop conducting. If turning off that diode results in forward biasing the lower diode in that phase, then the rectifier transitions to "ThreeTwoDown". Otherwise, it transitions to 'Two'. If $v_{dc} \leq 0$, all diodes are forward biased, and the rectifier transitions to "All" conduction mode. Depending on which transition condition is met, there are three (3) transition possibilities from this state, namely;

(i) Transition to 'Two' state wherein only two diodes conduct. To transition from this state to 'Two' state, the condition that must be **true** is that $v_{ng} > 0$.

(ii) Transition to 'ThreeTwoDown' state (with 2 of the 3 conducting diodes at the bottom of the diode rectifier configuration). To transition to 'ThreeTwoDown' state, it must be **true** that $v_{ng} \geq v_{dc}$.

(iii) Transition to 'All conducting state (where all the diodes conduct). To transition to 'All' state, it must be **true** that $v_{dc} \leq 0$.

6.4.4 The 'ThreeTwoDown' State

Again, this state is so named to naturally represent number of conducting diodes and their location in the diode rectifier configuration. In this state, there are three diodes conducting (with two of the three conducting diodes at the bottom). The state variables are the dc currents, i_{dc} and i_{ns} through the conducting diodes. The current and voltage selector matrices is used to assign values to the conducting and nonconducting diodes. That is, the selector matrices selects values based on diode conditions. The current selector matrix assigns a value which may be (-1,0,1) to the diodes. These values mainly indicate whether the diode is conducting or not, and the sign (+ or -) indicate the direction of the flow of current. For instance, the upper active diode are assigned the value of -1; indicating that:

1. It is actively conducting

2. The current flow is in the reverse direction away from the rectifier into the machine.

In the same vein, the lower conducting diode is assigned a value of 1 to indicate that:

1. It is actively conducting

2. The current flow is into the rectifier.

Through the voltage selector matrix, a value of 1 is assigned to each of the conducting diodes. $\mathbf{P_i}$ and $\mathbf{P_v}$ are defined such that

$$\mathbf{i_{abcs}} = \mathbf{P_i} \begin{bmatrix} i_{dc} \\ i_{ns} \end{bmatrix} \tag{6.13}$$

$$\mathbf{v_{abcg}} = \mathbf{P_v} v_{dc} \tag{6.14}$$

(6.1) –(6.3) are then solved to obtain values for the unknown variables such as dc voltage; v_{dc}, and the derivative of the state variables (currents); pi_{dc} and pi_{ns}. The value of the ac currents and voltages in the $q - d$ axis is then calculated using

$$\mathbf{i^r_{qds}} = \mathbf{K_s P_i} \begin{bmatrix} i_{dc} \\ i_{ns} \end{bmatrix} \tag{6.15}$$

$$\mathbf{v^r_{qds}} = \mathbf{K_s P_v} v_{dc} \tag{6.16}$$

If one of the two lower conducting diode's current (and derivatives) become non-positive, that diode will become reverse biased and stop conducting. If turning off that diode results in forward biasing the upper diode in that phase, then the rectifier

94

transitions to "ThreeTwoUp". Otherwise, it transitions to 'Two". If $v_{dc} \leq 0$, all diodes are forward biased, and the rectifier transitions to "All" conduction mode. Depending on which transition condition is met, there are three (3) transition possibilities from this state, namely;

(i) Transition to 'Two' state wherein only two diodes conduct. To transition from this state to 'Two' state, the condition that must be **true** is that $v_{ng} < v_{dc}$.

(ii) Transition to 'ThreeTwoUp' state (with 2 of the 3 conducting diodes at the top of the diode rectifier configuration). To transition to 'ThreeTwoUp' state, it must be **true** that $v_{ng} \geq v_{dc}$. To transition to 'All' state, then it must be **true** that $v_{dc} \leq 0$.

(iii) Transition to "All" conducting state (where all the diodes conduct).

6.4.5   The 'All' State

In this state, all six diodes conduct. The state variables are the dc currents i_{dc}, and ac currents in the $q - d$ axis (i_{qs}^r and i_{ds}^r). Also, the dc voltage v_{dc}, and ac voltages (v_{qs}^r and v_{ds}^r) are 0. (6.1) –(6.3) are then solved to obtain values for the unknown variables such as dc voltage; the derivative of the state variables (currents); pi_{dc}, pi_{qs}^r, and pi_{ds}^r. Depending on which transition condition is met, there are two (2) transition possibilities from this state, namely;

(i) Transition to 'ThreeTwoUp' state (with 2 of the 3 conducting diodes at the top of the diode rectifier configuration). To transition from the "all" state to 'ThreeTwoUp' state, the condition that must be **true** is that:

    a) the dc current must be less than or equal to the sum of positive ac currents.

    b) Also, this dc current derivative must be less than or equal to the sum of the derivatives of this positive ac currents.

c) In addition, the median value of the ac currents should be less than 0.

(ii) Transition to 'ThreeTwoDown' state (with 2 of the 3 conducting diodes at the bottom of the diode rectifier configuration). To transition from the "all" state to 'ThreeTwoDown' state, the condition that must be **true** is that:

   a) the dc current must be greater than the sum of positive ac currents.

   b) Also, this dc current derivative must be greater than the sum of the derivatives of this positive ac currents.

   c) In addition, the median value of the ac currents should be greater than 0.

6.5   Rectifier Conduction Modes Using Model Demonstration

There are basically four rectifier conduction modes; so named to signify transition from one state to another. The conduction modes are 0-2, 2-3, 3-3 and 3-6 conduction modes. The discussion below focuses on demonstrating the various conduction modes in simulation. Appropriate load resistances that demonstrate the desired conduction modes are utilized. Furthermore, to test for the model conduction modes, the model parameters used are listed in Table 6.1.

The parameters for demonstrating the rectifier conduction modes are shown in Table 6.1.

Table 6.1: Rectifier Conduction Modes Test Parameters

$\omega_b = 2\pi 60$ rad/s	$r_{dc} = 0$ Ω
$L_q'' = 2.7$ mH	$L_d'' = 1.9$ mH
$r_q'' = 1.57$ Ω	$r_d'' = 1.49$ Ω
$L_{dc} = 1.19$ mH	$C_{dc} = 4.9$ mF
$e_q'' = 32$ V	$e_d'' = -76$ V

6.5.1   0-2 conduction mode

In this rectifier switching mode, the conduction is such that it switches between no diode conducting to two diodes conducting. The condition under which this happens is generally under very high load resistance scenarios. Figure 6.3 shows a block diagram indicating the transitions occuring in this conduction mode. The actual mode transitions, the voltage, and current waveforms are shown for this conduction mode in Figure 6.4. The dc load resistance, R_{load} used to test for this conduction mode is 10 kΩ.

6.5.2   2-3 Conduction Mode

In this rectifier switching mode, the conduction is such that it switches between two diodes conducting to three diodes conducting. Figure 6.5 shows a block diagram indicating the transitions occuring in this conduction mode. The actual mode transitions, the voltage, and current waveforms are shown for this conduction mode in Figure 6.6. The dc load resistance, R_{load} used to test for this conduction mode is 100 Ω.

6.5.3   3-3 Conduction Mode

In this rectifier switching mode, the conduction is such that it switches between three diodes (two up) conducting to three diodes(two down) conducting. Figure 6.7 shows a block diagram indicating the transitions occuring in this conduction mode. The actual mode transitions, the voltage, and current waveforms are shown for this conduction mode in Figure 6.8. The dc load resistance, R_{load} used to test this conduction mode is 1 Ω.

6.5.4   3-6 Conduction Mode

In this rectifier switching mode, the conduction is such that it switches between three diodes conducting to six diodes conducting. The condition under which this
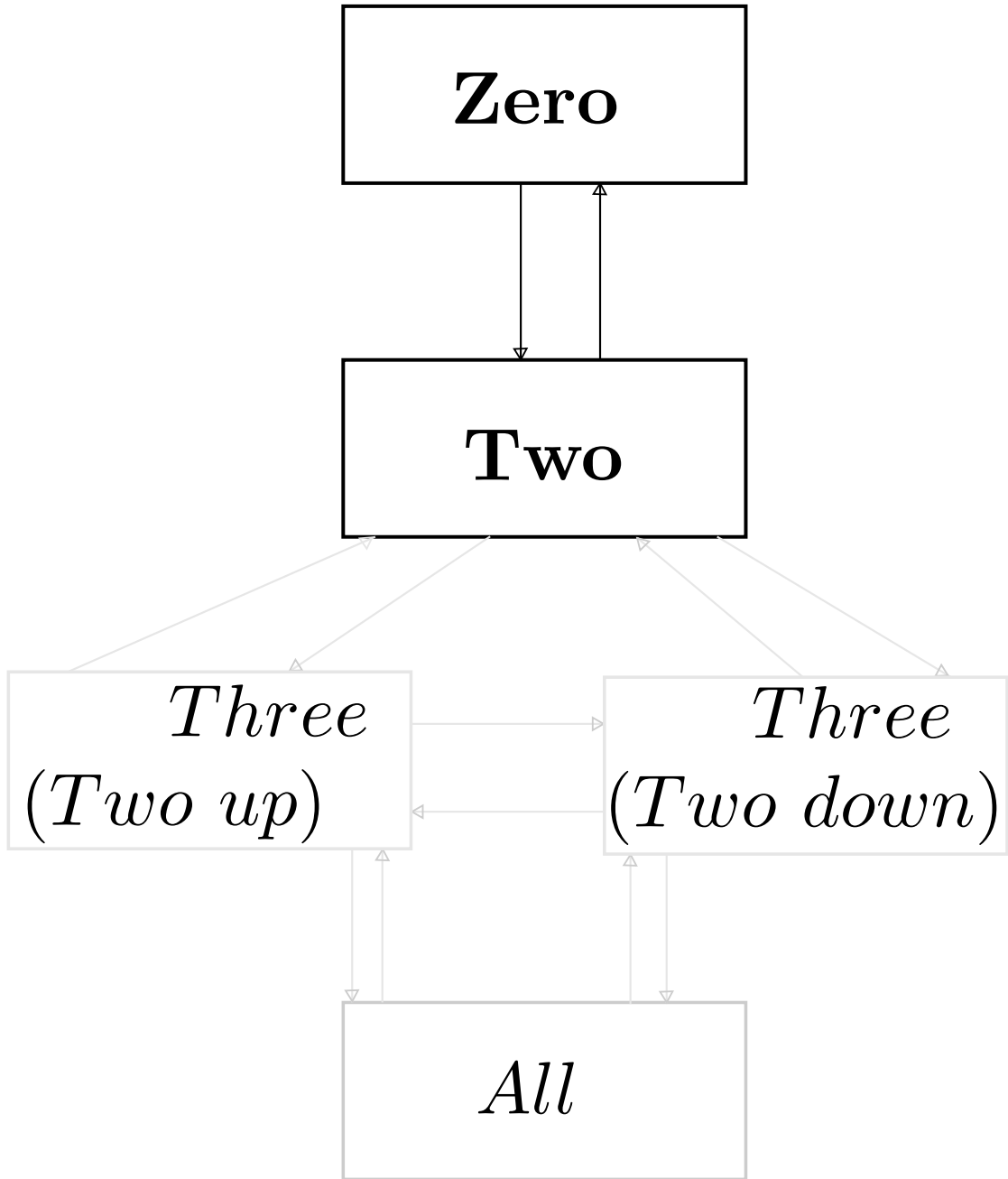
Figure 6.3: Rectifier model for 0-2 conduction mode

happens is generally in very low load resistance scenarios. Figure 6.9 shows a block diagram indicating the transitions occuring in this conduction mode. The actual mode transitions, the voltage, and current waveforms are shown for this conduction mode in Figure 6.10. The dc load resistance, R_{load} used to test this conduction mode
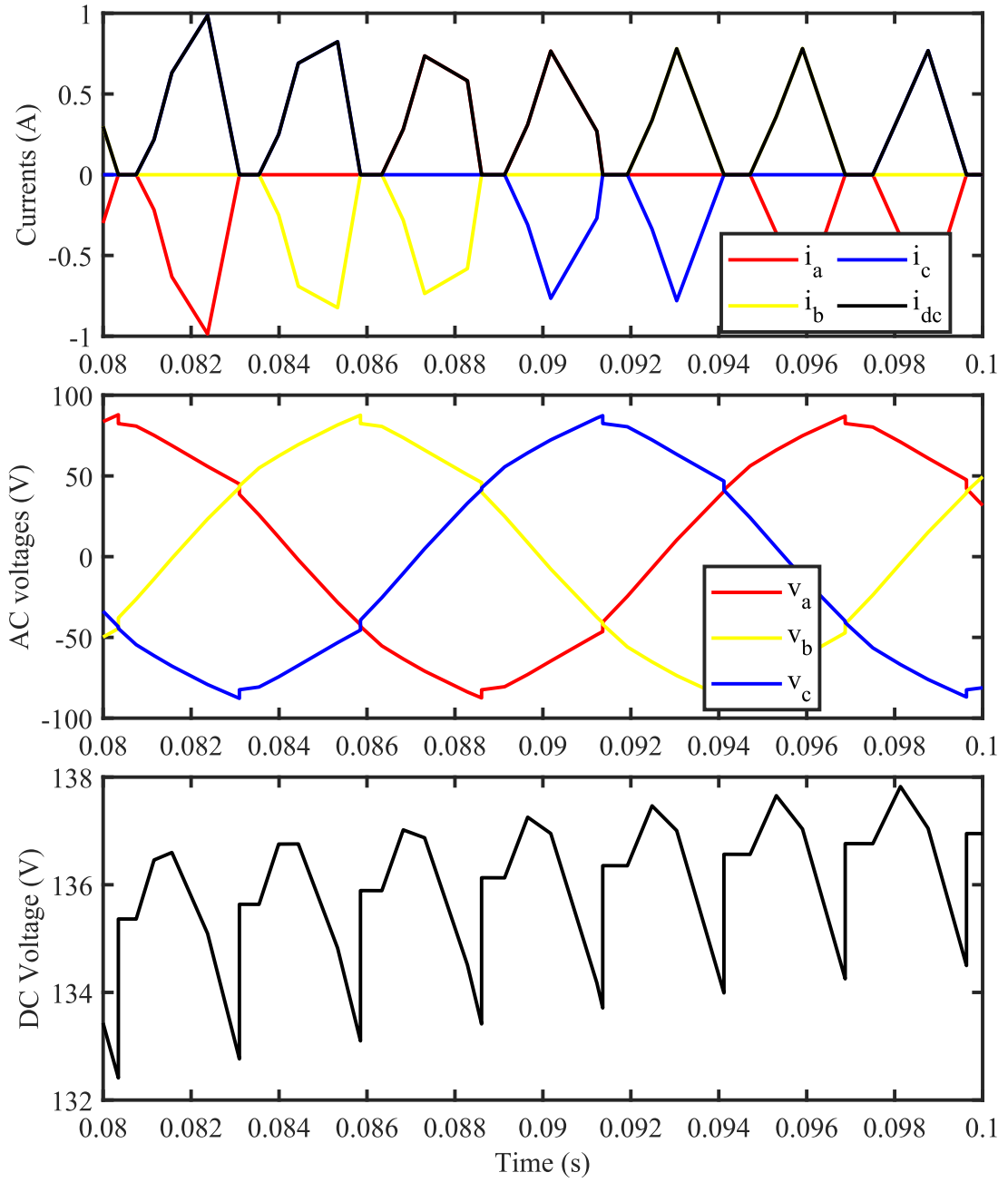
Figure 6.4: Rectifier at 0-2 conduction mode with a dc load of 10 kΩ

is 10 mΩ.
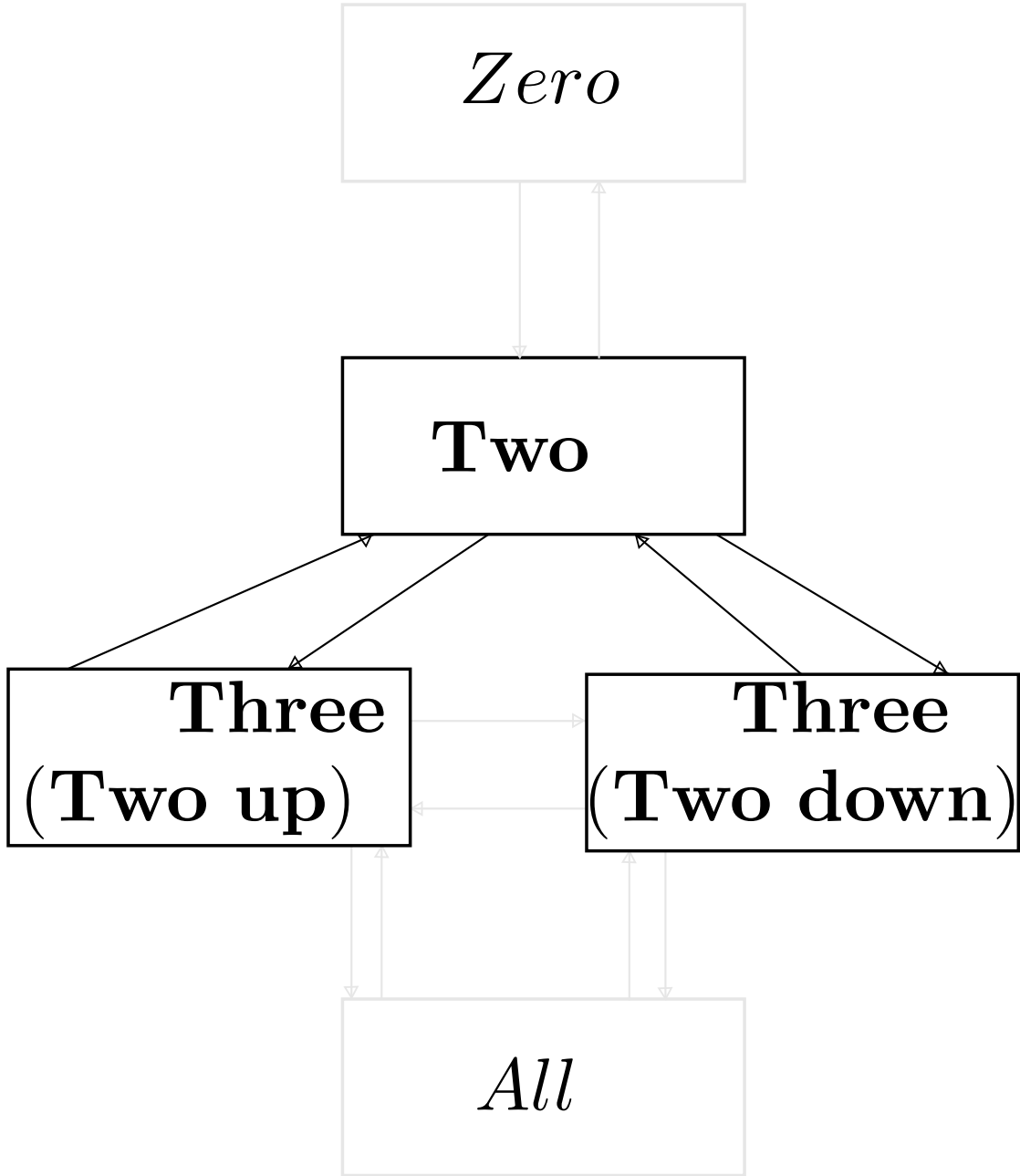
Figure 6.5: Rectifier model for 2-3 conduction mode
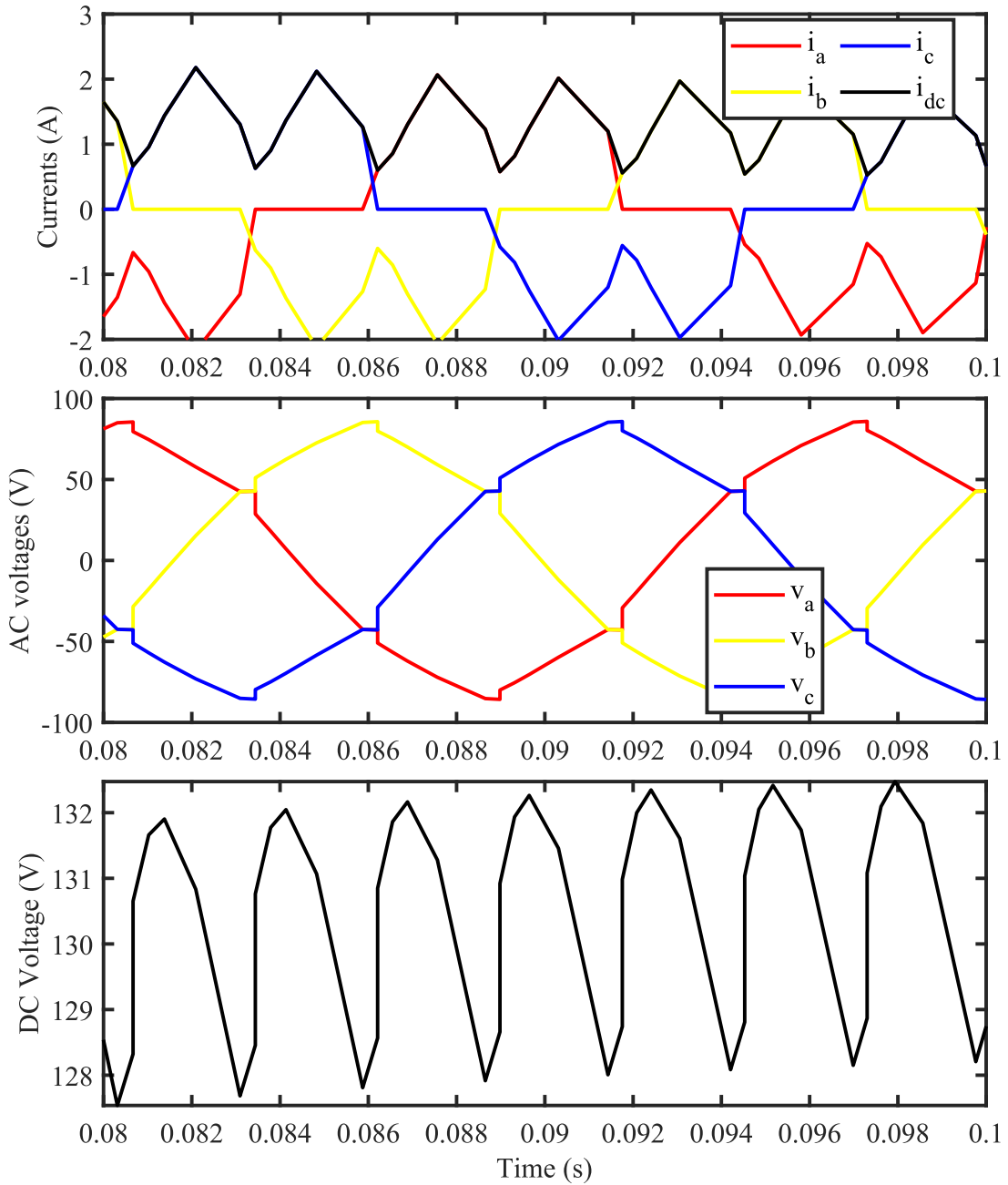
Figure 6.6: Rectifier at 2-3 conduction mode with a dc load of 100 Ω

Figure 6.7: Rectifier model for 3-3 conduction mode

Figure 6.8: Rectifier at 3-3 conduction mode with a dc load of 1 Ω

Figure 6.9: Rectifier model for 3-6 conduction mode
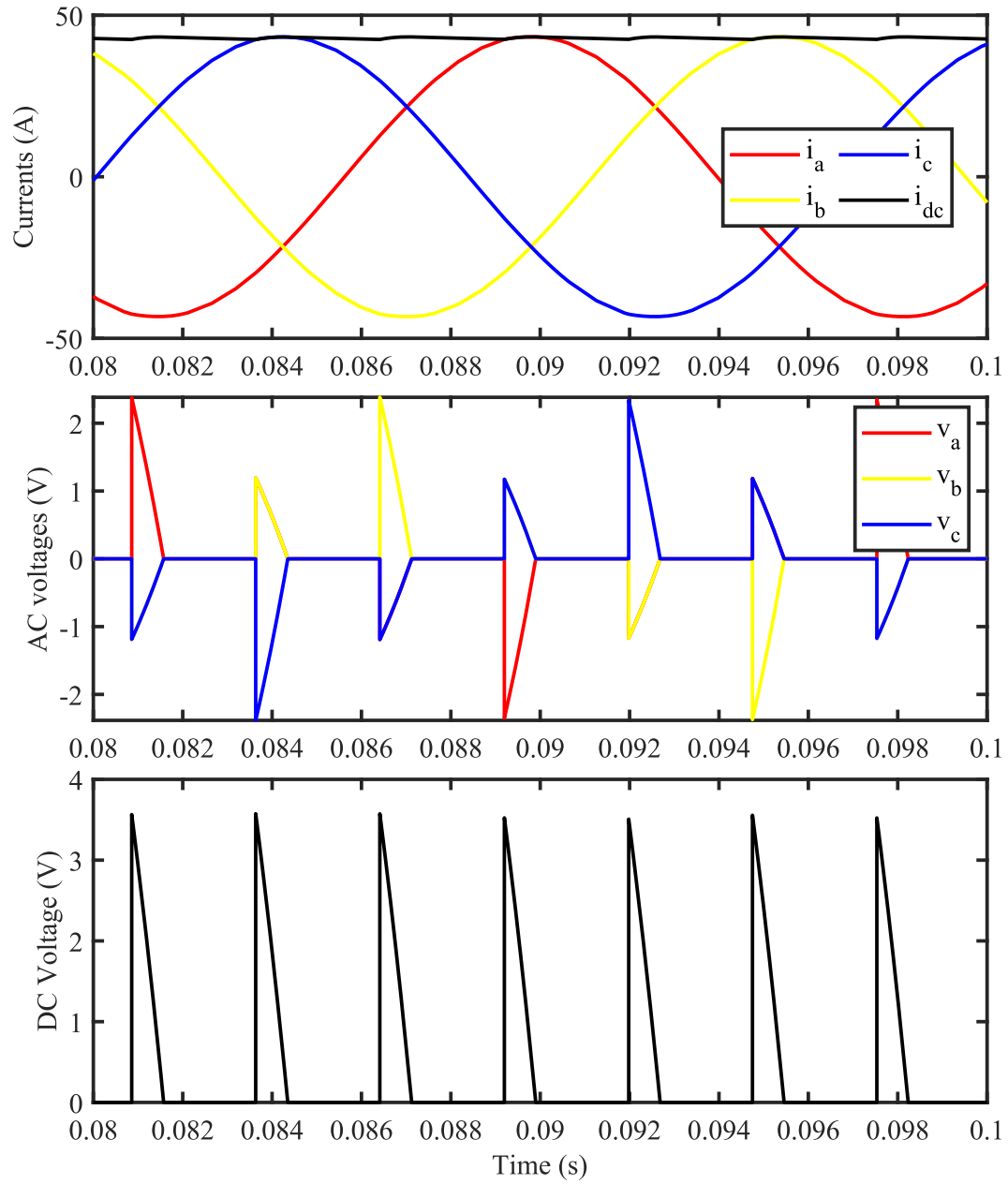
Figure 6.10: Rectifier at 3-6 conduction mode with a dc load of 10 mΩ

Chapter 7 Conclusion and Future Work

7.1 Conclusion

The work presented herein describes a novel SSPAVM of the synchronous machine-rectifier systems. Unique to the formulated model is its superior accuracy in predicting the system's behavior; particularly for a more salient machines with dyn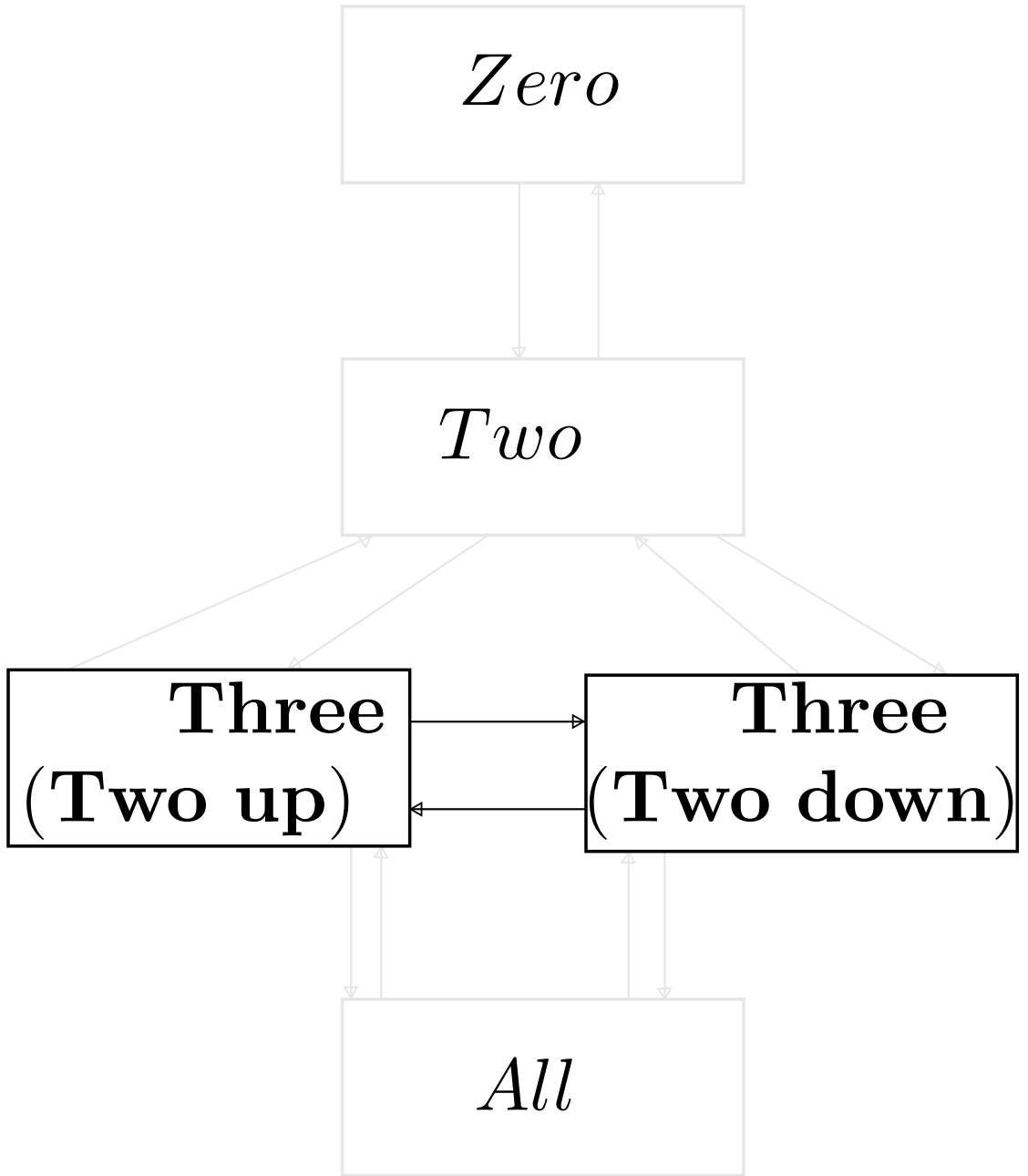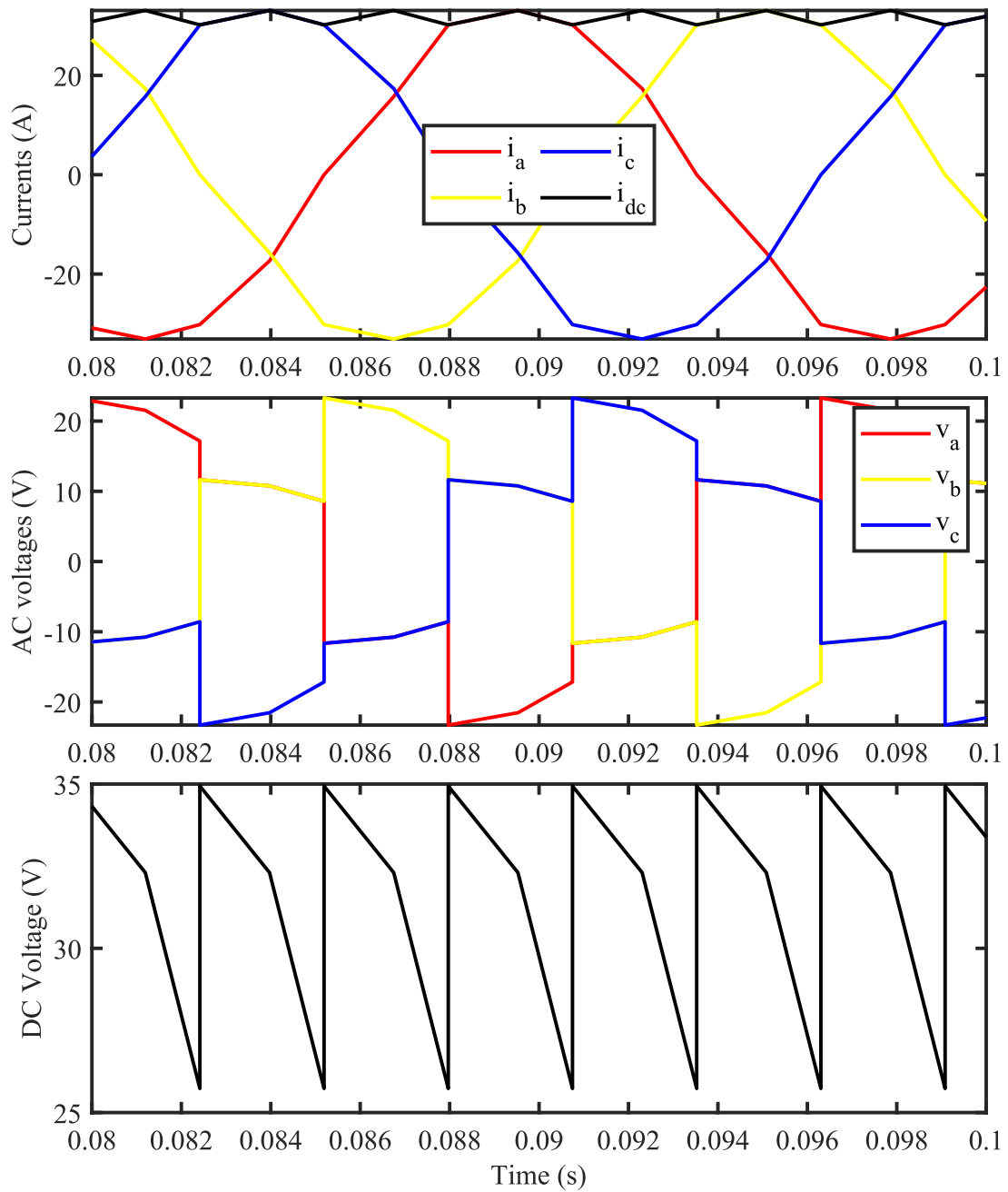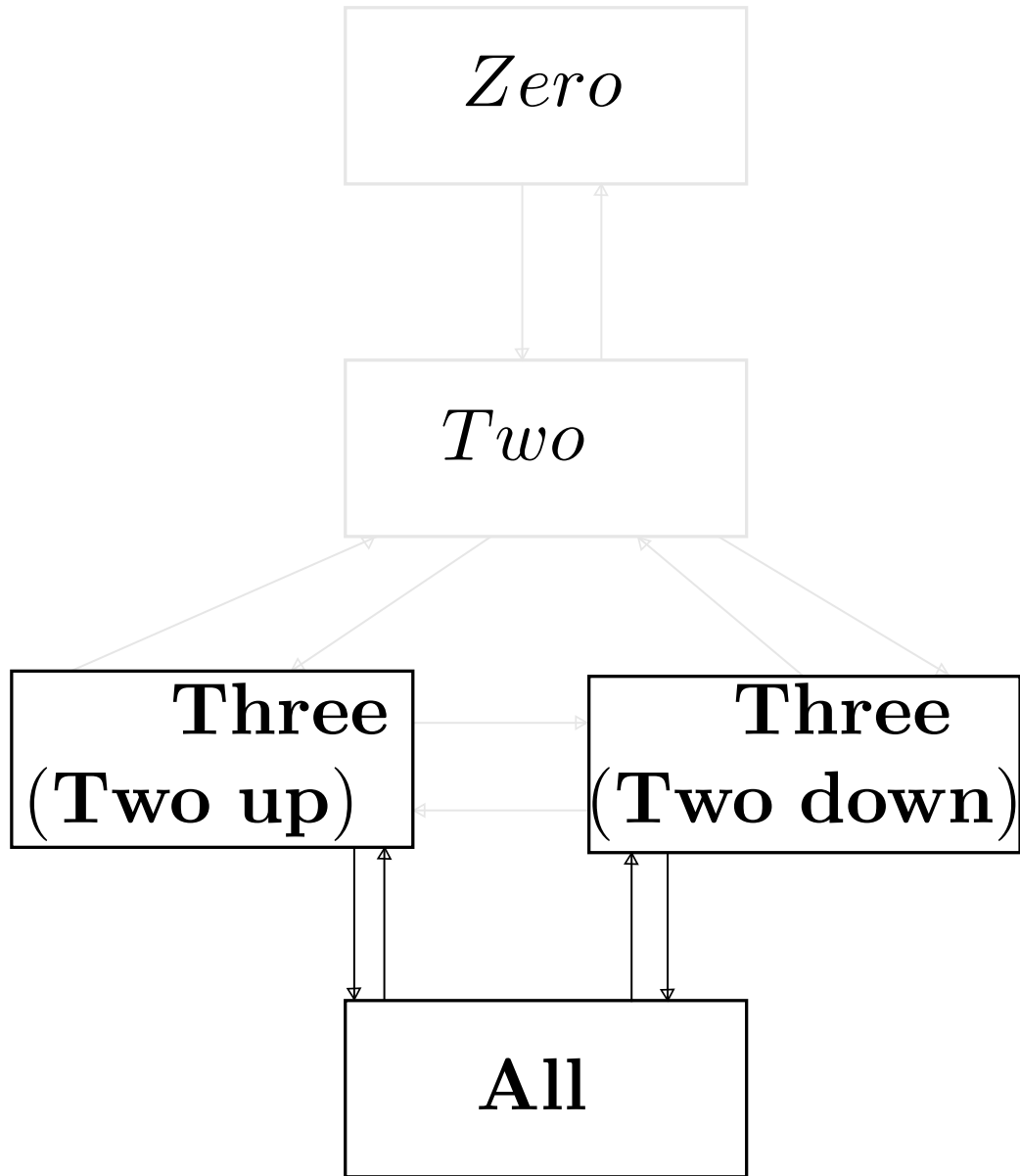amic and pulsed loading scenarios. The parametric relationships of the proposed SSPAVM use the dynamic impedance and the current angle as defined in previous sections as inputs. In nearly all the scenarios in which the proposed SSPAVM is validated against the detailed switched model and a previous PAVM, it is found that the proposed SSPAVM waveforms follow more accurately the detailed model waveforms than the previous PAVM. Also, in terms of computational efficiency, the proposed SSPAVM is more computationally efficient than the detailed model (as expected) and exhibits comparable computational efficiency with the previous PAVM.

A novel approach for obtaining the essential nonlinear parametric functions required to develop a SSPAVM of the synchronous machine-rectifier system is also discussed herein. This procedure provides the necessary lookup table values required for the application of the SSPAVM (developed in [82]). This procedure is demonstrated and compared with the lookup table values that are obtained when using the previous PAVM. Furthermore, specific situations in which the previous PAVM is not able to represent the parametric relationship between the dc and ac rectifier variables are demonstrated. In particular, these previous PAVM does not always represent the parametric functions accurately during transients, and this is particularly evident with machines with higher subtransient saliency.

Furthermore, the characterization method is extended to a 'fast procedure', wherein instead of multiple steady state simulations with a single value of the load resistance

and machine's ac current angle at each simulation loop, the approach utilizes a single transient exponential load increase for each current angle at each simulation loop. This multidimensional fast procedure greatly improves simulation times; and computational overhead associated with the multidimensional steady-state method.

Finally, an exact detailed model of the rectifier, in which all modes of operation/switching are accounted for is developed using stateflow-simulink hybrid state variable simulation environments. To achieve this, the exact differential equations with their appropriate state variable governing each state is utilized.

7.2   Future Work

- Looking forward, an approach in which the developed method of implementing the averaged model may be extended to alternative rectifier/converter topologies and machine structures should be explored. A specific example is developing a SSPAVM for active rectifiers.

- Another area of possible exploration is to investigate the relationship between the rectifier numerical functions (α, β and ϕ) and the rectifier switching functions. The hypothesis is that the ON and OFF switching characteristics of the rectifier is suspected to have an effect on the rectifier characterization. Therefore, one of the future efforts would be to find out if this is the case, and if so, to what extent and what mathematical relationship exist between both functions.

- A current-based average-value model wherein beta (β) numerical function and the current angle ($\angle \vec{i}$) will serve as lookup table inputs can be developed for the synchronous machine/converter systems. This aproach will likely improve upon the model proposed in [77]

Bibliography

[1] P. C. Krause, O. Wasynczuk, S. D. Sudhoff, and S. D. Pekarek, *Analysis of electric machinery and drive systems.* John Wiley & Sons, 2013.

[2] J. Jatskevich, S. D. Pekarek, and A. Davoudi, "Parametric avarage-value model of synchronous machine-rectifier systems," *IEEE Trans. Energy Convers.*, vol. 21, pp. 9–18, Mar. 2006.

[3] E. Mouni, S. Tnani, and G. Champenois, "Synchronous generators output voltage real-time feedback control via h_∞ strategy," *IEEE Trans. Energy Convers.*, vol. 24, pp. 329–337, June 2009.

[4] G. Grater and T. Doyle, "Propulsion powdered electric guns-a comparison of power system architectures," *IEEE Trans. Magnetics*, vol. 29, pp. 963–968, Jan 1993.

[5] Y. Zhang and A. M. Cramer, "Unified model formulations for synchronous machine model with saturation and arbitrary rotor network representation," *IEEE Trans. Energy Convers.*, vol. 31, no. 4, pp. 1356–1365, 2016.

[6] F. Kutt, M. Michna, and G. Kostro, "Multiple reference frame theory in the synchronous generator model considering harmonic distortions caused by nonuniform pole shoe saturation," *IEEE Trans. Energy Convers.*, vol. 35, no. 1, pp. 166–173, 2020.

[7] U. Karaagac, J. Mahseredjian, O. Saad, and S. Dennetière, "Synchronous machine modeling precision and efficiency in electromagnetic transients," *IEEE Transactions Power Del.*, vol. 26, no. 2, pp. 1072–1082, 2011.

[8]   L. Wang and J. Jatskevich, "A phase-domain synchronous machine model with constant equivalent conductance matrix for EMTP-Type solution," *IEEE Trans. Energy Convers.*, vol. 28, no. 1, pp. 191–202, 2013.

[9]   Y. Xia, Y. Chen, Y. Song, S. Huang, Z. Tan, and K. Strunz, "An efficient phase domain synchronous machine model with constant equivalent admittance matrix," *IEEE Trans. Power Del.*, vol. 34, no. 3, pp. 929–940, 2019.

[10] L. Quéval, M. Sekino, and H. Ohsaki, "A coupled FE phase-domain model for superconducting synchronous machine," *IEEE Trans. Applied Supercond.*, vol. 22, no. 3, pp. 5200804–5200804, 2012.

[11] K. Guo, Y. Li, L. Shi, H. Chen, S. Zhou, J. Liu, and M. Fan, "A phase-domain model of dual three-phase segmented powered linear PMSM for hardware-assisted real-time simulation," *IEEE Trans. Industry Appl.*, pp. 1–1, 2022.

[12] L. Wang and J. Jatskevich, "Magnetically-saturable voltage-behind-reactance synchronous machine model for EMTP-Type solution," *IEEE Trans. Power Syst.*, vol. 26, no. 4, pp. 2355–2363, 2011.

[13] A. P. Yadav, S. Xu, B. C. Schafer, and A. Davoudi, "Hardware-assisted simulation of voltage-behind-reactance models of electric machines on FPGA," *IEEE Trans. Energy Convers.*, vol. 35, no. 3, pp. 1247–1257, 2020.

[14] O. Rodriguez and A. Medina, "Synchronous machine stability analysis using an efficient time domain methodology: unbalanced operation analysis," in *IEEE Power Eng. Soc. Summer Meeting,*, vol. 2, pp. 677–681 vol.2, 2002.

[15] O. Rodriguez and A. Medina, "Efficient methodology for stability analysis of synchronous machines," vol. 150, pp. 405–412, IET, 2003.

[16] O. Rodriguez and A. Medina, "Efficient methodology for the transient and periodic steady-state analysis of the synchronous machine using a phase coordinates model," *IEEE Trans. Energy Convers.*, vol. 19, no. 2, pp. 464–466, 2004.

[17] K. Chan, E. Acha, M. Madrigal, and J. Parle, "The use of direct time-phase domain synchronous generator model in standard EMTP-Type industrial packages," *IEEE Power Eng. Rev.*, vol. 21, no. 6, pp. 63–65, 2001.

[18] L. Wang, J. Jatskevich, and H. W. Dommel, "Re-examination of synchronous machine modeling techniques for electromagnetic transient simulations," *IEEE Trans. Energy Conversion*, vol. 22, pp. 1221 – 1230, Aug 2007.

[19] S. J. Salon, ed., *Finite element analysis of electrical machines.* Norwell, MA: Kluwer, 1995.

[20] G. Slemon, "An equivalent circuit approach to analysis of synchronous machines with saliency and saturation," *IEEE Trans. Energy Conversion*, vol. 5, pp. 538–545, Sep 1990.

[21] Y.Xiao, G. Slemon, and M. Iravani, "Implementation of an equivalent circuit approach to the analysis of synchronous machine," *IEEE Trans. Energy Conversion*, vol. 9, pp. 717–723, Dec 1994.

[22] A. Lebsir, R. Rebbah, M. Larakeb, H. Djeghloud, and A. Bentounsi, "Modeling and analysis of a salient poles synchronous machines using finite-elements method," in *2014 International Symposium on Power Electronics, Electrical Drives, Automation and Motion*, pp. 363–367, 2014.

[23] H. Liu, L. Xu, M. Shangguan, and W. N. Fu, "Finite element analysis of 1 MW high speed wound-rotor synchronous machine," *IEEE Trans. on Magn.*, vol. 48, no. 11, pp. 4650–4653, 2012.

[24] S. Liu, O. A. Mohammed, and Z. Liu, "An improved FE-based phase variable model of PM synchronous machines including dynamic core losses," *IEEE Trans. Magn.*, vol. 43, no. 4, pp. 1801–1804, 2007.

[25] X. Xiao, W. Xu, D. Luo, and I. Boldea, "Improved 2D FEA model for homopolar linear synchronous machine," in *2020 IEEE 9th International Power Electronics and Motion Control Conference (IPEMC2020-ECCE Asia)*, pp. 3410–3414, 2020.

[26] I. Brown, G. Sizov, and N. Demerdash, "Rapid high fidelity finite element-based synchronous machine model for system simulations," in *2013 International Electric Machines and Drives Conference*, pp. 944–951, 2013.

[27] Y. Xiao, L. Zhou, J. Wang, and R. Yang, "Transient parameters calculation of salient-pole synchronous machine by finite element analysis," in *2016 IEEE Conference on Electromagnetic Field Computation*, pp. 1–1, 2016.

[28] A. Larson, S. Pekarek, R. Wang, M. L. Bash, and R. Van Maaren, "An efficient circuit model for design of synchronous machines," in *2015 IEEE International Electric Machines and Drives Conference (IEMDC)*, pp. 84–89, 2015.

[29] D. Luo, W. Xu, X. Xiao, and I. Boldea, "Three dimensional magnetic equivalent circuit analysis of the modified homopolar linear synchronous machine," in *2021 13th International Symposium on Linear Drives for Industry Applications (LDIA)*, pp. 1–6, 2021.

[30] J. Jatskevich, S. D. Pekarek, and A. Davoudi, "Fast procedure for constructing an accurate dynamic avarage-value model of synchronous machine-rectifier systems," *IEEE Trans. Energy Convers.*, vol. 21, pp. 435–441, June 2006.

[31] R. H. Park, "Two-reaction theory of synchronous machines generalized method of analysis-part I," *Transactions of the American Institute of Electrical Engineers*, vol. 48, no. 3, pp. 716–727, 1929.

[32] H. C. Stanley, "An analysis of the induction machine," *Electrical Engineering*, vol. 57, no. 12, pp. 751–757, 1938.

[33] D. Brereton, D. Lewis, and C. Young, "Representation of induction-motor loads during power-system stability studies," *Transactions of the American Institute of Electrical Engineers. Part III: Power Apparatus and Systems*, vol. 76, no. 3, pp. 451–460, 1957.

[34] G. Kron, *Equivalent circuits of electric machinery*. Wiley, 1951.

[35] P. C. Krause and C. Thomas, "Simulation of symmetrical induction machinery," *IEEE trans. power app. and syst.*, vol. 84, no. 11, pp. 1038–1053, 1965.

[36] P. T. Krein, "Elements of power electronics," 1998.

[37] D. W. Hart, *Power electronics*. Tata McGraw-Hill Education, 2011.

[38] P. Pejovic, *Three-phase diode rectifiers with low harmonics: current injection methods*. Springer Science & Business Media, 2007.

[39] R. W. Erickson and D. Maksimovic, *Fundamentals of power electronics*. Springer Science & Business Media, 2007.

[40] S. Ebrahimi, N. Amiri, and J. Jatskevich, "Hybrid parametric average-value/detailed modeling of line-commutated rectifiers," *IEEE Trans. Energy Convers.*, vol. 35, pp. 1494–1504, Sept. 2020.

[41] D. C. Aliprantis, S. D. Sudhoff, and B. T. Kuhn, "A brushless exciter model incorporating multiple rectifier modes and priesach's hysteresis theory," *IEEE Trans. Energy Convers.*, vol. 21, pp. 136–147, Mar. 2006.

[42] C. A. Platero, F. Blázquez, P. Frías, and M. Pardo, "New on-line rotor ground fault location method for synchronous machines with static excitation," *IEEE Trans. Energy Convers.*, vol. 26, no. 2, pp. 572–580, 2011.

[43] L. Xu, J. M. Guerrero, A. Lashab, B. Wei, N. Bazmohammadi, J. C. Vasquez, and A. Abusorrah, "A review of dc shipboard microgrids - Part I: Power architectures, energy storage, and power converters," *IEEE Trans. on Power Electron.*, vol. 37, no. 5, pp. 5155–5172, 2022.

[44] A. M. Cramer, X. Liu, Y. Zhang, and J. Stevens, "Early-stage shipboard power system simulation of operational vignettes for dependability assessment," in *2015 IEEE Elect. Ship Technol. Symp.*, pp. 382–387, June 2015.

[45] A. M. Cramer, J. D. Stevens, and I. Ojo, "Mission-based optimal control for the evaluation of power and energy system capability," in *2019 IEEE Elect. Ship Technol. Symp.*, pp. 311–316, 2019.

[46] B. Zahedi and L. E. Norum, "Modeling and simulation of all-electric ships with low-voltage dc hybrid power systems," *IEEE Trans. Power Electron.*, vol. 28, no. 10, pp. 4525–4537, 2012.

[47] S. Kim, S.-N. Kim, and D. Dujuc, "Impact of synchronous generator deexcitation dynamics on the protection in marine dc power distribution networks," *IEEE Trans. Transp. Electrific.*, vol. 7, pp. 267–275, Mar. 2021.

[48] E. Skjong, R. Volden, E. Rødskar, M. Molinas, T. A. Johansen, and J. Cunningham, "Past, present, and future challenges of the marine vessel's electrical power system," *IEEE Trans. Transp. Electrific.*, vol. 2, no. 4, pp. 522–537, 2016.

[49] M. Sabah, I. T. Ojo, and A. M. Cramer, "Evolution of operability-based performance metrics for assessment of mission performance," in *2021 IEEE Elect. Ship Technol. Symp.*, pp. 1–6, 2021.

[50] T. Skvarenina, S. Pekarek, O.Wasynczuk, P. Krause, R. Thibodeaux, and J.Weimer, "Simulation of a more-electric aircraft power system using an automated state model approach," in *IECEC 96 Proc. of the 31st Intersociety Energy Convers. Eng. Conf.*, pp. 133–136, Aug. 1996.

[51] A. Cross, A. Baghramian, and A. Forsyth, "Approximate, average, dynamic models of uncontrolled rectifiers for aircraft applications," *IET Power Electron.*, vol. 2, no. 4, pp. 398–409, 2009.

[52] G. Chunyi, Z. Yi, A. Gole, and Z. Chengyong, "Analysis of dual-infeed HVDC with LCC-HVDC and VSC-HVDC," *IEEE Trans. Power Del.*, vol. 27, no. 3, pp. 1529–1537, 2012.

[53] X. Lyu, J. Zhao, Y. Jia, Z. Xu, and K. Po Wong, "Coordinated control strategies of PMSG-Based wind turbine for smoothing power fluctuations," *IEEE Trans. Power Syst.*, vol. 34, no. 1, pp. 391–401, 2019.

[54] Q. Zhang, J. He, Y. Xu, Z. Hong, Y. Chen, and K. Strunz, "Average-value modeling of direct-driven PMSG-Based wind energy conversion systems," *IEEE Trans. Energy Convers.*, vol. 37, no. 1, pp. 264–273, 2022.

[55] "Simulink:user's guide." `https://www.mathworks.com/help/pdf_doc/simulink/simulink_ug.pdf`. Accessed: 2022-07-06.

[56] "PLECS: The simulation platform for power electronic systems user manual version 4.6." `https://www.plexim.com/sites/default/files/plecsmanual.pdf`. Accessed: 2022-07-06.

[57] "Simpowersystems: For use with simulink (user's guide version 2)." `https://matlab4engineers.com/wp-content/uploads/2019/09/powersys.pdf`. Accessed: 2022-07-06.

[58] "User's guide on the use of power systems computer aided design PSCAD." `https://www.pscad.com/uploads/ck/files/reference_material/PSCAD_User_Guide_v4_3_1.pdf`. Accessed: 2022-07-06.

[59] "MicroTran Reference Manual (Transient Analysis Program for Power Electronic Circuits)." `http://microtran.com/goodies1/mt.pdf`. Accessed: 2022-07-06.

[60] T. Zouaghi and M. Poloujadoff, "Modeling of polyphase brushless exciter behavior for failing diode operation," *IEEE Trans. Energy Convers.*, vol. 13, pp. 214–220, Sept. 1998.

[61] S. Chiniforoosh, J. Jatskevich, A. Yazdani, V. Sood, V. Dinavahi, J. Martinez, and A. Ramirez, "Definitions and applications of dynamic average models for analysis of power systems," *IEEE Trans. Power Del.*, vol. 25, pp. 2655–2669, Oct. 2010.

[62] J. Lin and J. Marti, "Implementation of the CDA procedure in EMTP," *IEEE Trans. Power Syst.*, vol. 5, pp. 394 – 402, May 1990.

[63] A. M. Gole, S. Filizadeh, R. W. Menzies, and P. L. Wilson, "Optimization-enabled electromagnetic transient simulation," *IEEE Trans. Power Del.*, vol. 20, no. 1, pp. 512–518, 2005.

[64] S. Chiniforoosh, H. Atighechi, and J. Jatskevich, "A generalized methodology for dynamic average modeling of high-pulse-count in transient simulation programs," *IEEE Trans. Energy Convers.*, vol. 31, pp. 228–239, Mar. 2016.

[65] H. A. Petroson and P. Krause, "A direct -and quadrature - axis representation of a parallel ac and dc power system," *IEEE Trans. Power App. Syst.*, vol. PAS - 85, pp. 210–225, Mar. 1966.

[66] P. C. Krause and T. A. Lipo, "Analysis and simplified representations of a rectifier-inverter induction motor drive," *IEEE Trans. Power App. Syst.*, no. 5, pp. 588–596, 1969.

[67] S. D. Sudhoff, K. Corzine, H. Heigner, and D. Delisle, "Transient and dynamic average-value modeling of synchronous machine fed load-commutated converters," *IEEE Trans. Energy Convers.*, vol. 11, pp. 508–514, Sept. 1996.

[68] T. H. Warner and J. Kassakian, "Transient characteristics and modeling of large turboalternator-driven rectifier/inverter systems based on field test data," *IEEE Power Eng. Rev.*, vol. PER-5, no. 7, pp. 47–47, 1985.

[69] S. D. Sudhoff and O. Wasynczuk, "Analysis and average-value modeling of line-commutated converter-synchronous machine systems," *IEEE Trans. Energy Convers.*, vol. 8, pp. 92–99, Mar. 1993.

[70] M. Shahnazari and A. Vahedi, "Improved dynamic average modeling of brushless excitation system in all rectification modes," *IET Electric Power Appl.*, vol. 4, pp. 657–669, Sept. 2010.

[71] D. Borkowski, "Analytical model of small hydropower plant working at variable speed," *IEEE Trans. Energy Convers.*, vol. 33, no. 4, pp. 1886–1894, 2018.

[72] I. Jadric, D. Borojevic, and M. Jadric, "Modeling and control of a synchronous generator with an active dc load," *IEEE Trans. Power Electron.*, vol. 15, pp. 303–311, Mar. 2000.

[73] J. Jatskevich and T. Aboul-Seoud, "Impedance characterization of a six-phase synchronous generator-rectifier system using average - value model," in *Canadian Conference on Electrical and Computer Engineering*, pp. 2231–2234, May 2004.

[74] J. Jatskevich and S. D. Pekarek, "Numerical validation of parametric average-value modeling of synchronous machine-rectifier systems for variable frequency operation," *IEEE Trans. Energy Convers.*, vol. 23, pp. 342–344, Mar. 2006.

[75] H.Atighechi, S. Chiniforoosh, K. Tabarraee, and J. Jatskevich, "Average-value modeling of synchronous machine-fed-thyristor-controlled-rectifier," *IEEE Trans. Energy Convers.*, vol. 30, pp. 487–497, June 2015.

[76] Y. Zhang and A. M. Cramer, "Numerical average-value modeling of rotating rectifiers in brushless excitation systems," *IEEE Trans. Energy Convers.*, vol. 32, pp. 1592–1601, Dec. 2017.

[77] Y. Zhang and A. M. Cramer, "Formulation of rectifier numerical average-value model for direct interface with inductive circuitry," *IEEE Trans. Energy Convers.*, vol. 34, pp. 741–749, June 2019.

[78] S. Ebrahimi, N. Amiri, and J. Jatskevich, "Average-value modeling of multi-phase machine-converter systems with asymmetric internal faults," in *IECON 2021 – 47th Annual Conf. of the IEEE Industrial Electron. Society*, pp. 1–6, 2021.

[79] Z. Hong, S. Ebrahimi, Y. Xu, J. Jatskevich, and J. He, "Average-value modeling of line-commutated inverter systems with commutation failure," *IEEE Trans. Power Del.*, pp. 1–1, 2021.

[80] S. Ebrahimi, N. Amiri, H. Atighechi, Y. Huang, L. Wang, and J. Jatskevich, "Generalized parametric average-value model of line-commutated rectifiers considering ac harmonics with variable frequency operation," *IEEE Trans. Energy Convers.*, vol. 33, no. 1, pp. 341–353, 2018.

[81] S. Pekarek and E. Walters, "An accurate method of neglecting dynamic saliency of synchronous machines in power electronic based systems," *IEEE Trans. Energy Convers.*, vol. 14, no. 4, pp. 1177–1183, 1999.

[82] I. T. Ojo, A. M. Cramer, and M. Sabah, "Saliency-sensitive parametric average-value modeling of machine-rectifier systems—Part I: Modeling and simulation." Unpublished.

[83] I. Ojo, "Saliency-sensitive parametric average-value modeling of machine-rectifier systems–Part I: Modeling and simulation," 2022.

[84] S. Ebrahimi, N. Amiri, and J. Jatskevich, "Interfacing of parametric average-value models of LCR systems in fixed-time-step real-time EMT simulations," *IEEE Trans. Energy Convers.*, vol. 35, no. 4, pp. 1985–1988, 2020.

[85] W.-S. Im, C. Wang, L. Tan, W. Liu, and L. Liu, "Cooperative controls for pulsed power load accommodation in a shipboard power system," *IEEE Trans. Power Syst.*, vol. 31, no. 6, pp. 5181–5189, 2016.

[86] J. M. Crider and S. D. Sudhoff, "Reducing impact of pulsed power loads on microgrid power systems," *IEEE Trans. Smart Grid*, vol. 1, no. 3, pp. 270–277, 2010.

[87] M. Steurer, M. Andrus, J. Langston, L. Qi, S. Suryanarayanan, S. Woodruff, and P. Ribeiro, "Investigating the impact of pulsed power charging demands on shipboard power quality," in *2007 IEEE Elect. Ship Technol. Sympos.*, pp. 315–321, 2007.

[88] I. T. Ojo and A. M. Cramer, "Saliency-sensitive parametric average-value modeling of machine-rectifier systems—Part II: Multidimensional characterization." Unpublished.

[89] I. Ojo, "Saliency-sensitive parametric average-value modeling of machine-rectifier systems–Part II: Model characterization," 2022.

[90] A. Davoudi and J. Jatskevich, "Realization of parasitics in state-space average-value modeling of PWM dc-dc converters," *IEEE Trans. Power Electron.*, vol. 21, no. 4, pp. 1142–1147, 2006.

[91] H. Atighechi, S. Chiniforoosh, S. Ebrahimi, and J. Jatskevich, "Using multiple reference frame theory for considering harmonics in average-value modeling of diode rectifiers," *IEEE Trans. Energy Convers.*, vol. 31, no. 3, pp. 872–881, 2016.

[92] Y. Huang, L. Dong, S. Ebrahimi, N. Amiri, and J. Jatskevich, "Dynamic phasor modeling of line-commutated rectifiers with harmonics using analytical and parametric approaches," *IEEE Trans. Energy Convers.*, vol. 32, no. 2, pp. 534–547, 2017.

[93] I. T. Ojo and A. M. Cramer, "Multidimensional fast procedure for extracting parametric functions for salient machine-rectifier systems." Unpublished.

[94] B. Wu and M. Narimani, *High-power converters and AC drives*. John Wiley & Sons, 2017.

Vita

Personal Information

Name: Isuje Taiye Ojo

Nationality: Nigeria

Education Background

Bachelor of Engineering (B.Eng), Electrical/Electronics Engineering, 2011

Master of Engineering (M.Eng), Electrical/Electronics Engineering, 2018

Publications

1. A. M. Cramer, J. D. Stevens and **I. T. Ojo**, "Mission-Based Optimal Control for the Evaluation of Power and Energy System Capability," 2019 IEEE Electric Ship Technologies Symposium (ESTS), 2019, pp. 311-316.

2. M. Sabah, **I. T. Ojo** and A. M. Cramer, "Evolution of Operability-Based Performance Metrics for Assessment of Mission Performance," 2021 IEEE Electric Ship Technologies Symposium (ESTS), 2021, pp. 1-6.

3. **I. T. Ojo**, A. M. Cramer and M. Sabah, "Saliency-Sensitive Parametric Average-Value Modeling of Synchronous Machine-Rectifier Systems–Part I: Modeling and Simulation", submitted in IEEE Transactions on Energy Conversion, July 2022.

4. **I. T. Ojo** and A. M. Cramer, "Saliency-Sensitive Parametric Average-Value Modeling of Synchronous Machine-Rectifier Systems–Part II: Model Characterization", submitted in IEEE Transactions on Energy Conversion, July 2022.

5. **I. T. Ojo** and A. M. Cramer, "Multidimensional Fast Procedure for Extracting Parametric Functions for Salient Machine-Rectifier Systems", in preparation for submission in IEEE Transactions on Energy Conversion, August 2022 .